Development of paper-based 3D cell culture devices and real-time biosensing applications

Miss Naricha Pupinyo

จุฬาลงกรณ์มหาวิทยาลัย
CHULALONGKORN UNIVERSITY

A Dissertation Submitted in Partial Fulfillment of the Requirements

for the Degree of Doctor of Philosophy in Clinical Biochemistry and Molecular Medicine

Department of Clinical Chemistry

FACULTY OF ALLIED HEALTH SCIENCES

Chulalongkorn University

Academic Year 2019

การพัฒนาอุปกรณ์โครงร่างฐานกระดาษสำหรับเพาะเลี้ยงเซลล์แบบสามมิติและการประยุกต์ใช้
ทางไบโอเซนเซอร์แบบตามเวลา

น.ส.นริชา ภู่ภิญโญ

จุฬาลงกรณ์มหาวิทยาลัย
CHULALONGKORN UNIVERSITY

วิทยานิพนธ์นี้เป็นส่วนหนึ่งของการศึกษาตามหลักสูตรปริญญาวิทยาศาสตรดุษฎีบัณฑิต
สาขาวิชาชีวเคมีคลินิกและอณูทางการแพทย์ ภาควิชาเคมีคลินิก
คณะสหเวชศาสตร์ จุฬาลงกรณ์มหาวิทยาลัย
ปีการศึกษา 2562
ลิขสิทธิ์ของจุฬาลงกรณ์มหาวิทยาลัย

Thesis Title	Development of paper-based 3D cell culture devices and real-time biosensing applications
By	Miss Naricha Pupinyo
Field of Study	Clinical Biochemistry and Molecular Medicine
Thesis Advisor	Associate Professor WANIDA LAIWATTANAPAISAL, Ph.D.
Thesis Co Advisor	Professor Jenny Emnéus, Ph.D.

Accepted by the FACULTY OF ALLIED HEALTH SCIENCES, Chulalongkorn University in Partial Fulfillment of the Requirement for the Doctor of Philosophy

.... Dean of the FACULTY OF ALLIED HEALTH SCIENCES

(Associate Professor PALANEE AMMARANOND, Ph.D.)

DISSERTATION COMMITTEE

.... Chairman

(Assistant Professor TEWIN TENCOMNAO, Ph.D.)

.... Thesis Advisor

(Associate Professor WANIDA LAIWATTANAPAISAL, Ph.D.)

.... Thesis Co-Advisor

(Professor Jenny Emnéus, Ph.D.)

.... Examiner

(Assistant Professor TEWARIT SARACHANA, Ph.D.)

.... Examiner

(NADNUDDA RODTHONGKUM, Ph.D.)

.... External Examiner

(Somponnat Sampattavanich, Ph.D.)

นริชา ภู่ภิญโญ : การพัฒนาอุปกรณ์โครงร่างฐานกระดาษสำหรับเพาะเลี้ยงเซลล์แบบสามมิติและการประยุกต์ใช้ ทางไบโอเซนเซอร์แบบตามเวลา. (Development of paper-based 3D cell culture devices and real-time biosensing applications) อ.ที่ปรึกษาหลัก : รศ. ดร.วนิดา หลายวัฒนไพศาล, อ.ที่ปรึกษาร่วม : Jenny Emnéus

ปัจจุบันกระดาษสามารถใช้เป็นโครงร่างสำหรับเพาะเลี้ยงเซลล์ เนื่องจากกระดาษประกอบไปด้วยเส้นใยที่สามารถค้ำจุนเซลล์ได้ในรูปแบบสามมิติ การศึกษามะเร็งผิวหนังในปัจจุบันอาศัยการตรวจวัด 2 วิธีหลัก คือการศึกษาปริมาณการสร้างเมลานินและการบุกรุกของเซลล์มะเร็งผิวหนังต่อสิ่งเร้าชนิดต่างๆ ในงานวิจัยนี้ผู้วิจัยได้พัฒนาอุปกรณ์โครงร่างฐานกระดาษสำหรับเพาะเลี้ยงเซลล์เมลาโนมาแบบสามมิติ ระหว่างการพัฒนา ผู้วิจัยได้ประยุกต์ใช้พารามิเตอร์ต่างๆเพื่อพัฒนางานวิจัย 3 งาน ได้แก่ อุปกรณ์ตรวจวัดฤทธิ์การยับยั้งการสร้างเมลานินของสารประกอบทางธรรมชาติ วิธีการตรวจคัดกรองสารออกฤทธิ์คล้ายเอสโตรเจนแบบตามเวลา และอุปกรณ์การตรวจวัดการบุกรุกของเมลาโนมาแบบตามเวลา การใช้กระดาษสีขาวสำหรับเพาะเลี้ยงเซลล์เมลาโนมาช่วยให้การสังเกตสีของเมลานินซึ่งมีสีดำง่ายขึ้น โดยสีของเมลานินสามารถมองเห็นได้ด้วยตาเปล่า และประเมินปริมาณความเข้มได้โดยใช้คอมพิวเตอร์โปรแกรม ในงานวิจัยแรกนี้ผู้วิจัยพบว่าอุปกรณ์ดังกล่าวสามารถใช้ตรวจหาฤทธิ์การยับยั้งการสร้างเมลานินในสารประกอบทางธรรมชาติภายในเวลาอันรวดเร็วและง่าย ต่อมาผู้วิจัยได้ศึกษาค่าพารามิเตอร์เบื้องต้นสำหรับเลี้ยงเซลล์ ค่าพารามิเตอร์ดังกล่าวได้ถูกนำไปประยุกต์ใช้เพื่อพัฒนาวิธีการตรวจวัดสารออกฤทธิ์คล้ายเอสโตรเจนแบบตามเวลา โดยอาศัยการจับของเอสโตรเจนบนเซลล์มะเร็งเต้านม ซึ่งส่งผลให้เซลล์เพิ่มจำนวนมากขึ้น จำนวนของเซลล์ดังกล่าวทำให้ค่าอิมพิแดนซ์สูงขึ้นตามความเข้มข้นของเอสโตรเจน วิธีดังกล่าวสามารถตรวจหาการออกฤทธิ์คล้ายเอสโตรเจนของ Bisphenol-A และ Irgarol 1051 ได้แบบตามเวลาและให้ผลรวดเร็วกว่าวิธีดั้งเดิม หลังจากนั้นผู้วิจัยได้นำสภาวะที่เหมาะสมสำหรับการเลี้ยงเซลล์เมลาโนมาบนกระดาษจากงานวิจัยแรก และค่าพารามิเตอร์สำหรับการตรวจวัดอิมพิแดนซ์จากงานวิจัยที่สองมาประยุกต์ใช้ในการพัฒนางานวิจัยที่สาม เพื่อพัฒนาอุปกรณ์การตรวจวัดการบุกรุกของเซลล์เมลาโนมาแบบตามเวลาโดยใช้กระดาษเป็นเยื่อเลือกผ่าน อุปกรณ์ดังกล่าวได้พัฒนาภายใต้หลักการการอุดตันของเซลล์ที่บุกรุกผ่านกระดาษ ซึ่งส่งผลให้การไหลของกระแสไฟฟ้ายากขึ้นและทำให้ค่าอิมพิแดนซ์สูงขึ้นตามลำดับ อุปกรณ์ดังกล่าวได้นำไปใช้ศึกษาการบุกรุกของเซลล์เมลาโนมาภายใต้การทดสอบร่วมกับ Insulin growth factor-1 ผู้วิจัยพบว่า การบุกรุกของเซลล์เมลาโนมาสามารถตรวจพบได้ภายใน 7 ชม. หลังจากใส่สาร Insulin growth factor-1 ทำให้ลดระยะเวลาการติดตามและสามารถลดผลกระทบของการเจริญเติบโตของเซลล์ต่อการวัดปริมาณเซลล์บุกรุกลงได้

สาขาวิชา ชีวเคมีคลินิกและอณูทางการแพทย์	ลายมือชื่อนิสิต ....
ปีการศึกษา 2562	ลายมือชื่อ อ.ที่ปรึกษาหลัก ....
	ลายมือชื่อ อ.ที่ปรึกษาร่วม ....

5876954437 : MAJOR CLINICAL BIOCHEMISTRY AND MOLECULAR MEDICINE

KEYWORD: Paper-based cell culture, Melanoma, anti-melanogenic effect, E-screen, Invasion assay, Impedance measurement

Naricha Pupinyo : Development of paper-based 3D cell culture devices and real-time biosensing applications. Advisor: Assoc. Prof. WANIDA LAIWATTANAPAISAL, Ph.D. Co-advisor: Prof. Jenny Emnéus, Ph.D.

Due to its micro fibrous pores, paper has gained traction in the use as a scaffold for 3D cell culture. To study melanoma mechanism, screening the amount of melanin production and invasion study are major keys for drug development. In this work, we developed paper-based devices for culturing melanoma cells. Through the development process, we obtained the optimal parameters, which were applied for 3 different projects; 1) Anti-melanogenic effect screening, 2) Impedance-based E-screen assay, and 3) A membrane insert for real-time invasion assay. As a result of melanin production from melanocytes, the cells can be easily observed after a few days of culturing due to their black color. Fortunately, this color change can easily be visualized when melanocyte is cultured in the paper due to the white color of the paper. The paper was then applied for anti-melanogenic screening of the natural compounds with short analysis time and easy steps. In order to develop the real-time invasion assay, we primarily study the impedance characteristics of cells. The obtained impedance parameters were applied for real-time estrogen screening as a parallel project. Based on the estrogen receptor on breast cancer cells, the binding of estrogen can increase cell proliferation, resulting in the increased impedance magnitude. The estrogenic effect of the test compounds, Bisphenol-A and Irgarol 1051, were then monitored in real time. After that, we applied the obtained impedance parameters for the development of real-time invasion assay device using paper as a membrane insert. The concept was based on the blockage of invasive cells within paper pores, resulting in the increased impedance magnitude. The device was applied for real-time invasion study of melanoma cells under the treatment of IGF-1. Melanoma invasion could be tracked within 7 h after IGF-1 treatment. Thus, the invasion of melanoma cells was less likely affected by cell proliferation.

Field of Study:	Clinical Biochemistry and Molecular Medicine	Student's Signature ....
Academic Year:	2019	Advisor's Signature ....
		Co-advisor's Signature ....

ACKNOWLEDGEMENTS

TABLE OF CONTENTS

LIST OF FIGURES

LIST OF TABLES

CHAPTER I Introduction

1.1 Background and rationale

The incident of melanoma has been increased specially in western countries. Besides, melanoma is one the main cause from cancer (1) and also associated with high rates of mortality (2, 3). Nevertheless, melanoma patients tend to have a good prognosis when the cancer was detected before metastasis (4). The obvious melanoma pathogenesis is the dark spot on patient skin, which is caused by the over pigmentation from UV exposure and genetic susceptibility. Hence, those genetic mutations result in an increased melanocyte proliferation, blood vessel growth, tumor invasion, evasion of immune response, and ultimately metastasis (5). The histopathology of primary melanoma is often found in the different types of lesion, ranging from benign naevi and dysplastic naevi to melanoma *in situ* (6). These lesions tend to present as a flat or slightly elevated brown lesion with variegated pigmentation (7). In order to study in-depth regarding melanoma mechanism, the process of melanogenesis and cancer metastasis for targeted gene identification are crucial.

For melanoma treatment, researchers have used the synthesized melanogenesis inhibitors as well as the natural compounds (8, 9). In order to qualify those compounds, the *in vitro* melanin content analysis is applied. Furthermore, melanin quantification is the important *in vitro* experiment for melanoma study because melanin amount can provide the information about the progression from benign to malignant melanoma. The most extensively used method nowadays is the absorbance spectroscopy. In brief, melanocytes are collected after seeding and treatment. Next, the produced melanin is solubilized in 1 N NaOH. The total amount of melanin is measured by absorbance spectroscopy comparing with the standard curve of synthetic melanin or melanin isolated from *Sepia officinalis.* However, the absorbance measurement is time-consuming due to the incubation step of melanin solubilization, labor intensive process, and low sensitivity and specificity (10). Thus, conventional melanin quantification takes at least 1 hour for the incubation step of melanin solubilization and takes around 2 h for the complete steps. Another method using for melanin quantification is Electro spin resonance spectrometry *(ESR),* which allows the measurement of electron spin resonance signal based on free radicals derived from melanin. ESR is specific to melanin but lacks of sensitivity (11). High

performance liquid chromatography *(HPLC)* is another method used for melanin quantification, which can also differentiate between eumelanin and pheomelanin. However, HPLC requires the specific equipment and expertise (12). Rosenthal *et al.* originally developed the fluorescent quantification of melanin by subjecting melanin with the hydrogen peroxide solution. The advantage of fluorescent quantification of melanin is that the fluorescent signal from melanin is not affected by proteinaceous or lipid contamination. Nonetheless, the fluorescent quantification of melanin still needs multiple steps, which take around 4-5 h to complete the experiment (13, 14).

Another crucial test for understanding melanoma mechanism is the invasion assay. Studies on the factors involved in the mechanism of melanoma invasion are, therefore, important for the development of anti-metastatic drugs. Various *in vitro* methods have been developed to overcome the limitations of existing devices. The most popular approach to study cell invasion is the transwell assay, also known as the Boyden chamber assay. In brief, a transwell invasion assay device consists of two compartments separated by a commercially available polycarbonate or polyethylene terephthalate membrane insert, which is coated with an extracellular matrix (ECM) based gel. A known number of cells is seeded on top of the gel-coated membrane insert and the lower compartment is filled with a chemoattractant of interest. Once the cells invade through the membrane, the experiment is stopped. The non-invasive cells are then swabbed out, stained and counted under a microscope (15-17). A conventional transwell assay is simple and easy to use. However, the invasion of cells cannot be tracked in real-time (18). Even though the plastic membrane inserts are translucent, allowing staining and direct visualization of the cells, they are only available in certain sizes and designs and expensive. Additionally, the invasion of cells is based on 2D cell formation. Hence, the invasion of cells is not able to imitate the *in vivo* metastatic conditions.

To overcome these problems, researchers have developed the real-time invasion assay device using Electrochemical Impedance Spectroscopy (EIS) (19). When cells are seeded on an electrode surface, adherent cells act as insulators, which impede the passage of alternating current (20). An increasing number of cells on an electrode surface results in a correspondingly increasing impedance. This principle has been used to develop different real-time migration and invasion assay devices. For

example, the commercial xCELLigence system was used for migration and invasion study of various cell types including placental and endothelial cells (21, 22). EIS was used in a simple invasion assay by integrating the electrodes in a transwell-inspired device (23). The assay was performed by placing chemoattractant under the membrane insert and cellular invasion was followed in real time by an increasing impedance due to movement of cells.

Currently, paper is the alternative scaffold for cell culture because they contain micro fibrous pores. Whitesides's group has demonstrated the "Cell-in-Gel-in-Paper or CiGiP" technique which is the use of hydrogel to encapsulate cancer cells and place the encapsulated cells in the paper (24). This technique has also been adapted for various applications for culturing cell in the paper such as paper-based cell culture platforms for the construction of *in vitro* disease models (24-26), drug screening (27), and cell cryopreservation (28, 29) applications. In particular, paper is biocompatible and can easily be established with the extremely low costs. Moreover, the paper is white, which is suitable for color screening. Thus, as a result of melanin production from melanocytes, the cells can be easily observed after a few days of culturing due to their black color. Fortunately, this color change can easily be visualized when melanocyte is cultured in the paper-based scaffold due to the white color of the paper. Mosadegh *et al.* demonstrated a paper-based invasion assay by constructing a device comprising multiple paper layers. Fluorescently labelled cells were then encapsulated in a gel and placed in the middle of the stacked multilayer (30). This approach requires, however, a paper destacking step to analyze the invading cells in each layer. Paper-based 3D cell culture devices have also been coupled with electrochemical measurements. Lei *et al.* demonstrated paper-based 3D cell culture for quantifying cell proliferation using EIS (31), which shows the potential of paper as an alternative scaffold for 3D cell cultures in combination with electrochemical techniques.

In order to reduce the cost of melanoma study and improve the *in vivo* like melanoma model, paper could serve as an alternative scaffold for melanoma 3D cell culture. In this work, we demonstrated the novel applications of paper-based 3D cell culture for two melanoma studies; melanin content analysis and its invasion. In the first model, we optimized the suitable conditions for melanoma cell culture on the

paper and applied for the screening of anti-melanogenic compounds. In this model, we aim to simplify the method for rapid screening the amount of melanin production. Due to its black color, the melanin produced by the melanocytes can be easily observed on the white paper-based scaffold after a few days of culturing. Afterwards, paper-based device was applied for screening the effect of Kojic acid and Arbutin on melanin production. In the first model, we successfully demonstrated that paper-based scaffolding can be beneficial for 3D cell culture, allowing melanoma cells to behave similar to the *in vivo* structure. Furthermore, the melanin amount can be easily screened by scanning the paper and analyzing the melanin intensity with ImageJ software, thus decreasing the duration of conventional melanin content analysis (absorbance spectroscopy). Moreover, the color on the paper was confirmed as melanin by the treatment of α-MSH at various concentrations. The amount of melanin production in every experiment was confirmed by absorbance spectroscopy. After we obtained the optimal condition for paper-based melanoma cell culture, we further developed the device for melanoma invasion study as the second model.

In order to develop the impedance-based invasion assay device, we began with the primary study of cellular impedance characteristics of Mardin Darby Canine Kidney (MDCK) and MCF-7 breast cancer cells using the commercial electrode-containing cell cultureware. The cultureware contains gold interdigitated electrode, which provide the suitable conditions for optimizing parameters including potential and frequency in cell culture system. After obtaining the impedance information for MCF-7 cell culture, we further applied this model for xenoestrogenic screening as a parallel project. Xenoestrogen is the major group of the endocrine disrupting chemicals (EDCs), which is found to inhibit or activate the estrogenic effect *in vivo* based on their binding on estrogen receptor (ER) (32). The binding of xenoestrogen on ER causes adverse effects in various systems including, nervous (33), reproductive (34), and immunological system (35). Currently, there are plenty synthetic compounds that are found to contaminate in the environment, such as Bisphenol-A (BPA), Phatalate, Nonylphenol, and pesticides (36). BPA is one of the serious harmful substances, which have shown adverse effects not only in the reproductive system (37), but also other developmental systems (38, 39). Though FDA has announced that the low-dose exposure of FDA is not harmful (40), the application in plasticware and their environmental contamination should be aware. Since BPA was banned in

the plastic use, some plasticware was produced by using an alternative Bisphenol compounds such as Bisphenol-AF (BPAF) and Bisphenol-F (BPF) (41). However, the concern of the alternative Bisphenol should be raised due to their similarity of chemical structures to BPA. In a recent study, seven BPA analogues (BPAF, BPAP, BPB, BPE, BPF, BPS, and BPZ) show the agonist activities to both ERα and ERß (41, 42). Mesnage *et al.* have also demonstrated the estrogenic activity of six Bisphenol analogues (BPB, BPZ, BPA, BPF, BPAP, and BPS), which could increase cell proliferation of ER positive breast cancer cell line (43). Other than bisphenol, researchers have been concerned about estrogenic contamination in the sea water, due to the adverse effect on marine ecosystem and indirect effect on human from seafood consumption (44). One crucial example of seawater estrogenic contaminants is the antifouling agents, due to the direct exposure into the seawater when painted on boats (45). Irgarol 1051 are the well-known antifouling chemical that is toxic to marine animals (46). Other than the toxicity of Irgarol, its estrogenic effect has also been studied. In 2006, Noguerol *et al.* have determined the estrogenic effect of Irgarol 1051 with the recombinant yeast assay (RYA) (47). However, the Irgarol shows no response on ER of the recombinant yeast. In 2019, Park *et al.* have found the estrogenic effect of Irgarol by detecting Vitellogenin production, caused by estrogen exposure in Mud crab (48). Therefore, the xenoestrogenic effect of Irgarol is still varied depending on testing methods. The further study should be performed in various method including E-screen assay as well as the newly developed method with higher sensitivity.

To detect the estrogenic compounds in environmental contaminants, various methods have been developed including both *in vivo* and *in vitro*. Based on the estrogen exposure, Vitellogenin, the protein of egg yolk produced by fish, was used as a marker of estrogenic screening. Therefore, the level of increased Vitellogenin in fish can indicate the amount of estrogen, which was later developed as the antibody-based Vitellogenin assay (49-51). However, this assay is labor intensive and cannot be applied for large-scale screening (52). Based on the recognition of biomolecules, cell-based assay is widely used due to the availability to detect the toxic effects to living cells. In addition to minimize the assay, Yeast Estrogen Screening (YES) assay has been developed based on the expression of human estrogen receptor (hER) gene on *Saccharomyces cerevisiae,* and a combination with

a plasmid-containing lac-Z reporter gene (encoding ß-galactosidase enzyme). The binding of xenoestrogen results in the production of ß-galactosidase enzyme, which can change the substrate color (53-55). YES assay is scalable and easy to perform. However, the diffusion of secreting enzyme is slow due to the composition of yeast cell wall, results in time consuming (56). Moreover, the use of recombinant yeast cells showed the variation in receptor levels and protein proteolysis mechanisms, non-receptor cell-specific factors, and metabolic capabilities (57, 58). Therefore, the use of naturally ER-expressed cells can overcome these problems. MCF-7 (breast cancer) cell line is a suitable model for cell-based xenoestrogen study. The method was developed by Soto and colleagues, called E-screen assay. In brief, the binding of xenoestrogen on ER of MCF-7 caused the increased cell proliferation. The amount of increased cells was compared to the negative control and converted to proliferative effect of tested substances respectively (59). The E-screen assay relies on the human cells, which can properly reflect the *in vivo* response after xenoestrogen exposure better than the genetically modified cells. Moreover, the assay is simple to perform with the scalability. Nonetheless, it takes six days until the proliferative effect of the tested substance is evaluated. Besides, E-screen assay provides only the end-point readout (60). Therefore, the kinetic of cell proliferation during the xenoestrogen treatment cannot be studied.

Due to the fast estrogen detection and precise data acquisition, biosensors have shown a potential to accomplish the analytical requirements for xenoestrogen detection (61). Electrical impedance spectroscopy (EIS) was applied in various developed biosensors for xenoestrogenic detection. For instance, the work of Granek and Rishpon demonstrated the application of EIS on estrogen detection manifested as conformational changes in an ER-loaded lipid bilayer deposited on a gold electrode, causing the alteration of electrical components which can be detected by impedance measurements (62). However, the bioavailability and biological effect of a tested substance cannot be determined by this approach. Electrical Cell Substrate Impedance Sensing (ECIS), originally developed by Giaever and Keese (63), is widely used for studying cellular behavior. The detection is based on culture of cells adhering on electrodes at the bottom of a culture substrate. By applying an alternating sinusoidal potential across the two electrodes and measuring the generated in-phase and out-of-phase current, the impedance relating the potential

to the measured current can be determined (20, 64). The advantage of ECIS is that it is non-invasive and facilitates continuous real-time measurements on a cell population that functions as its own control. When cells adhere on the electrodes, the cell membrane acts as an insulator, impeding the current flow between the electrodes. This causes an increase in the determined impedance, which is proportional to the number of adhering cells (65), responding to their motion (66), and morphological changes (62). Furst *et al.* have demonstrated the use of EIS for cell-based detection of EDCs based on genetically modified ERα-expressing *Escherichia Coli* (67). The EDCs present in a sample can bind to both ERα expressed in *E. Coli* and monobody protein-coated electrode in a sandwich form. The binding of *E. coli* on the electrode increased the impedance, which correlates with the concentration of EDCs. This work has shown the advantages of using EIS for label-free EDC detection. However, the assay relies on genetically engineered bacteria, which behave differently than human cells, only allowing detection of the presence of EDCs instead of their biological effect.

In this parallel project, we developed the rapid impedance-based E-screen assay for real-time xenoestrogen screening, based on the kinetic monitoring of MCF-7 cell proliferation on the electrode. Xenoestrogenic effect was accessed by determining MCF-7 cell growth rate after acquiring impedance spectra. The developed assay was validated by detecting xenoestrogenic effect of BPA. Besides, Irgarol 1051 was firstly tested its xenoestrogenic effect by both conventional E-screen assay and our developed impedance-based E-screen assay.

Next, the optimal potential from the impedance-based E-screen assay was applied for the developed impedance-based melanoma invasion assay due to the feasibility for long term cell culture. In the second paper-based melanoma culture model, paper-based scaffold was applied as a membrane insert for invasion assay device. In order to overcome the high cost of commercially available membrane inserts and make real-time invasion assay more accessible, we developed a low-cost real-time invasion assay device using paper as an alternative membrane insert. The device was applied for the invasion study of B16 melanoma 4A5 cells under the treatment of Insulin-growth factor-1 (IGF-1). The ability of melanoma invasion was then real-time

tracked, based on their ability to break extracellular matrix (Matrigel coated on the paper) and penetrate into the pores of paper using EIS.

Due to the advancement of 3D cell culture in the *in vivo* mimicking microenvironment, papers have shown a promising possibility to be used as a scaffold for various cell models. In this thesis, we firstly applied the use of paper-based 3D cell culture for melanoma cell model. Author has divided the projects into 3 parts, based on the application of each study. The first part is the study of basic conditions required for melanoma culture on the paper and its application for melanin content screening. The second part is the initial characteristic study of cells, which was later developed as the impedance-based E-screen assay. Afterwards, the optimal impedance parameters were applied in the third project, which was the development of paper-based cell culture as a membrane insert for real-time invasion assay.

1.2 Research objectives

1.2.1 To develop paper-based scaffold for melanoma cell culture

1.2.2 To develop the paper-based cell culture devices for screening melanin content by naked eye and evaluate by a computer software

1.2.3 To demonstrate paper-based cell culture for anti-melanogenic screening by treatment with natural compounds

1.2.4 To primarily study the impedance characteristics of 2 cell types; MCF-7 and MDCK cell line in order to apply for melanoma invasion study

1.2.5 To apply the impedance characteristic study of MCF-7 cells for developing real-time xenoestrogenic screening in environmental contaminants (Irgarol 1051 and Bisphenol-A)

1.2.6 To develop the low cost and real-time invasion assay device by using paper as a membrane insert

1.2.7 To demonstrate paper-based cell culture for real-time invasion assay by using impedance measurement

1.2.8 To demonstrate the application of developed invasion assay device by studying melanoma invasion under the treatment of IGF-1

1.3 Research questions

1.3.1 Can a paper be used as a scaffold for 3D cell culture?

1.3.2 Can a paper-based melanoma cell culture improve the methods for accessing melanoma mechanism i.e. melanin production and its invasion?

1.3.3 Can a paper-based cell culture be a device for detecting the anti-melanogenic effect of natural compounds?

1.3.4 Can EIS be applied for the real-time estrogenic effect screening based on the principle of E-screen assay?

1.3.5 Can the developed invasion assay device improve the accessibility to perform real-time invasion study?

1.3.6 Can a paper-based cell culture serve as a membrane insert for real-time melanoma invasion assay by using impedance measurement?

1.4 Research hypotheses

1.4.1 Paper-based cell culture can be used for melanin quantification by using a computer software

1.4.2 Paper-based cell culture can be a device for detecting the effect of natural compounds on melanin production.

1.4.3 The impedance characteristic study of MDCK and MCF-7 cells be applied further for melanoma invasion study.

1.4.4 The optimal impedance parameters obtained from MDCK and MCF-7 cell culture can be further applied for xenoestrogenic screening, based on the binding of contaminants (Estrogen mimicking compounds) and estrogen receptor on MCF-7 cells, results in increased cell proliferation and impedance signal respectively.

1.4.5 Paper-based cell culture can be used as a membrane insert for real-time melanoma invasion assay by using impedance measurement

1.4.6 Melanoma invasive mechanisms under IGF-1 treatment can be studied by using paper membrane insert, integrated with the developed real-time invasion assay device.

1.5 Research utilization

  1.5.1 Paper-based melanoma cell culture can be used for screening melanin content and application for screening anti-melanogenic effect in 2 natural compounds including Kojic acid and Arbutin. This work was published in Analyst entitled "In situ paper-based 3D cell culture for rapid screening of the anti-melanogenic activity".

  1.5.2 Paper-based melanoma cell culture can be used as a membrane insert for melanoma invasion study using impedance measurement. Melanoma could be monitored in real time and label free manner and confirmed by confocal imaging. The result of the work has been submitted in Sensing and Bio-sensing research entitled "Impedimetric melanoma invasion assay device using a simple paper membrane and stencil-printed electrode on PMMA substrate".

  1.5.3 Optimized impedance parameters can be applied for MCF-7 cell culture and developed for E-screen assay. The assay was applied for real-time screening xenoestrogenic effects of 2 environmental contaminants including Irgarol and BPA. The result of this work is under the manuscript preparation for submitting in the international journal.

1.6 Conceptual framework

Lack of cell-cell contact and poor *in vivo* mimicking of 2D cell culture

3D cell culture

The need of developed scaffold for 3D cell culture due to the cost of scaffold production, complication of use, unstable 3D spheroid formation

Lack of the report on paper-based melanoma cell culture application

Development of paper-based 3D cell culture devices for melanoma cells

Paper-based 3D cell culture device for anti-melanogenic screening

Paper-based cell culture as a membrane insert for invasion assay using impedance measurement

Primary study of the cell-based impedance measurement using MDCK and MCF-7 cells

Optimization of applied potential and frequency for the impedance-based cell culture

Conventional melanin content analysis is
- time consuming
- require multiple steps
- high solution consumption
- based on 2D cell culture: cells behave poorly different from *in vivo*

− melanin

+ melanin

Counter electrode

Paper–Working electrode

Melanoma cells

Chemo-attractant

Device and electrode fabrication of real-time invasion assay for paper integration

Application of real-time invasion monitoring of melanoma under IGF-1 treatment

Optimization of culture conditions of melanoma cells in paper-based device

Confirmation of melanin color on the paper

Confirmation of 3D formation of melanoma cell inside paper

Application of paper-based melanoma culture devices for anti-melanogenic screening of Kojic acid and Arbutin

Rapid and easy screening anti-melanogenic effect of natural compounds

More reliable result due to the better cell behavior in 3D cell culture system

Faster detection of cell invasion through the paper membrane

Cell invasion was less likely influenced by cell proliferation

Application for real-time xenoestrogen screening

The conventional E-screen assay is
- time consuming
- End point readout
- Require cell labelling

Impedance signal / Incubation time (xenoestrogen)

Optimization of cell seeding number of MCF-7 cells

The application of estrogenic effect screening of 10beta-Estradiol and co-treatment with its antagonist

Real-time estrogenic effect screening of Bisphenol-A and Irgarol 1051

Faster and easy method of estrogen and xenoestrogen screening

CHAPTER II Literature review

2.1 3D cell culture

Recently, the *in vitro* 3D culture becomes an important model for studying cell change. Cells in the 3D culture environment can develop morphology and physiology similar to that of analogous cell types *in vivo.* Moreover, the extracellular matrix that surrounds cells can influence the distribution of cell-cell and cell-matrix contacts on the surface of the cells which affects the cell polarity and cell signaling (68). Therefore, 3D cell culture can reflect the *in vivo* condition better than the rigid 2D culture (Table 1). Currently, to cultivate cells in 3D structure, there are 4 main methods including suspension, hydrogel, scaffold, and paper-based 3D cell culture. We here describe each method below.

Table 1 A summary of differences between 2D and 3D cell culture

Properties	2D cell culture	3D cell culture
Ease of establishment	Easier	More complicated
Cost	Cheaper	More expensive
Interaction between cells	Worse	Better
In vivo imitation	Could not replace the animal use due to the lack of tumor formation	Alternative method for the animal model due to the 3D organ formation
Formation time	A few hours	A few hours to a few days
Culture quality	High performance, reproducibility, long-term culture, easy to interpret	Worse performance and reproducibility, difficult to interpret because of an unstable spheroid formation
Characteristic of cells	Loss of diverse in phenotype and polarity	Preserved morphology and way of divisions

Table 1 A summary of differences between 2D and 3D cell culture (continue)

Properties	2D cell culture	3D cell culture
Molecular mechanisms	Change in gene expression, topology, and biochemistry of cells	Gene expression, topology, and biochemistry of cells are more similar to *in vivo*.

2.1.1 Methods of 3D cell culture

2.1.1.1 Suspension

The simplest method for 3D cell culture was developed during 1800's. The 3D formation based on the agitation of large amount of cells in the non-treated culture flask. The 3D cell formation was used for protein expression study for therapeutics as well as bio-reactor applications (69-71). Afterwards, the suspension technique has been developed to a so-called hanging drop cell culture (figure 1B). Cell suspension was placed in the culture well that has a semicircle shape which facilitates spherical-shaped formation (72). However, the hanging drop technique is time consuming, low throughput, and requires many pipetting steps (73).
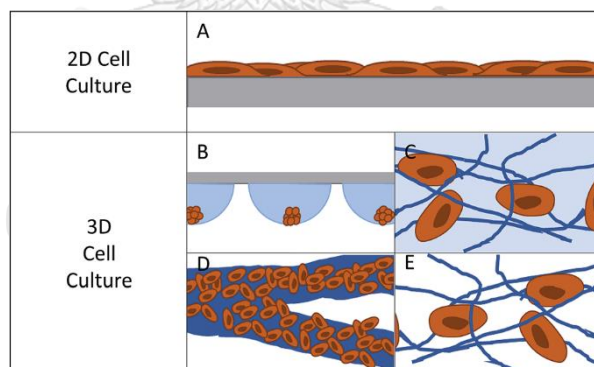
Figure 1 Schematic illustration of the comparison between A) 2D, B) Hanging drop, C) Hydrogel-based, D) Paper-based, and E) Fiber-based 3D cell culture.

(This picture was taken from ref 73.)

Wu *et al*. have combined hanging drop technique with microfluidic device (Figure 2). The microfluidic device was made of PDMS. Afterwards, the device was connected to the reservoir for medium flow in the system. In this work, researchers have

developed the high throughput 3D cell culture device which can reduce the pipetting steps. (74)
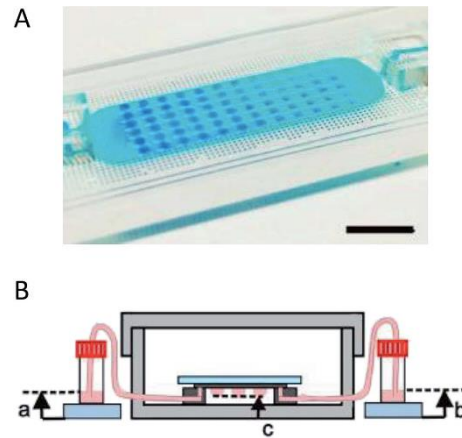
Figure 2 Schematic representation of A) microfluidic hanging drop 3D cell culture device and B) the side viewed illustration when the device was combined with culture medium reservoir.

(This picture was taken from ref 74.)

The hanging drop microfluidic device was further developed by Frey *et al*. by integrating the valve and mixing channels with the device (Figure 3). The device allows users to select cell loading in each column via the cell loading ports. In this work, researchers represented the reproducibility of spheroid formation for more than 10 days. This method could reduce the pipetting steps and labor intension (75).
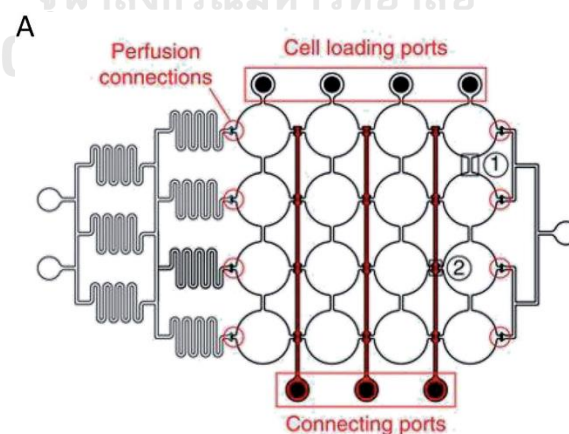
Figure 3 Schematic illustration of the PDMS based hanging drop microfluidic device with the integration of valves and mixing channels.

The device was able to select cell loading channels.

(This picture was taken from ref 75.)

2.1.1.2 Hydrogel

In order to mimic *in vivo* cell proliferation, the use of synthetic extracellular matrix (ECM) has emerged as a solution (76, 77). Hydrogel serves as one of the ECM, researchers are using nowadays. Hydrogel composes of the polymers that contain pores, allowing cellular movement (Figure 1C). The hydrogel pores provide the scaffold for supporting cells in 3D structure.

There are 2 main types of hydrogel. The first one is the synthetic ECM such as polyacrylamide, polyethylene glycol, and polyacrylic acid. The second is the natural polymers such as collagen, fibrin, and hyaluronic acid. The properties of hydrogel should be considered before using in the specific conditions, for instance, porosity, stiffness, and matrix degradation. Even though there are many choices of commercial hydrogel, there are still the variation from batch-to-batch (76, 78).

To select the hydrogel for 3D cell culture, there are many types and properties that users should consider including:

Collagen is typically extracted from rat tail or bovine skin and tendon. Collagen could exhibit structural and mechanical properties reminiscent of native tissues. The use of collagen provides the possibility for future implantation due to the availability of an enzymatic degradation, using collagenase (76). Beebe's group has utilized hydrogel in the microfluidic device using passive pumping arrays (79-81). The passive pumping is responsible for solution feeding, based on the pressure in the microfluidic device. This work used collagen gel for human breast cancer cell culture with the co-culture condition with fibroblasts (82). Beebe's group has demonstrated the advantages of collagen gel which can provide high cell viability with a high throughput manner.

Fibrin is separated from human plasma. Fibrin is normally used in *in vitro* wound healing study, including angiogenesis (83) and platelet mechano-sensing (84). It is degradable by fibrinolytic enzyme. However, fibrin has low mechanics which limit the utilization (76).

Alginate is derived from brown algae. Users normally modified alginate with adhesive ligand to increase cellular binding. However, due to their weak bonding, the additional covalent crosslinking is needed (76).

Polyacrylamide (PA) is a synthetic polymer that could provide wide range of mechanics. PA is the base of most commercial hydrogel nowadays. Though, PA can only be used for 2D cell culture because of the toxicity of the hydrogel precursors (76). Hence, PA should be crosslinked before cell seeding, make it unable to be used for cell encapsulation before adding precursors.

Polyethylene glycol (PEG) is known as a blank state hydrogel because it can be modified for various types of culture and applications (76). The PEG crosslinkers are available in either nondegradable or MMP-degradable forms. To form hydrogel, users just simply mix all precursors and their crosslinkers together. Due to the cytocompatibility, users can add cells in the same step as the components mixing step (85).

Prior to cell mixing, hydrogel needed to be sterilized due to the cell culture protocol. Most of the cell culture grade hydrogels are already sterilized. However, when users have modified the base hydrogel, the further sterilization is needed. Hydrogels can be sterilized by various methods including gamma or germicidal UV irradiation, ethylene oxide exposure, ethanol treatment of already formed hydrogels, or dense carbon dioxide gas sterilization (86). The precursors for gel formation can be sterilized by using UV radiation or filter. Nonetheless, the use of radiation should be careful due to the breakage of polymers. For example, UV treatment can denature collagen and promote peptide degradation within functionalized hydrogels (87). Also, gamma radiation can degrade alginate (88).

2.1.1.3 Paper-based cell culture

Papers are made of a bundle of cellulose microfibers and also contain micro fibrous pores, which are suitable for constructing the 3D scaffold (89). In particular, a paper is biocompatible and can be easily established with the extremely low costs. In this regard, paper would be an interesting scaffold for 3D cell culture. Therefore, we here describe the process of paper fabrication, modification, as well as their applications in 3D cell culture.

2.1.1.3.1 Paper fabrication

To limit the zone for cell seeding, there are 2 methods used for paper fabrication. The first method is wax printing technique. In brief, the paper is designed to have cell culture zone in the desired shape by using the available software such as Adobe Illustrator, AutoCAD, or Adobe Photoshop. A paper is then printed the design on top by using wax printer. The wax was then melted through the thickness of a paper by using hot plate. The temperature and time for wax melting are needed to be optimized according to the paper types and printed pattern (90). The wax pattern is then become hydrophobic wall which surround the hydrophilic zone as known as cell culture zone (Figure 4) (91, 92). The second method is hot embossing. Instead of using a wax for the hydrophobic zone, plastic can also be used for the cell culture zone limitation. Similar to wax printing, a plastic, e.g. polyvinyl carbonate, is placed between 2 pieces of paper. The paper/plastic sandwich is then placed in hot embossing machine. The hot plates are pressed upon the paper/plastic sandwich. Plastic is then melted through a paper and become a hydrophobic wall (93).
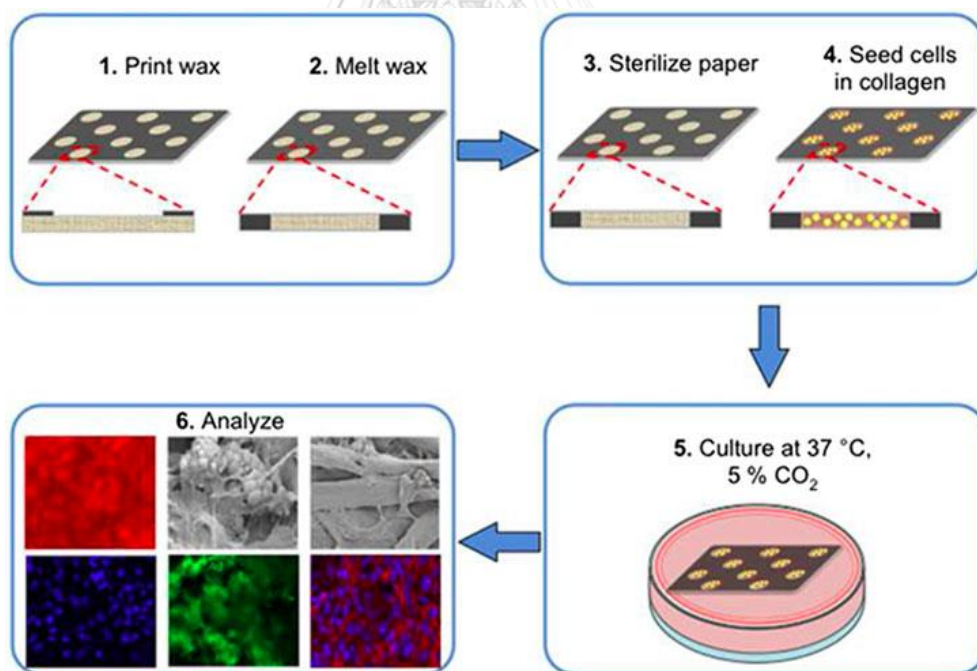
Figure 4 Wax printing technique used for filter paper patterning.

Osteoblast cells were seeded on the wells of the paper scaffolds in a collagen matrix. After culturing the samples for 21 days, SEM, colorimetric assays, and immunostaining were performed to evaluate the deposition of minerals in the paper scaffolds.

(This picture was taken from ref 93.)

2.1.1.3.2 Paper modification

Modification of chemical properties of paper for cell culture

Some applications of paper-based cell culture require a high specificity of the test. Thus, the correct amount and type of cells on the paper is important One method that is used to increase the cellular attachment on the paper is the chemical modification (Figure 5). The chemical modification on the paper should provide the increase cell adhesion, proliferation, and cell viability on the paper (94, 95). For example, Chen *et al.* have conjugated the paper with small molecules including nucleotides and peptides (96).

Initiator chemical vapor deposition (iCVD) is a method for flowing the initiater and monomer together in the vacuum. An initiator breaks down into radicals, beginning a free-radical polymerization of the monomer at the substrate surface in a vapor free atmosphere. This method allows thin film forming on many kinds of polymers (97). Park *et al.* have used iCVD to deposit glycidyl methacrylate polymer (pGMA) on perfluorodecyl acrylate polymer (pPFDA)-on a paper. pGMA and pPFDA have shown to increase cell adhesion on a paper (89).

Corona discharge surface treatment or air plasma is a method used for surface modification at a low temperature. The corona plasma is generated by the application of high voltage to an electrode and form the plasma at the tip of electrode. The polymers that pass the plasma will change the surface energy. This method can induce the bond sites by increasing the surface energy without losing the positive properties of materials (98). For instance, Janus paper was treated with corona discharge which leads to the increase of wettability. Thus, Janus paper has a better flow in the microchannel platform. Cells, that were culturing on Janus paper, were found to have an increase cell viability (99).

The printing method was also used for printing chemicals to increase cellular adhesion on the paper. For instance, the extracellular and adhesion proteins, including vitronectin and fibronectin, were printed onto the paper (100-103). Plasmonic gold nanorod was also used for paper coating. Gold nanorod coating has increased the smoothness of paper surface. The Plasmonic gold nanorod-coated

paper can promote cell growth of human arising retinal pigment epithelia cells (ARPE-19) because of its ability to smoothen the surface of paper (24, 25).
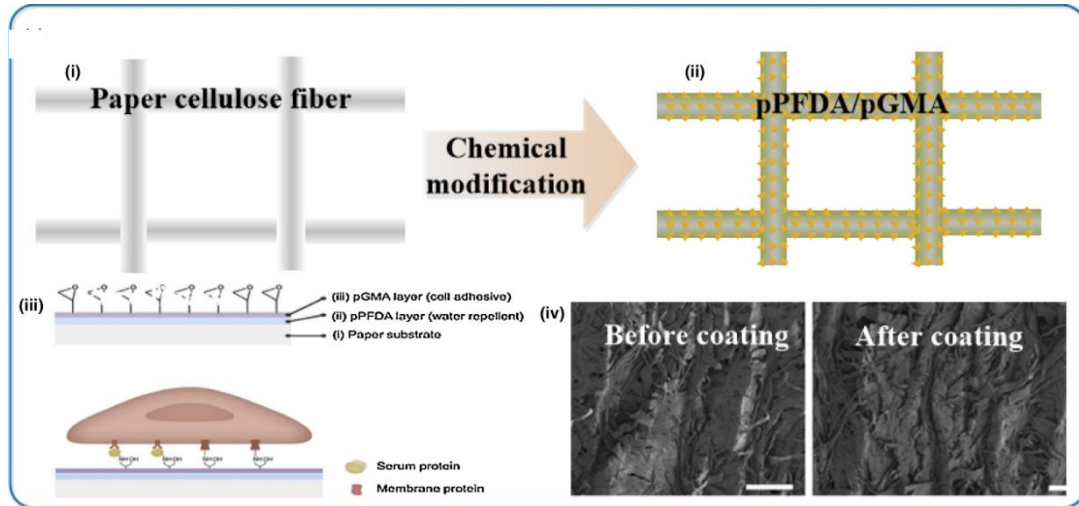
Figure 5 Chemical modification through iCVD coating on the paper of various components on paper scaffold for the enhanced cell attachment.

(This picture was taken from ref 282.)

Modification of physical properties of paper for cell culture

Physical properties of paper consist of many factors including topography, stiffness, roughness, and water permeability. The smoothness of paper surface also has the effect on a better growth, spreading, and attachment of epithelial cells (95, 104-106). Cellular behavior, including stem cell proliferation, adhesion, locomotion, spreading, morphology, striation, and even differentiation has reported to be influenced by the paper (107). Creating hydrophobic and hydrophilic zone allows researchers to area for cell culture by printing or coating a paper with hydrophobic materials. For instance, PDMS was printed on a paper to create 96 cell culture zone similar to the 96-well plate. PDMS could prevent the lateral flow of aqueous medium and cell growth across each zone (24, 26, 108). Other than PDMS, wax and Teflon have also been used to create cell culture zone on a paper (Figure 6) (109-111).
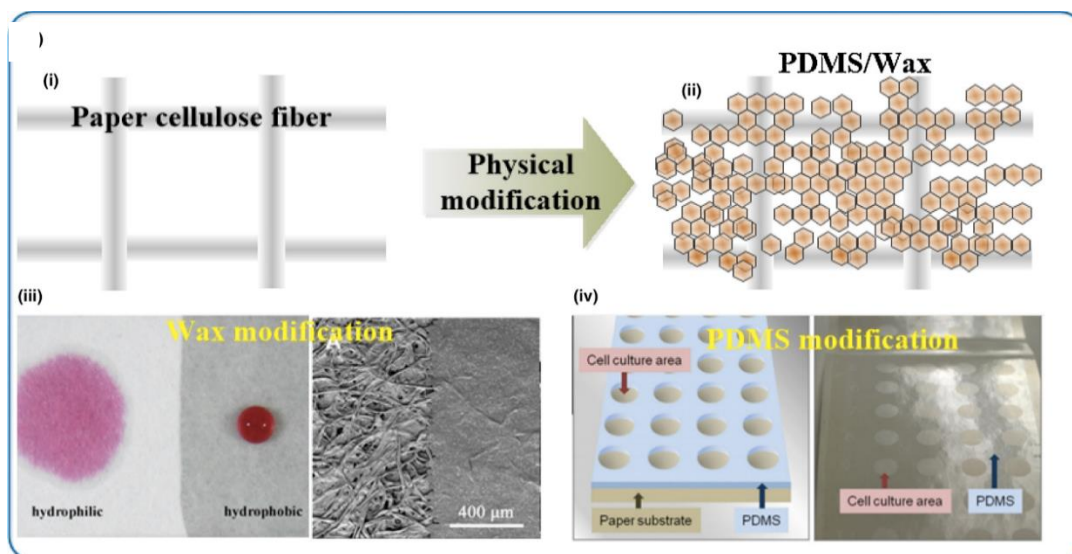
Figure 6 Physical modification of paper using wax and polydimethylsiloxane (PDMS) to modify the hydrophobicity and hydrophilicity of the paper surface.

(This picture was taken from ref 282.)

2.1.1.3.3 Advantages and drawbacks of paper-based cell culture

According to the low cost of papers, researchers have been focusing on the modification of papers for many applications. Other than the price, paper has a wide availability and accessibility due to the regular use in most laboratories. The most famous choice of paper for cell culture is Whatman filter paper, because of its various pore sizes, filter rates as well as their grades. Unlike hydrogels, ceramics, metal, or polymers, papers are easily fabricated by just print and cut (112-116). Their mechanical properties are also various depending on the available grades. Papers are also available in many pore sizes, which researchers can choose according to the cell size or the experimental purpose (117). In order to culture cells, the scaffold needs to be sterilized before cell seeding step. Even though most of the available polymers have various chemical choices for material sterilization, the chemical reactions between the chemical used for sterilization and polymers are concerned. On the other hand, papers are easily sterilized by using UV radiation. By using the UV, papers can remain their integrity better than soaking in the available sterilized solution e.g. 70% ethanol.

Other than the advantages mentioned above, papers also have some drawbacks in order to culture cells. However, their drawbacks have come with the available solutions. We here list their drawbacks and solutions in table 2.

Table 2 The drawbacks and solutions for the use of paper as a scaffold for cell culture

Drawback	Solution
Difficult to acquire fluorescent images	Use two-photon microscope
Mechanical properties decrease upon wetting	Stack papers
Changes of chemical structure due to the chemical sterilization	Choose other choices for sterilization e.g. UV, autoclave, ethanol immersion
Some types are hard to degrade (not suitable for *in vivo* implantation)	Use an enzymatic approach such as cellulase
Inability to quantify small molecules because of its opaque fibers	Develop a new analytical method in a paper scaffold

Paper-based cell culture for cancer research

Cancer, the deadliest disease nowadays, is influenced by multiple factors. To develop the therapeutic agents, understanding the cancer invasion mechanism is important. The crucial mechanism that leads to the malignant stage is metastasis. Cancer metastasis begins with the step of cell adhesion, extracellular matrix *(ECM)* proteolysis, and migration respectively *(118)*. Once cancer cells invade through the ECM and migrate to various organs in the body, it can lead to a poor prognosis in patients. Thus, researchers have been focusing on the metastatic step to develop the treatment and understand the mechanism of cancer invasion. To date, the transwell assay is the most conventional method used to assess the invasion activity of cells. However, transwell assay can only be used for end-point measurement. Besides, cells are formed in 2D monolayer which could not well reflect the *in vivo* condition. The gradient of oxygen and other small molecules is also the key to study cancer invasion. In order to study cancer invasion under the gradient of substances of

interest, transwell assay could not overcome this problem. Paper has been used as a scaffold for 3D invasion assay in various experimental design. For instance, paper was used as a scaffold for 3D breast cancer cell line in the invasion study. Cell-containing paper was placed in the gradient generator device. The device can create the gradient of oxygen in a horizontal direction (Figure 7). Thus, the invasion of cells under gradient of oxygen were tracked in real time using fluorescent microscope (68).
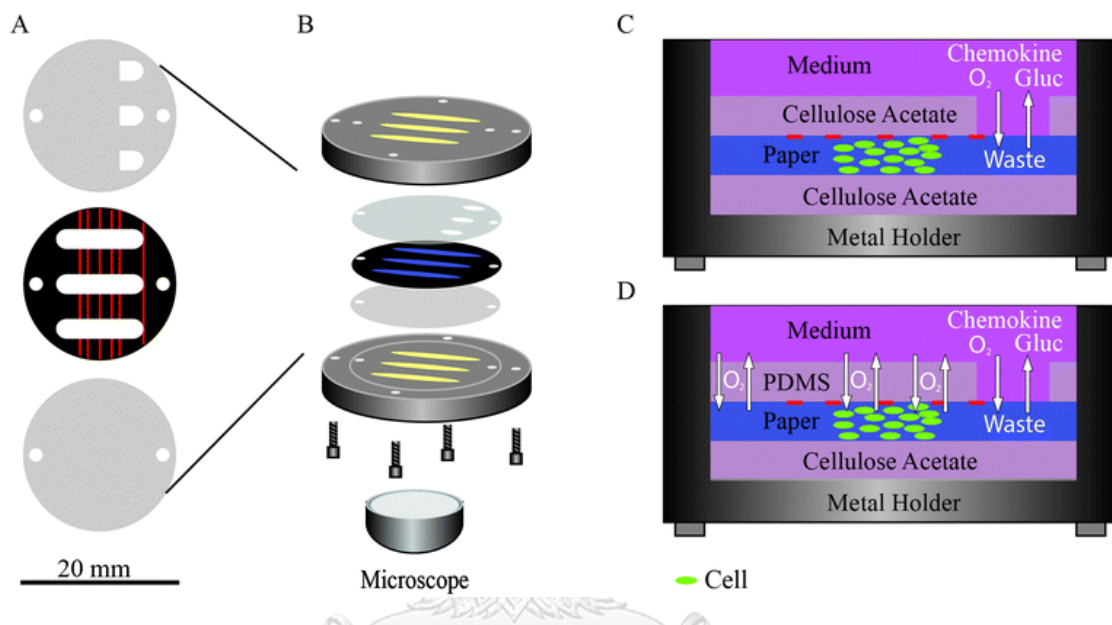
Figure 7 Schematic of a paper-based scaffold, patterned to contain three channels in which we cultured cells for the invasion assays under gradient of oxygen.
(This picture was taken from ref 68.)

Another cancer invasion study under the gradient of oxygen was also performed in a vertical direction. Whitesides group has utilized a gradient generator for paper-based containing device to create a gradient of oxygen in a vertical direction. Multi layers of paper were stacked up. A cell-containing paper was placed in a middle of the stack. After the incubation period, paper were destacked and performed LIVE/DEAD staining to measure the distance of invasive cells in each paper layer (Figure 8) (30). In this study, researchers found that oxygen acts as a chemoattractant to cancer cells. Cells tended to move toward high concentration of oxygen than the hypoxic side. In the same experimental design as Mosadegh *et al.*, the oxygen consumption of cells were studied under the gradient of oxygen by using a luminescent thin film (119). Other than the oxygen supply, researchers have also found the effects of fibroblast releasing factors on cancer cell invasion. By co-culturing fibroblast and human lung

cancer cells in paper stack device, the releasing factors from fibroblast could induce the invasion of VXN2 cells towards the fibroblast at the bottom of the device (93). The cellular invasion study was able to perform in a high throughput format due to the ease of patterning paper (108). Derda *et al.* developed a 96-well pattern on a paper for cell culture by using Teflon as a support material. Paper in Teflon support was found to increase prptide systhesis and cell attachment on a paper (25).
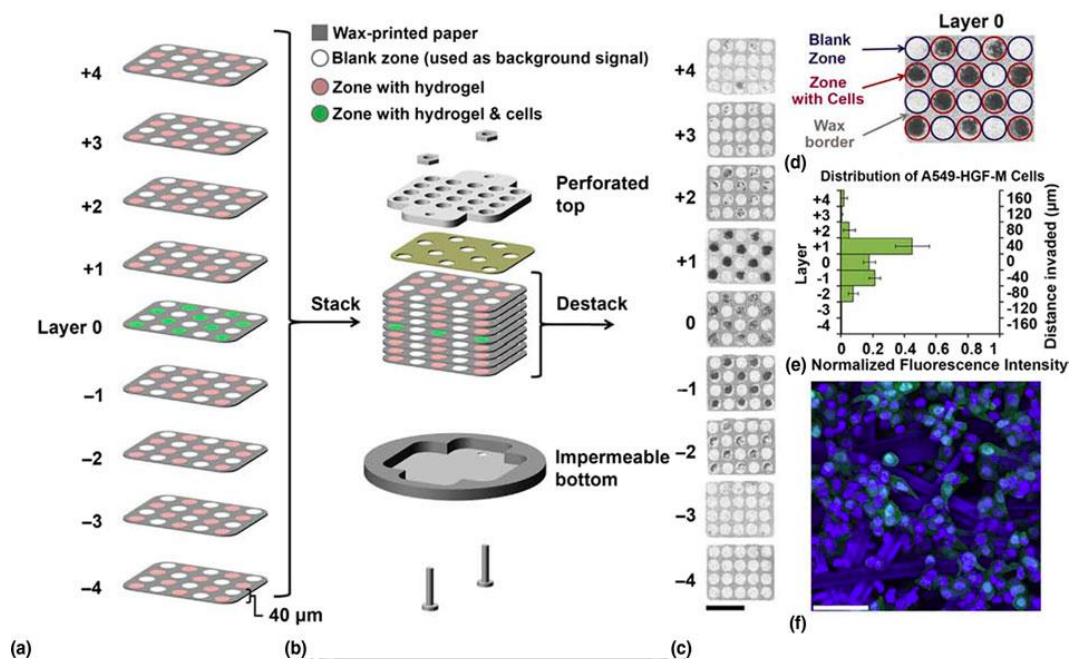
Figure 8 Schematic representation of paper scaffolds for the cancer invasion assay under the gradient of oxygen

(a) Multi-layered, wax-printed paper scaffolds. In layer 0, cells encapsuted in hydrogel were seeded in cell culture zone (white color). Only hydrogel was added to the paper in layers 1–4. (b) All the layers were assembled in the device (c) After culturing for 24 h, invasive cells in each layer were characterized by fluorescence scanner. The dark zones represent the cells, which were stained using a fluorescent reagent. (d) The cell culture area in layer 0. (e) The distance invaded by cells. (f) Fluorescent cells in layer 0 imaged by a confocal microscope.

(This picture was taken from ref 30.)

For cancer treatment, doxorubicin (dox) has a well ability to kill cancer cells. In many cancer apoptosis assays, dox was chosen as a positive control. Though when treating tumor with dox, the well-known drug penetrated to the tumor in a gradient manner.

To study the ability of dox on cancer apoptosis, the gradient of dox was generated into the gradient concentration by using the paper-based cell culture. Paper was designed to have Christmas-tree shape (Figure 9). Paper was assembled in the microfluidic device which contains cell seeding and drug adding inlets. Hela cells were cultured at the bottom of paper-based gradient generator before adding dox in the inlets (120). Using paper to create a gradient of drug concentration could reduce the drug consumption due to the stable flow on a paper (92). The radiation is nowadays used for cancer treatment. Simon *et al*. have utilized a paper-based 3D cell culture for studying the metabolic response of lung cancer cells to the exposure of ionizing radiation. This platform facilitates the regulation of oxygen to cells in 3D structure (92, 121).
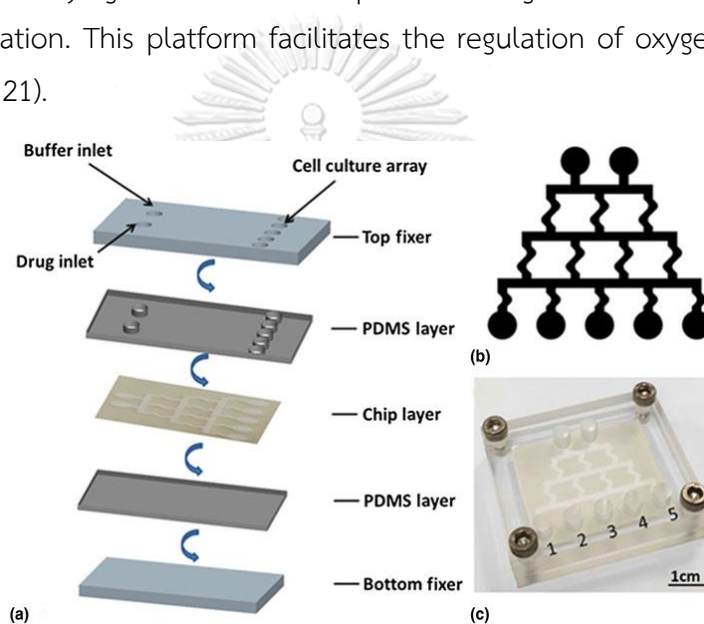
Figure 9 A Christmas tree paper-based microfluidic device for generating gradient of drug concentrations.

(This picture was taken from ref 120.)

Paper-based cell culture for cardiovascular disease

Calcific aortic valve disease (CAVD) is a hardening disease, happens when calcium deposit to the aortic valve. Aortic valvular interstitial cells (VICs) are crucial for the production and turnover of leaflet extracellular matrix (ECM) (122, 123). Thus, VICs have been interested by many researchers on the development protocols for study their ECM turnover mechanism. In order to replicate the *in vivo* conditions, researchers have focused on 3D re-model of VIC. Paper-based 3D cell culture was

applied for the VICs culture. VICs were cultured in multi layers of paper to mimic different aortic valve leaflet thicknesses to monitor cell migration (124).

By stacking the paper, Mosadegh *et al*. have also used this model for cardiac ischemia study. Primary rat cardiomyocytes were co-cultured with cardiac fibroblasts. This work has demonstrated the migration of fibroblast towards the ischemic region in the paper stack (26).

Induced pluripotent stem cells (iPSC) have shown many great properties over stem cells, in order to use in the regenerative medicine (125). To differentiate iPSC into cardiomyocytes, paper was used as a scaffold for cell culture. Paper was coated with Matrigel prior to cell seeding step. In this work, researchers showed the successful differentiation protocol of iPSC into beating cardiomyocytes on the paper (Figure 10) (126).
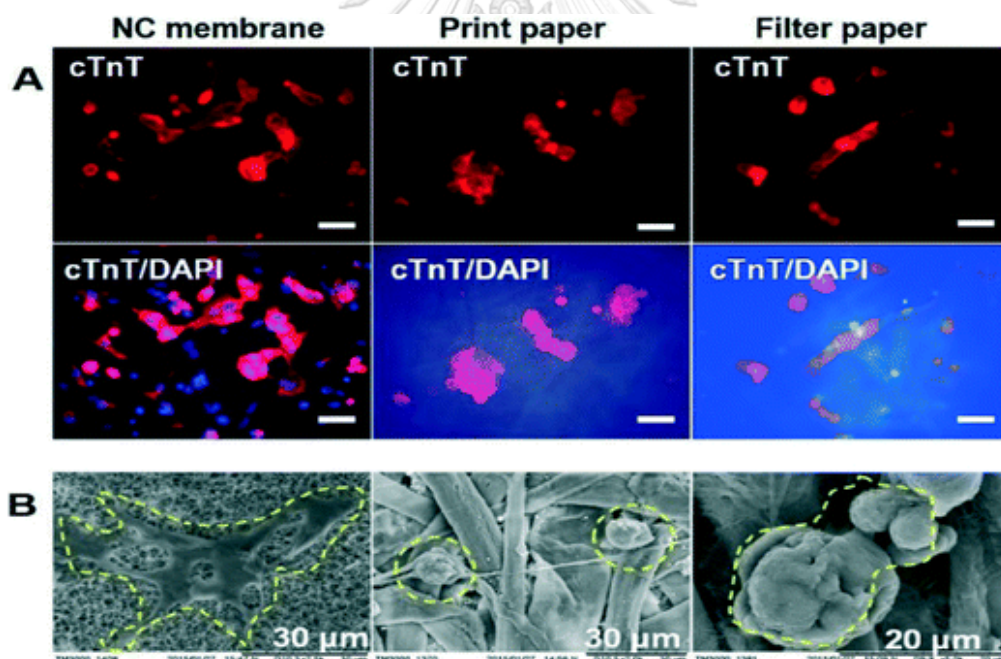
Figure 10 Cardiomyocytes derived from human iPSCs on paper.

A: identification of cardiomyocytes on three kinds of paper substrate with cTnT antibody; bottom images: cTnT staining merged with DAPI staining. B: SEM images of cardiomyocytes on different paper substrates. The regions surrounded by a yellow dotted line indicate the cardiomyocytes.

(This picture was taken from ref 126.)

Paper-based for bone research

In order to repair the bone damage, tissue engineering is typically used with the integration of existing scaffolds, cells, growth factors (127). The scaffold used for bone engineering should provide proper porosity, stiffness, swelling, degradation, and biological activity, for guiding bone formation (92). Paper has demonstrated as an alternative scaffold for tissue engineering due to their biocompatibility, ease of fabrication, right geometrical structures.

In order to generate the bone for tissue regeneration, researchers have used stem cells and iPSC as a tissue substrate. Park *et al*. have demonstrated the application of paper as a scaffold for bone regeneration (89). By using the human adipose-derived stem cells, bone lineage was generated directly on a paper construct before implanted into mouse model. This work has shown the ability of paper to generate bone for tissue engineering as well as *in vivo* implantation (Figure 11).
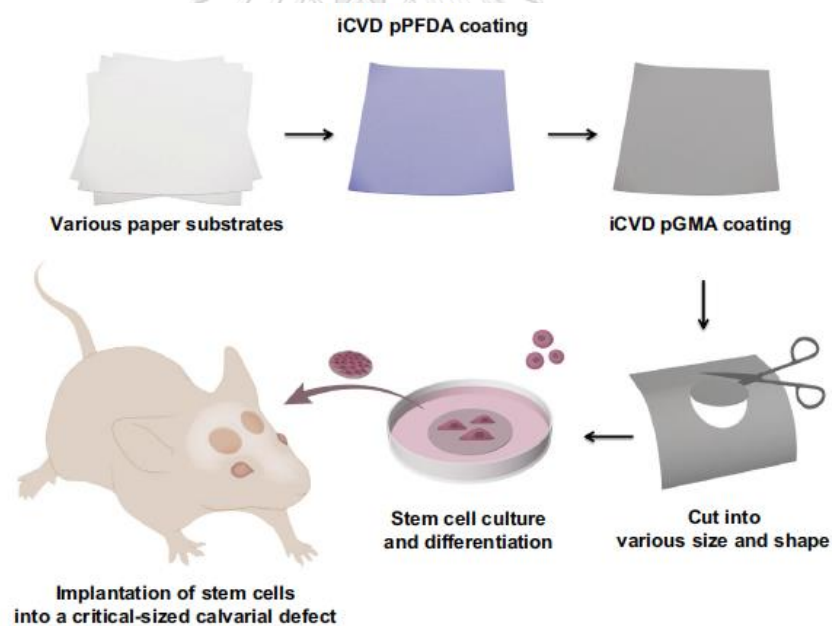
Figure 11 Schematic illustration of paper-based scaffold for bone engineering. The paper was modified for human adipose-derived stem cells culture. After stem cell differentiation, paper-based bone tissue was implanted in a mouse model with calvarial bone defect.

(This picture was taken from ref 89.)

Other than the single piece of paper, an origami-inspired paper construct was applied for bone tissue engineering by Camci-Unal *et al.* (91). The paper construct was embloyed for guiding the mineralization process of mouse osteoblasts. In this work, researchers observed the calcium phosphate deposition on the bone tissue within a paper construct (Figure 12). Together with Park *et al.*'s work (89), paper could be suitable material for the future bone tissue engineering and implantation.

Cell cultures in folded paper scaffolds
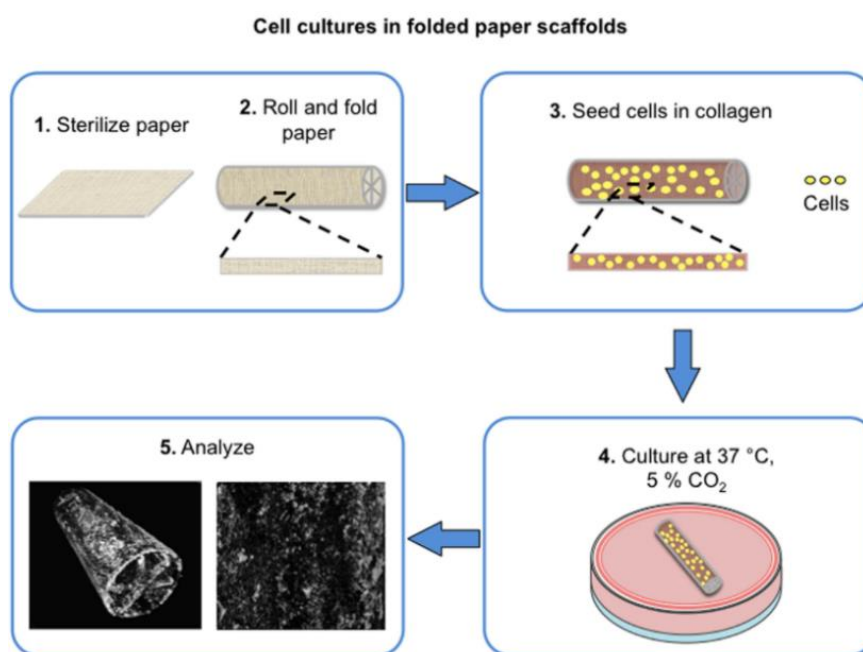
Figure 12 Schematic representation of the origami-inspired paper construct for bone tissue engineering. The micro-CT analysis, after mouse osteoblast culture on a paper, demonstrated the deposition of minerals in the origami-inspired paper constructs.

(This picture was taken from ref 91.)

According to the paper properties, many researchers have applied paper for cell study including cancer, cardiovascular, and bone tissue engineering applications. In order to ease readers to choose the proper paper types for future works, we here summarize types, properties, advantages, and applications have papers that have been used in the 3D cell culture research in table 3.

Table 3 Paper types and their characteristics in biomedical applications

Paper type	Whatman filter paper #114	Weighing paper	Nitrocellulose membrane	Janus paper
Thickness /(µm) (128)	190	200	130-160	200
Pore size /(µm) (128)	25	-	10	-
Mechanical strength (128)	2.8 MPa	150-650 kPa	1.8-2.6 MPa	392 kPa
Applications	Drug screening	Disease model	Tissue modeling	Disease model
Advantages	Optimal pore size for diffusion	Stimulate osteogenic differentiation	Uniformity of pore size, easy to stack, mechanical robustness	High biocompatibility
Ref.	(24-26, 30, 117, 124, 129)	(89, 130)	(131)	(99)

Table 3 (continue). Paper types and their characteristics in biomedical applications

Paper type	Kimwipes Kimberly Clark 34155	Printing paper	Whatman No.1	Whatman no.4
Thickness /(µm) (128)	100-160	100-200	180	205
Pore size /(µm) (128)	-	-	11	20-25
Mechanical strength	-	-	-	-
Applications	Cryopreservation	Culturing and differentiating stem cells	Screening melanin production, Hydrogen peroxide sensing	Cell proliferation
Advantages	Mechanical robustness	Facilitate myogenic differentiation	Suitable pore size for melanoma cells, easy to observe melanin color	Possible for EIS sensing
Ref.	(29)	(126)	(111, 129)	(31)

2.2 Electrochemical paper-based 3D cell culture devices

Electrochemical analysis has been coupled with cellular study due to low cost, point-of-care testing, and miniaturization capacity (132). The electrochemical biosensors are based on 3 measurements including potentiometry, Amperometry, and Electrochemical impedance spectroscopy (EIS). The potentiometry is the measurement of changed potential, based on the ion selective electrode. However, potentiometry is less sensitive to the big analytes e.g. cells when compared to amperometry and EIS. Currently, amperometry is often used in paper-based 3D cell culture. The technique is used for measuring the current generated by the redox of species produced in response to analyte-bioreceptor interaction (133). The EIS has been widely used in cell study according to Giaever and Keese study. Recently, the combination of EIS and paper-based cell culture system has been applied for only one application so far. The assay was developed for monitoring cell proliferation. The detail can be found in the section of Impedance-based cellular study below. Besides, EIS has been the fundamental technique that was used in most of paper-based 3D cell culture device for electrode characterization. The following paragraphs describe in detail about how the mentioned electrochemical measurements have been applied in paper-based cell culture system.

2.2.1 Electrode and paper modification for electrochemical paper-based cell culture analysis

To improve the conductivity for electrochemical response from cells, researchers have modified the electrode directly before combining with paper-based cell culture device. Besides, the paper itself has also been developed as an electrode sensor for *in situ* cell analysis. The detail of both modifications is described below.

Commercial screen-printed electrode modification

The commercial screen-printed electrode (SPE) was widely chosen by electrochemist due to its ease of use and high reproducibility. To couple with paper-based 3D cell culture, paper was directly attached to the SPE. In order to increase the conductivity and current response, Liu *et al.* have modified SPE with gold nanoparticles (Au NPs) and nafion for detecting released dopamine from PC12 cell line (134). Nafion is a synthetic polymer which can act as proton conductor. Thus, the modification of electrode surface with nafion could definitely increase the conductivity. Besides, Au

NPs has shown the ability to increase the electrochemical signal after the modification with SPE (135). The Au NPs-nafion modified SPE showed the characteristic reductive peak of gold at the potential of 0.5 V and oxidation peak at 1.0 V while the bare SPCE could not show the redox peak (figure 13). Besides, Liu *et al.* suggested that the modification with nafion could be beneficial for superfluous absorption and enhance the selectivity through the electrostatic repulsion (134).
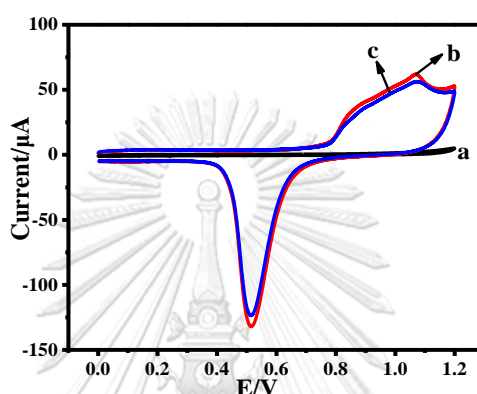
Figure 13 Cyclic voltammograms of stepwise modified SPCE in 0.5 mol/L H_2SO_4 solution. (a) bare SPCE; (b) Au NPs/SPCE; (c) nafion/Au NPs/SPCE.

(This picture was taken from ref 135.)

The carbon paper electrode (CPE) modification

Instead of culturing cells directly on conductive carbon paper electrode (CPE), Shi *et al.* have demonstrated the use of carbon paper as the working electrode (WE). By connecting cell culture zone on a paper with a carbon paper using silver paste, the electrochemical response could then be tracked. In order to improve the conductivity of carbon paper electrode, the hydrogel was fabricated from the mixture of carbon nanotube (CNT), graphene oxide (GO), and MnO_2 (figure 14). To functionalize the CPE, CNT/graphene/MnO_2 aerogel was deposited on CPE before casting with nafion. The functionalized was then attached to the paper-based 3D cell culture. The CNT/graphene/MnO_2 aerogel was found to increase the electrochemically active surface area and low charge transfer resistance, when characterized with EIS Nyquist plot (136).
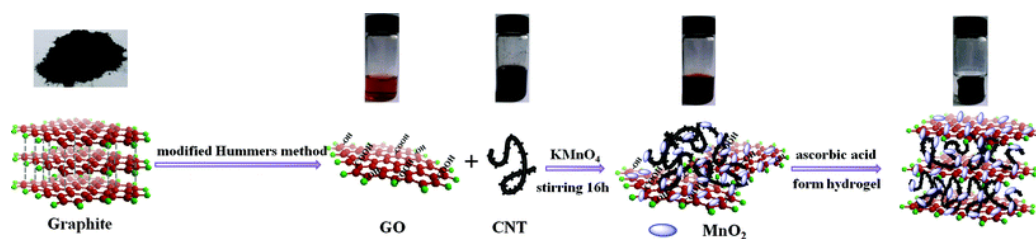
Figure 14 Schematic illustration of the fabrication of CNT/graphene/MnO₂ hydrogel. GO: graphene oxide, CNT: carbon nanotube, MnO₂: manganese dioxide.

(This picture was taken from ref 136.)

Paper as the electrode sensors

Instead of relying on the commercial SPE, paper itself could be used as an electrode sensor by screen printing. Jiang and Yu group have used the same concept for the paper modification as an electrode by screen printing technique. One paper was modified as RE and CE by screen printing Ag/AgCl as RE and carbon as CE. Another paper was modified as WE by screen printing carbon (Figure 15). Afterwards, the RE/CE and WE paper were attached together and directly used for cell culture (137, 138).
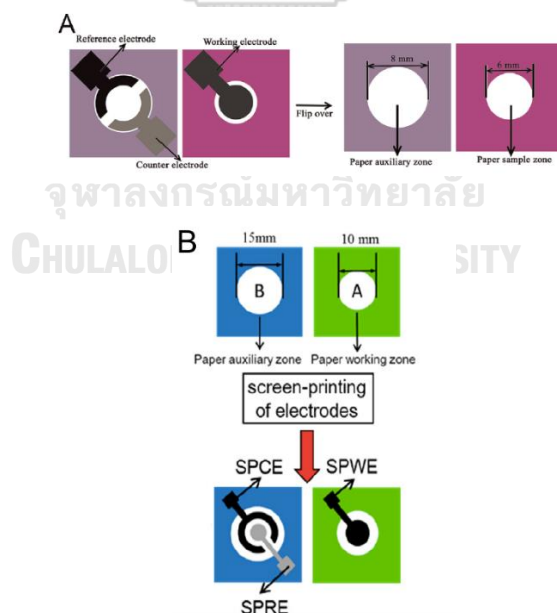
Figure 15 A schematic representation of paper-based screen-printed electrode for cell culture from A) Yu and B) Jiang group.

(Picture 15A was taken from ref 137. Picture 15B was taken from ref 138.)

Yu's group has also further modified the paper-based screen-printed electrode for cell culture. The paper origami consisted of 4 parts of paper that can be folded and assembled together. A paper was designed to have 4 cell culture zones that consisted of 4 WE in the back side of the paper. The RE/CE was screen printed on another piece of paper before assembled with the WE paper. The paper was further modified with aptamer for single cell detection in each cell culture zone (Figure 16) (129, 139, 140).
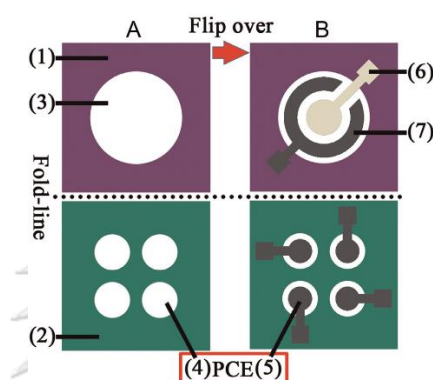
Figure 16 A paper screen printed electrode developed by Yu's group consisted of 1) paper auxiliary tab, 2) paper cell tab, 3) paper auxiliary zone, and 4) paper cell zone. (B) The reverse side of (A) with screen-printed electrodes: 5) SPCWE, 6) SPARE, and 7) SPCCE.

(This picture was taken from ref 140.)

Applications

Hydrogen peroxide sensing

Hydrogen peroxide (H_2O_2) is one of the reactive oxygen species that plays an important role in cellular modification, including cell signaling, proliferation, and migration. H_2O_2 is cytotoxic due to its ability to penetrate to any compartments of cell, causing peroxidation at, for example, cell membrane and DNA bases. In mammalian cells, H_2O_2 was produced from mitochondrial electron transport chain, lipoxygenase, cytochrome P450, oxidase, uncoupled endothelial nitric oxide synthase (eNOS) and other hemoproteins (Figure 17). The generated H_2O_2 in Figure 17 can directly react to lipid and protein, causing a DNA strand break. A very low concentration of H_2O_2 has also caused the change of molecular signaling, especially

endothelial cells. Cellular exposure to H_2O_2 exhibited an increase cell proliferation via the alteration of various molecular signaling, including ERK1/2 and NOX (141). Thus, the quantification of H_2O_2 in cells could reflect many pathological conditions.
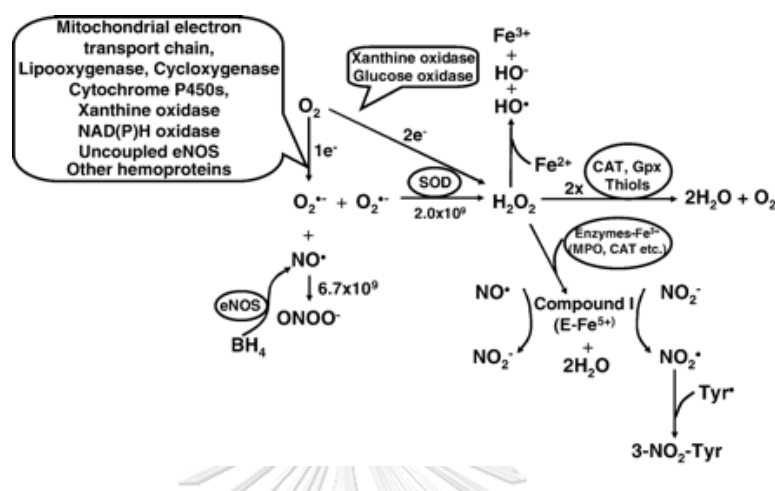
Figure 17 Biochemical pathways of hydrogen peroxide generation and metabolism. Molecular oxygen undergoes one or two-electron reduction (1 or 2e-) to form superoxide (O_2^-) or hydrogen peroxide (H_2O_2) respectively

(This picture was taken from ref 141.)

Paper-based 3D cell culture has been used for the direct H_2O_2 detection and indirect cellular pathological examination. The advantage of catalytic properties of various enzymes over H_2O_2 substrate could be coupled with electrochemical analysis. In order to perform the measurement, paper has an advance benefit to cellular response due to the 3D structure that is formed within a paper scaffold. The 3D morphology of cells could exhibit cellular responses better than the rigid 2D cell culture. Therefore, the production of H_2O_2 in a responsive of adverse pathological stimulation is more reliable. After culturing cells in the paper, the electrode was then coupled with a paper for electrochemical measurement. The direct H_2O_2 detection on the electrochemical paper-based cell culture was developed by Shi and colleagues. (136) A paper was fabricated by wax printing technique to create hydrophobic and hydrophilic (for cell culture) zone. WE and RE/CE were attached to the cell culture zone via silver paste. The device was used for larynx carcinoma cells produced H_2O_2. Phorbol 12-myristate-13-acetate (PMA), the chemical that is known as a stimuli of H_2O_2 production via $ERk_{1/2}$/CREB (142, 143), was also used to validate the device. Researchers applied PMA on paper-based cell culture to stimulate H_2O_2

production after culturing cells on the paper. In this work, the produced H_2O_2 gives a high current response which correlated with the concentration of H_2O_2 and PMA as expected. This result confirmed the validity of the develop paper device over the direct H_2O_2 detection. Accordingly, this paper has suggested the potential device for drug screening application via H_2O_2 detection (Figure 18). The same concept was also developed for SK-BR-3 breast cancer cells by Yu's group. The paper was modified by Platinum (Pt) nanoparticle to increase the conductivity. The aptamer was immobilized on the paper for cell specificity before adding the PMA. Cells then released H_2O_2, which could be measured by amperometry (129).
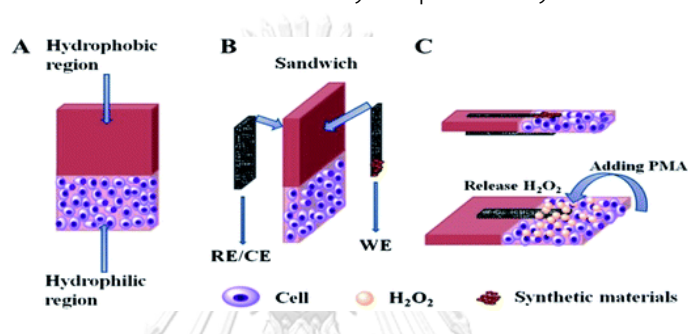
Figure 18 Electrodes/paper sandwich device and its validation for H_2O_2 detection after PMA stimulation. PMA: Phorbol 12-myristate-13-acetate.

(This picture was taken from ref 136.)

The indirect application of H_2O_2 detection is for cancer cell detection. Since it has been known that cells normally release H_2O_2 after the PMA stimulation. Thus, the release of H_2O_2 could also represent the existence of cells. Ge *et al*. have demonstrated the detection of leukemia cells via the release the H_2O_2 after PMA stimulation. The released H_2O_2 could oxidize thionine (TH), which resulted in an increased current response (Figure 19) (137).
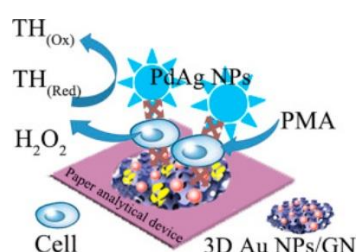
Figure 19 A schematic of paper-based device for leukemia cell detection via the release of H_2O_2 by PMA stimulation.

(This picture was taken from ref 137.)

Cell viability assay

Currently, cell viability assay is mostly performed in the end-point manner due to its ease of use and low cost. The end-point cell viability assay can be divided into 4 main concepts which are Tetrazolium reduction assay, Resazurin reduction assay, protease viability assay, and ATP assay. However, these end-point assays cannot be used for kinetic cytotoxic study due to the staining of specific reagents. The real-time cell viability assay was also developed by detecting luminescence product that is caused by the luciferase enzymatic reaction to the substrate produced by living cells. Thus, the kinetic of cell toxicity can be studied in real time (144). In addition, the fluorescent detection as also developed for real-time cell viability assay, the so called LIVE/DEAD staining, based on Calcein-AM (live cells) and Ethidium homodimer-1 (dead cells) staining (145). Nevertheless, both luminescence and fluorescence-based cell viability assay are expensive, time-consuming, and require the advance instrumentation (139). Consequently, the use of paper could reduce the cost of cell viability assay. Besides, paper could support cells in 3D morphology which exhibits the better *in vivo*-like structure. Other than luminescent and fluorescent detection, researchers also used electrochemical detection from real-time cell viability assay due to the simplicity of instrumentation which requires low electrical power, ease the in-field use (146).

In order to detect cell viability on the paper, researchers have used paper-based 3D cell culture technique by directly adding cells onto the paper. To increase the cell specificity of a paper, an aptamer was used for paper modification before cell seeding step. Su *et al*. have developed a paper-based electrochemical cyto-device or µ-PECD (Figure 20) for detecting cell apoptosis after anti-cancer drug treatment (139). DPV was used to detect cell apoptosis after Cycloheximide, Etoposide, Camptothecin treatment. The DPV response showed the direct correlation with cell apoptosis as the anti-drug concentrations increased.

The evaluation of multi-glycan expressions

Other than anti-cancer drug screening application, the **µ**-PECD was further developed for screening multi glycan expressions. Glycosylation on cancer cell surface plays a role in cancer metastasis due to the tumor adhesive alteration. The change in tumor

adhesion can either promote or inhibit cancer invasion (147). Hence, the screening of multi-glycan expressions on cancer cells is important in order to understand the invasive mechanism. Su *et al.* have applied **μ**-PECD to detect the multi-glycan expression by adding horseradish peroxidase (HRP) tagged with lectin that can specifically bind to glycan onto the cell-containing paper. H_2O_2 was then added for the result in enzymatic product, which could produce a DPV response. The DPV response represents different patterns, which correlated to the level glycan expressions.
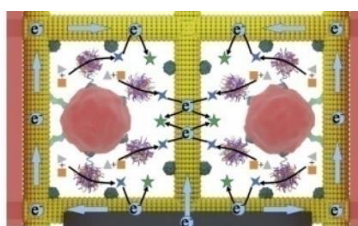
Figure 20 The scheme representing a paper-based electrochemical cyto-device or **μ***-PECD for screening anti-cancer drugs and multi-glycan expressions on cancer cells.*
(This picture was modified from ref 139 and 140.)

Impedance-based cellular study

Electrochemical Impedance spectroscopy (EIS) has been widely used as a method for studying cellular behavior. In brief, as the cell grows on the electrode surface, the current flow was impeded by the insulation of cell membrane, causing the increase of electrical resistance, which is known as impedance signal. This basic theory was proposed by Giaever and Keese (63, 148, 149). As the impedance signal change according to the cellular behavior, the impedance measurement was applied in various studies including cell proliferation, migration, invasion, and the tight junction integrity. For the better understanding of cellular behavior via the impedance measurement, researchers have been coupled 3D cell culture for the impedance measurement to improve the *in vivo*-like cellular responses.

The emerging of paper as an alternative scaffold for 3D cell culture was also coupled with EIS for measuring cell proliferation (31). The paper was used for culturing cells in various concentrations. The impedance measurement was performed throughout the incubation period (Figure 21). Lei and colleagues have demonstrated the direct correlation between cell amount on the paper and impedance signal. Their

developed paper was then used for quantifying cell proliferation in real-time manner for up to 72 h. This work has demonstrated the advantages of paper-based culture couple with EIS including, the non-invasive and real-time cell proliferation assay which was based on the 3D cell culture. This rises the potential of paper-based culture device for cellular study by using EIS.
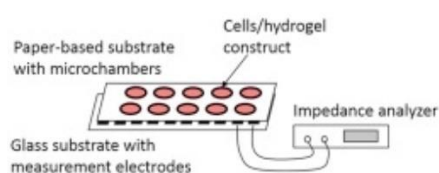
Figure 21 The schematic representing a paper-based culture device for cell proliferation assay using the impedance measurement.

(This picture was taken from ref 31.)

Table 4 A summary of paper-based 3D cell culture application using with the electrochemical analysis

Paper substrate	Cell line	Application	Electrochemical analysis	Ref.
Glass filter paper (CB08)	Hep2	Hydrogen peroxide sensing	CV, Amperometry	(136)
Whatman chromatography paper #1	SK-BR-3	Hydrogen peroxide sensing	DPV	(129)
Whatman chromatography paper #114	HL-60	Cancer cells detection Anti-cancer drug screening	DPV	(139)
Whatman chromatography paper #114	K562	Multi-glycan expression screening on cancer cells	DPV	(140)
Chromatographic paper	K562	Cancer cells detection via hydrogen peroxide sensing	DPV	(137)
Whatman No.4 filter paper	TW06	Cell proliferation	EIS	(31)
Whatman filter paper	PC-12	Cell viability	DPV	(134)
Cellulose A4 paper	RBL-2H3	Casein detection	CV, DPV	(138)

2.3 Melanogenesis

2.3.1 Biological roles and functions of skin and hair melanin and melanogenesis

Melanin have shown the significant properties on skin protection. Human with white skin are found to be more possibility to develop skin cancer than human with dark skin due to melanin's role of skin protection from UV radiation (UVR) (150, 151). By protecting melanocytes from UVR, melanin prevents DNA damage in both keratinocyte and melanocyte (152). Melanin consists of 2 main types which are eumelanin and pheomelanin. Eumelanin is a black brown melanin that is derived from the oxidative polymerization of L-DOPA via 5,6-dihydroxyindole intermediates. Pheomelanin is the yellow to red pigment that is derived from the oxidation of cysteinyldopa via benzothiazone and benzothiazole intermediates (Figure 22) (153). Eumelanin is found more in black hair, and decrease in dark brown, brown, light brown, blond, and red hair respectively. Pheomelanin is low in every hair color but remains constant, except red hair which has similar amount of eumelanin and pheomelanin (154).

Melanin also has the toxic effects. For instance, Pheomelanin contributes to the UVR damaging effects which generate hydrogen peroxide and superoxide anions (155-157). The effect of DNA damage can turn into melanocytes mutations (158). Insertion of melanoma oncoprotein BRAF into mice carrying $MC1R^{e/e}$ on MC1R gene caused the more invasive melanoma without the presence of UVR (159).

2.3.2 Melanin properties and control of melanogenesis

α-melanocyte stimulating hormone or α-MSH is an endogenous hormone of the melanocortin family. α-MSH is responsible for melanogenesis through the activation of melanocortin 1 receptor or MC1R (160, 161). The activation of MC1R through the binding of α-MSH and ACTH can result in the increased tyrosinase expression. The tyrosinase expression is based on the cAMP signaling and microphthalmia transcription factor. The cAMP signaling triggers the acidic melanosome into neutral state. The neutral melanosomal pH could enhance the catalytic efficiency of tyrosinase (162).

The activation of normal human melanocyte with α-MSH and ACTH increases the expression of Tyrosinase-related protein-1 (TRP1) and Tyrosinase-related protein-2

(TRP2) (163). The role of TRP1 and TRP2 are not yet clarified (164). There is also the evidence of TRP1 that is accountable for activation and stabilization of tyrosinase, melanosome synthesis, increased the ratio of eumelanin/pheomelanin (165, 166).

2.3.3 Chemical control of melanogenesis

Melanocytes produce two major types of melanin including eumelanin and pheomelanin. Melanin production depends on the availability of substrates and the function of melanogenesis enzymes (Figure 22). Firstly, tyrosinase (TYR) carries out tyrosine hydroxylation to L-3,4-dihydroxyphenylalanine (DOPA) which is rapidly oxidized to DOPAquinone.

In order to produce eumelanin, DOPAquinone is then removed cysteine, resulting in Cyclodopa. Cyclodopa then follows the redox exchange into Dopachrome and Dopa (167). Dopachrome rearranges itself into 5,6-Dihydroxyindole (DHI) and 5,6-Dihydroxylindole-2-carboxylic acid (DHICA). DHICA is produced in the less amount than DHI. Both DHI and DHICA are then oxidized into eumelanin (168).

In order to produce pheomelanin, DOPAquinone is added with cysteine before turning into 5-S-Cysteinyldopa (5-S-CD) and 2-S-Cysteinyldopa (2-S-CD). 5-S-CD and 2-S-CD are then turned into CD-quinone, 1,4-Benzothiazone intermediates, and pheomelanin (168).
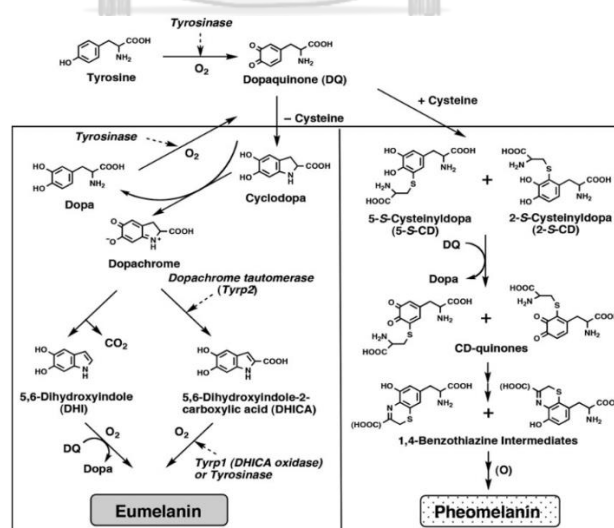
Figure 22 The process of melanin synthesis leading to eumelanin and pheomelanin production.

(This picture was taken from ref 168.)

2.3.4 Intrinsic regulation of skin pigmentation

Keratinocyte produces several factors that is caused by the UV exposure. These factors can both inhibit and stimulate melanogenesis. For instance, catecholamines produced by keratinocytes can bind to 1α and 2ß adrenogenic receptor in melanocytes. The binding results in melanogenesis by the cAMP pathway and PHC-ß (166, 169). cAMP production is responsible for the role of second messenger in melanogenesis (164). Figure 23 represents the additional significant pathways responsible for melanogenesis.
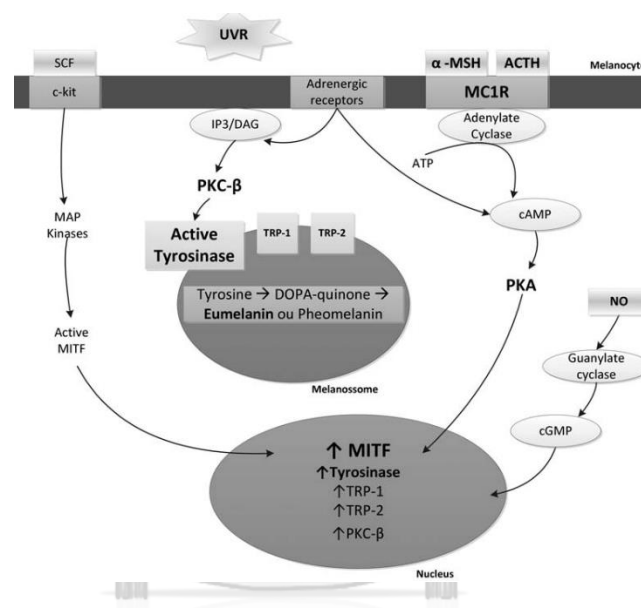
Figure 23 Signaling pathways in melanocytes that regulate melanogenesis.

(This picture was taken from ref 165.)

2.3.5 Extrinsic regulation of skin pigmentation by UVR

UVR exposure can cause 2 types of skin pigmentation. The first one is the immediate pigmentation which appears within 5-10 min after UV exposure. The immediate pigmentation is caused by UVA that does not result in the change of melanin production. Immediate pigmentation causes the oxidation of pre-existing melanin and redistribution of melanosomes. The second type is the delayed pigmentation which occurs 3-4 days after UV exposure. The delayed pigmentation causes by UVA and UVB that results in the increased epidermal melanin (170-173).

2.3.6 Melanin content analysis

Melanin amount is one of important factors for melanoma accessing procedures. In order to measure the amount of melanin that is produced from melanoma cells, researchers have been developed many methods including fluorescence spectrophotometry (14), Electron paramagnetic resonance (174-176), high performance liquid chromatography (177), and absorption spectroscopy (11, 178, 179). However, absorption spectroscopy has been widely used nowadays due to the ability to measure melanin in cells and the secreted one, its ease of use, does not need the large instrument, and skilled operator (180).

To perform the melanin content analysis by using absorption spectroscopy, cells are trypsinized from the culture plate before centrifugation. Cell pellet is then dissolved in 1 N NaOH at 80 °C for 1 hour to solubilize melanin. The melanin concentration is measured by the absorbance spectrophotometer at 475 nm. The absorbance value from commercial melanin from sepia (SIGMA) was measured at various concentration. The standard curve is plotted between melanin (sepia) concentrations and absorbance value. To calculate melanin concentration, the absorbance value from an unknown sample was then calculated from the standard curve (181-183).

2.3.7 Parameters for melanin content measurement

There are 2 parameters for melanin content measurement which are melanin content per cell (MC) and melanin content per culture or per area (MT). To calculate melanin content per culture, the melanin amount, that is obtained from the absorbance standard curve, is converted to nanogram (ng) unit before divided by the total number of cells. Thus, MC unit is shown in ng/ml unit. To convert MC to MT, the MC number in ng/ml unit is then multiplied by the total number of cells (181, 184-187).

In order to describe the melanin content in each cell line at a certain growth period, MC is suitable for comparison of melanin content among different cell lines (181, 188, 189). While the evaluation of the melanin content after the treatment of substance of interest, MT is more suitable due to the determination of biological effects of melanin *in vivo.* For instance, if the melanin content per cell is low but there are the large treatment area for the substance, the melanin content would then be increased due to the large surface area for treatment (190, 191).

2.3.8 Parameters for melanin production

There are 2 parameters for evaluating melanin production which are melanin content per culture in a given time period (MPT) and melanin production by each cell in a given period (MPC).

MPT can be calculated by using equation 1.

$$MPT = \frac{MTt - MTo}{t} \qquad [1]$$

MPT is the melanin production in a culture dish per day (ng per culture per day), t is the time period (day), MTo and MTt are the melanin content per culture dish at the beginning and at the end of culture respectively. (181)

MPC can be calculated by using equation 2.

$$MPC = \frac{MCt\ P - MCo}{1.3D} \qquad [2]$$

MPC is the melanin production per cell per day during the culture time (ng per cell per day). MCo and MCt are the melanin content per cell (ng per cell) at the beginning and at the end of culture respectively, t is time period (day), P is the cell population increase during culture time, and D is the doubling time of the cells which can be calculated by using equation 3. (192)

$$D = \frac{t \times log2}{log\ Nt - log\ No} \qquad [3]$$

No and Nt are the cell number at the beginning and at the end of the culture respectively, and t is the time period (day).

Similar to the melanin content evaluation, comparison of melanin production of cell lines at a certain growth period, MPC is more suitable than MPT. While the evaluation of melanin production after the treatment of biological substance, MPT should be used for determination (181, 188).

2.3.9 Melanin content analysis in 3D cell culture

Since 2D cell culture could not reflect the cellular condition *in vivo,* 3D cell culture has been widely used in many biological experiments including melanin content

analysis. Chung *et al*. demonstrated the evaluation of melanin content in 3D culture. Researchers formed the 3D spheroid from melanoma cell line by hanging drop technique. The spheroids were then transferred to ultra-low attachment (ULA) 96-well plate before adding the anti-melanogenic agents. After the incubation period, plate was read the absorbance at 490 nm (180). Thus, method had overcome the problem of 2D cell culture. However, the melanin content had been obtained from the secreted melanin only. Therefore, the total melanin content was not measured.

2.3.10 Other *in vitro* methods for melanin content analysis

Other than the spectrophotometric method, researchers have developed the HPLC-based melanin content analysis. The method is based on the formation of pyrrole-2,3,5-tricarboxylic acid (PTCA) by permanganate oxidation of eumelanin and of aminohydroxyphenylalanine (AHP) isomers, followed by hydriodic acid (HI). The products from degradative reaction were then analyzed by HPLC. This method allowed researchers to quantify in detail whether the melanin consist of eumelanin or pheomelanin more. Besides, the melanin derivatives can be quantified (10). Fernandes *et al*. have also developed the melanin content analysis by using fluorescence spectrophotometry. Similar to absorbance-based technique, trypsinized cells were centrifuged. The pellet was then solubilized in 1 N NaOH before adding hydrogen peroxide. Melanin is naturally acquire the fluorescence when subjected to oxidative conditions (heating in alkaline hydrogen peroxide solution) (13). Thus, the fluorescence, after hydrogen peroxide, adding was measured by fluorescence spectroscopy (14).

2.4 Electric Cell-Substrate Impedance Sensing (ECIS)

Electric Cell-Substrate Impedance Sensing (ECIS) is a technique, based on electrical impedance spectroscopy (EIS) for measuring cellular activities including cell proliferation and viability, cell cycle, cell metastasis, and cell migration and invasion. EIS is technology that is able to monitor specific information of cells by applying the voltage (V) in the electrodes that are placed with cells. (193). The impedance signal or Z_f is measured as a function of the frequency and represented by $Z_f=V_f/I_f$ when I_f is the current obtained from the electrode (194). Since EIS is non-invasive, real-time, and label-free method (195-198), it has gained the potential for applying in cellular study. ECIS was found by Giaever and Keese (63). Giaever and Keese have found that

when applying AC current while the frequency is sufficiently high, the resistance of the tight cell layer could be measured (199). According to Giaever and Keese ECIS system, researchers have been focusing on applying ECIS into various cell studies. Here, we review the theory, electrode design for ECIS and its applications.

2.4.1 Theory and Modelling of ECIS

The impedance signal can be obtained using a small AC voltage as the excitation before the electrical current is measured (200). The complex impedance (Z_ω) is then calculated as:

$$Z_\omega = \frac{U_{(\omega)}}{I_{(\omega)}} = Z_{RE} + jZ_{IM} \qquad (1)$$

where $j = \sqrt{-1}$ and ω is the frequency. The real (Z_{RE}) and imaginary (Z_{IM}) parts of the complex impedance are called resistance and reactance, respectively. The magnitude (Z) and phase angle (θ) of the complex impedance are

$$|z| = \sqrt{(Z_{RE})^2 + (Z_{IM})^2} \qquad (2)$$

$$\theta = \arctan\frac{Z_{IM}}{Z_{RE}}$$

Cells, that were measured in the ECIS system, are in 2 statuses which are the suspended in medium and adhered on the culture substrate (200).

For the suspended cells in the medium, the mammalian cells which consist of a lipid bilayer membrane and cytoplasm (no cell wall). This type of cells is referred to a single-shell model (201-203). The plasma membrane acts as the insulating shell, while the cytoplasm acts as the conducting sphere (Figure 24). The EIS is normally applied for the detection of cell metabolism/proliferation. Their shell (plasma membrane and/or cell wall) acts as the charged particle, while the ion released from cells can change the conductivity in the medium (204). After fitting with the equivalent circuit model, the resistance-capacitance can be determined from Nyquist plot.
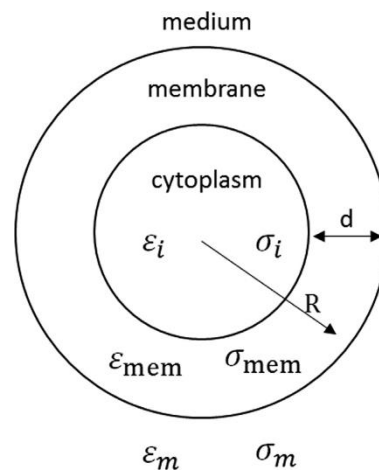
Figure 24 A single shell model of suspended cell in the medium represents the permittivity of the medium, cell membrane, and cytoplasm

(This picture was taken from ref 200.)

Asami *et al*. have demonstrated that normally the frequency that applied for the single shell model ranged from 1 Hz to 10 GHz (205). These range of frequency can be divided into 3 dispersions which are **α, β**, and **γ** (206). The **α**-dispersion is below 100 Hz which is interfered by the electrode polarization. The **β**-dispersion represents the insulating membrane which is usually discussed in the ECIS system (203). The **γ**-dispersion is higher than 1 GHz and is resulted from reorientation of water molecules (207).

For the adherent cells, Giaever and Keese have established the theory in 1991 (208). The character of cells adhered on the electrode can be described by the equivalent circuit models (Figure 25) (209, 210). Cells that adhered on the electrode acts as the capacitance, or a constant phase element (CPE) or a resistance-capacitance complex, depends on the equivalent circuit models (200). Basically, the impedance magnitude is increased when cells adhere on the electrode surface and more increased when cell proliferate due to the insulating properties of cell membrane which impeded the current flow in the system. When measuring the impedance signal without cells (Z_0), the impedance magnitude reflects the electrode-medium interface. In order to reflect impedance magnitude caused by cells, the impedance signal normally represented in the normalized term (Z/Z_0) or cell index ($Z-Z_0/Z_0$) (211).
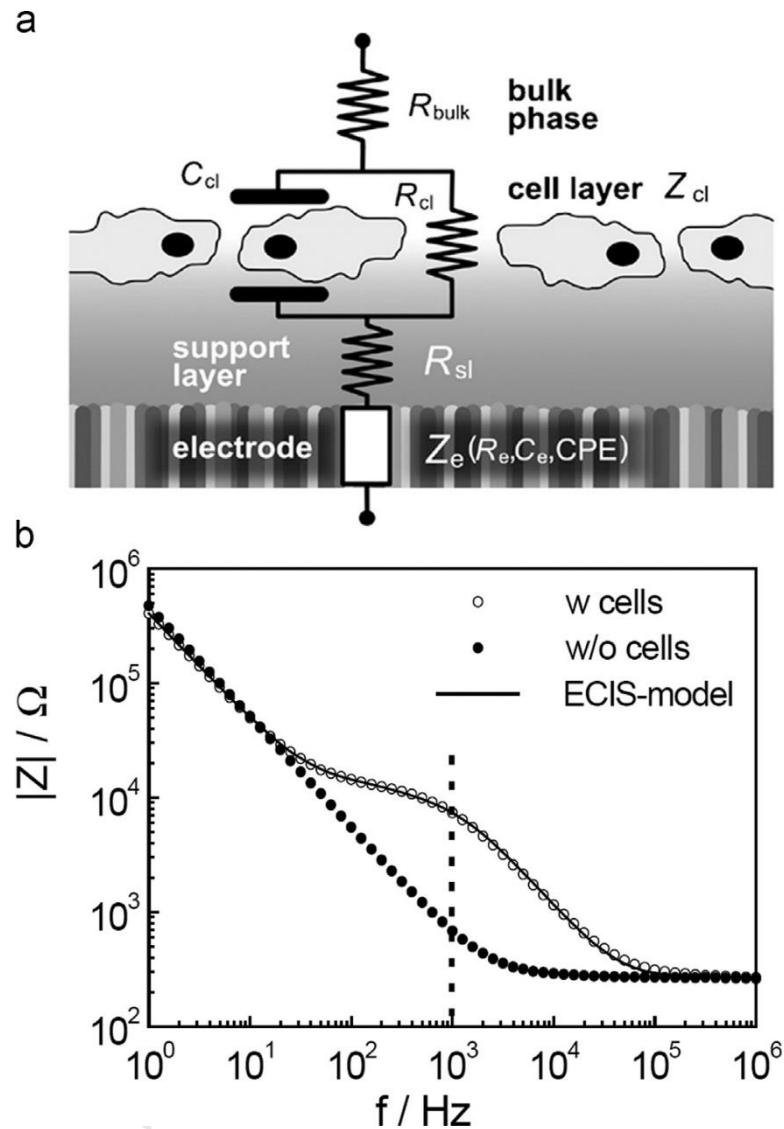
Figure 25 The equivalent circuit models explain the character of cells adhered on the electrode and the relationship between the applied frequency sweeping and the impedance magnitude with and without cells.

(The picture was taken from ref 211.)

2.4.2 Instrument

EIS measurement is based on the AC/DC power generator which connects to a potentiostat. A potentiostat is responsible for supplying the current to the counter electrode, in order to maintain the desired potential difference between working electrode and reference electrode. The data precision in EIS experiment also depends on the ability to manipulate the applied frequency. The wider range of the frequency, the more data acquisition. Noise and background currents generated by

the instrument were removed by adjusting variable resistor on the lock-in amplifier connected to the potentiostat. Lower frequency can give the accurate result but also causes longer experiment which may lead the change of sample surfaces (Figure 26) (212).
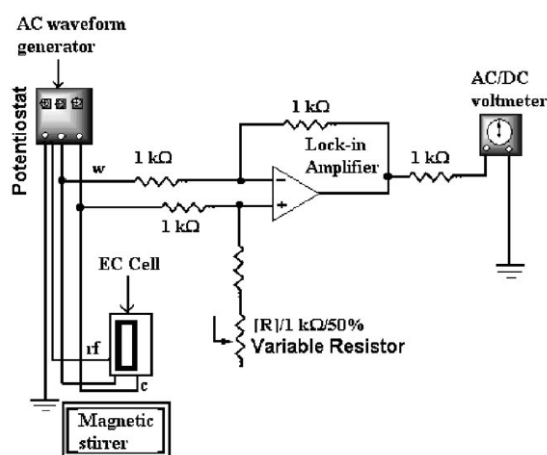
Figure 26 Schematic representation of the instrument acquired for EIS experiment

(The picture was taken from ref 212.)

2.4.3 Data representation

The basic curves acquired after EIS experiment consist of 2 types which are Nyquist plot and Bode plot. Nyquist plot is usually shown in a semicircle and straight line portion (Figure 27). The semicircle portion at high frequencies represents to electron-transfer limited process while the straight-line portion corresponds to diffusion limited electron transfer process at low frequencies. (Figure 27a) Thus, for the very fast electron transfer process, the impedance spectrum may possess only the straight line protion as shown in figure 27b. For the slow electron transfer process may give rise to a large semicircle as shown in figure 27c due to the thick layer of insulator on electrode materials (212). Normally, the Nyquist plot is used for the electrode characterization by measuring the charge transfer resistance (R_{ct}) from the curve. The lower R_{ct}, the better electrode will function.
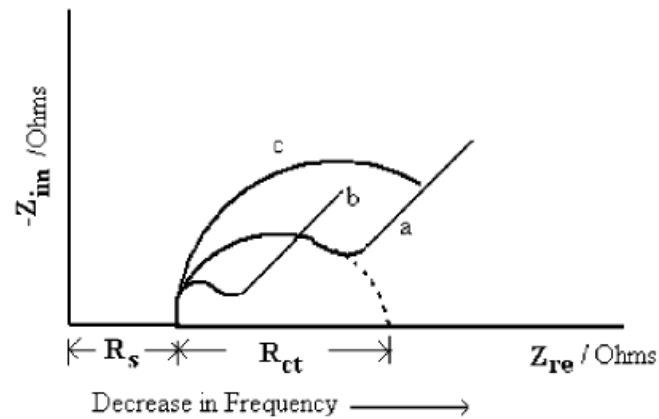
Figure 27 A schematic illustration of Faradaic impedance spectra in the form of Nyquist plots for various modifications of electrode.

(The picture was taken from ref 212.)

Bode plot is a combination of a magnitude plot, expressing the magnitude of the frequency response, and a phase plot, expressing the phase shift (Figure 28) (212, 213).
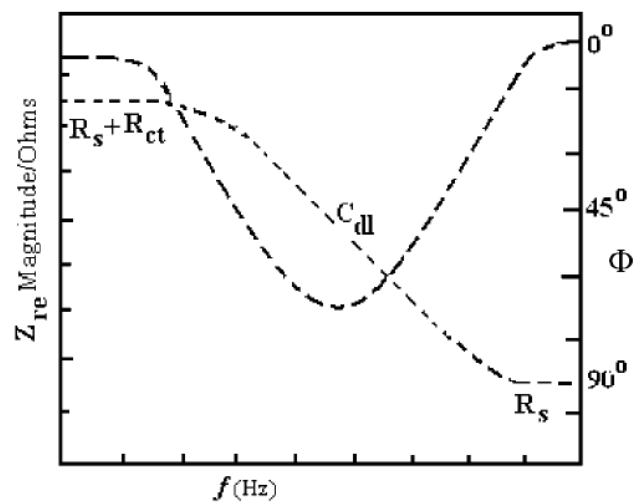
Figure 28 Bode Plots showing variations of impedance parameters with frequency

(The picture was taken from ref 212.)

2.4.4 Electrode design and fabrication

There are 2 factors that contribute to the optimal EIS signal. The first factor is the electrode which is responsible for applying the electric field to cell medium system.

The second factor is the device which should be able to integrate with electrode design and biocompatible with cell culture (200).

The materials used for the electrode substrate are glass (214, 215) and silicon (216-218). However, there is the limitation of using silicon as the electrode substrate due to its non-transparent property. Thus, the integration with microscopy is not possible. Glass substrate are more popular due to its transparency.

For the electrode material, gold (Au) is an ideal material used for electrode fabrication due to its good electrochemical properties and biocompatibility. Moreover, Au is easy to modified (219, 220). Other than Au, Silver/silver chloride (Ag/AgCl) (221), Platinum (Pt) (222), indium tin oxide (ITO) (223), Nickle (Ni) (224) have also been used as an electrode material in the ECIS system.

The electrode fabrication is based on various processes including metal deposition, lithography, and reactive ion etching (225). The process started with sputter coating or evaporation of Cr (30nm) and Au (300nm) on the glass substrate. Ti can also be used as an alternative material of Cr. The use of Ti or Cr can enhance the deposition of Au on the substrate. In order to connect to circuit pad, the electrode is bonded by using lithography and etching technique respectively. The electrode is then covered with the insulation layer that patterned as the desired electrode design. Afterwards, the electrode is exposed and the insulation layer is removed respectively (Figure 29) (200, 215).
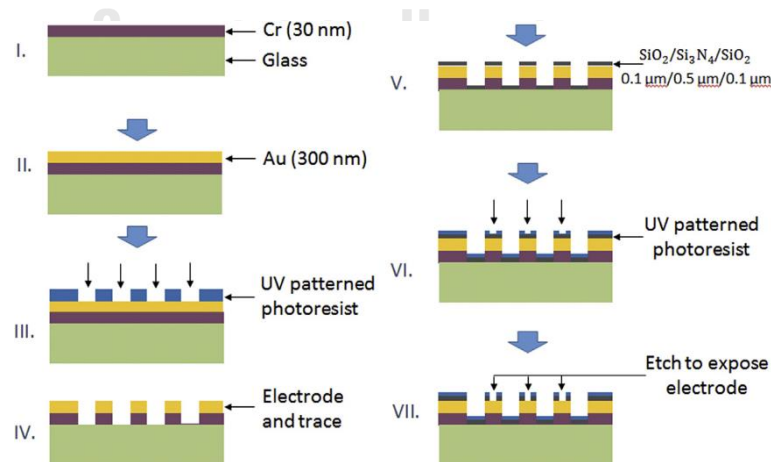
Figure 29 The microfabrication of Cr/Au electrode on glass substrate

(The picture was taken from ref 215.)

The electrode geometries used in the ECIS system consist of 2 main types. The first geometry is a pair of circular microelectrodes. The circular one has round working electrode and the large counter electrode (Figure 30A&C). This configuration has a wide area for cell culture (194). Thus, it is widely used for cell proliferation, attachment and spreading, wounding and migration (226-228). The second configuration is the interdigitated electrode. Interdigitated electrode consists of 2 fingers that mesh with each other (Figure 30B&D). By increasing the number of fingers, the electrode surface could be increased. The fingers can be arranged in parallel (229-231) or circular pattern (232).
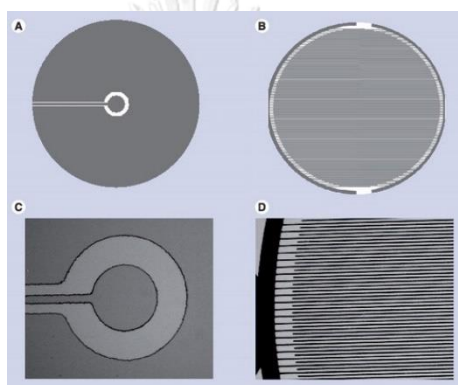
Figure 30 The microelectrode geometries used for EIS. A&B is a schematic view. C&D is a microscopic view. A&C represent the circular microelectrode pair. B&D represent the interdigitated electrode.

(The picture was taken from ref 194.)

2.4.5 Application of ECIS

2.4.5.1 Cell proliferation and viability

The conventional cell proliferation assay requires many steps and the end-point readout (233). To simplify the measurement, ECIS has served as the non- invasive, label free and real-time cell proliferation assay. To perform the experiment, a small quantity of cells is seeded on the electrode cultureware. When cells start dividing, the number of cells is increased and covered electrode surface, resulting the increased impedance magnitude. These impedance changes is related to cell proliferation rates or, more accurately, the rate at which the substrate becomes occupied with spread cells (226, 234).

Similar to cell proliferation assay, ECIS can be used for cell viability assay since the death of cells causes the decrease cell number attaching on the electrode surface. Mostly, ECIS was applied for studying the cytotoxicity of substances of interest to cells. For instance, the cytotoxicity of mercury chloride and 1,3,5-trinitrobenzene (TNB) was study by exposing to fibroblastic V70 cell line. In this work, the gold electrode was fabricated for measuring the concentration and time response function of cells to the substances (235). Other substances that are suspected as a non-biocompatible chemical were also studied by ECIS system including magnesium ion (236) and anti-cancer drugs (237).

Other than the compounds, the virus induced toxicity has also been tested using the ECIS. The fish cell lines were tested with 2 types of infectious viruses which were pancreatic necrosis virus and hematopoietic necrosis virus. In this work, researchers found that an approximate linear correlation exists between the log of the viral titer and the time of cell death (238). Muller *et al.* have also studied the titer-dependent cytotoxicity of adenoviral vector in IPI-21 cells (239). ECIS based cell proliferation assay improves the conventional methods in many ways as mentioned above. Moreover, the ECIS cell proliferation assay can be performed in high throughput manner by fabricating the multi-well electrode cultureware. The assay can be performed simultaneously by the multi-channel potentiostat.

2.4.5.2 Cell cycle

Deregulation of cell cycle is one of the approach to stop cancer metastasis (118). To track cell cycle, the fluorescence and flow cytometry are currently used. Wang *et al.* have developed the cell cycle detection based on impedance signal. Cells were synchronized before seeded on the electrode surface. When cycle changed, cells changed their shapes that corresponded with impedance signal. Researchers found that when cell cycle progress from G2 to M phase, cells detached from the electrode and round up to prepare for cellular division. While the progression from G1 to S phase, cell re-attached the electrode and spread themselves, resulting in increased impedance signal (211).

2.4.5.3 Cell migration and invasion

Conventional migration and invasion assay are based on transwell assay or Boyden chamber. The assay is easy to use and provides quantitative data. However, it can

only be performed in the end point manner. Thus, the kinetic of cell motility and invasion could not be studied. ECIS has served the purpose of real-time migration and invasion assay. AppliedBiophysics company has developed the automated ECIS wound healing assay which gives the precise wounding, highly reproducibility, and good matrix preservation. After cell scratching on the electrode, the healing process could be tracked from the electrical signal (240). For the invasion assay, the technique is based on the cell monolayer formation on the electrode. When cells form monolayer, the impedance magnitude will be increased as the cell-cell contact is getting tight. To perform the invasion assay, the invasive cells were placed on top of cell mono layer. Once the invasive cells destroy the cell adhesion on the electrode, the current will flow easier again, resulting the decreased impedance signal. This assay is called transepithelial/transendothelial electrical resistance (TEER) measurement. Applied Biophysics company had also developed the commercial device for TEER measurement. The device has a similar configuration as the transwell assay but contains electrode sensors upper and lower the membrane insert. Cellular invasion was then mapped from the electrical signal from the whole device (Figure 31) (241).
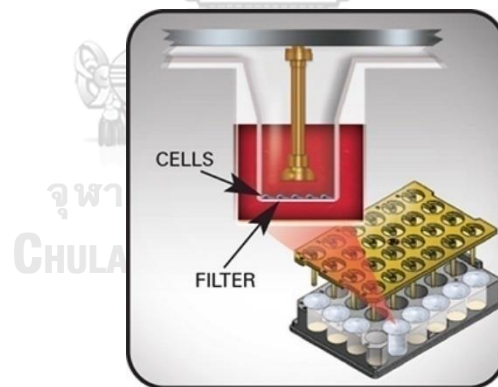
Figure 31 The illustration of the commercial ECIS TEER24 instrument from Applied Biophysics company.

(The picture was taken from ref 241.)

2.5 Microfabrication technique for microfluidic devices

The miniaturization of laboratory process has come to the popular research field known as Lab-on-a-chip. In order to fabricate Lab-on-a-chip system, the microfabrication is required due to the small structure that could recapitulate the experimental conditions such as the *in vivo* conditions. Microfluidic chip can be

made of 2 major types of material which are silicon or glass and polymers. Here, we discuss the microfabrication methods that was used for both silicon or glass and polymer substrate.

2.5.1 Silicon/Glass-based microfabrication

The silicon/glass/based microfluidic devices are mostly used in Micro-Electro-Mechanical system (MEMS) by integrating with the integrated circuit (IC). The use of silicon could provide the feature size down to 50 μm feature size (242). There are several methods used for microfabrication of rigid matters, described below.

2.5.1.1 Lithography

Lithography is the technique for transferring the three dimensional pattern onto the material surface (243). The method starts with designing the pattern using the computer-aided design (CAD). After that, the substrate (silicon, glass or the rigid matter) is coated with the light sensitive polymer called photoresist (PR). PR is then covered with mask that is fabricated according to CAD design. The PR is then exposed to light such as UV, laser, beam of electrons. The mask acts as the light protection. The PR after light exposure is then cured. In brief, there are 2 types of PR. Positive PR is the PR that becomes soluble when exposed to the light while the negative PR will become insoluble. After light exposure, PR will remain on the substrate as the desired pattern. This pattern will define etching regions or deposition regions in the subsequent steps (242).

2.5.1.2 Etching

The further technique after lithography can be done by etching which is the process to cut into the unprotected parts of a surface to create a design in the incised in the metal (244). There 3 types of etching. Wet etching is the method based on the chemicals used for etching. However, wet etching shows a slow etch rate but can be enhanced by tuning agitation or temperature. Chemical etching relies on the reaction from the free ion of used chemicals which reacts with the silicon atoms, results in the removal of silicon surface. The second type is dry etching which is based on the use of plasma to remove materials from silicon substrate at low pressure and low temperature. However, the combination of dry and wet etching can be used to achieve high resolution etching, called reactive ion etching (RIE). RIE starts with etching step with gases such as CH_4, SF_6 and BCl_2+Cl_2. Before further etching, the

bottom of etched pattern and side walls are protected by the deposition of polymer resistant layer. The process was repeated to obtain the deeper and vertical etch profile (242).

2.5.1.3 Additive techniques for pattern transfer

After etching the silicon into the desired shape, the addition material can be directly deposited. There are various methods for material deposition. Physical vapor deposition (PVD) is the technique for depositing thin film by the condensable vapor through the low pressure or vacuum gases. The vapor can be delivered to the substrate by using various methods such as sputtering, thermal evaporation, ion plating and cluster deposition (242). After the transportation of vapor to the substrate, the vapor is condensed on the surface of substrate. This layer can then be used as a sacrificing layer for the subsequent device layers fabrication.

2.5.2 Polymer-based microfabrication

Polymers are gaining attention as an alternative material for microfabrication due to its low cost. Moreover, polymers are replicable, transparent, biocompatible. There are 2 main types of polymers that are often used in microfabrication technique currently, which are elastomer, such as polydimethylsiloxane (PDMS), and thermoplastics.

2.5.2.1 Elastomers: PDMS

PDMS is used in microfabrication technique in the rapid prototyping of microfluidic devices. The technique is called soft lithography. Soft lithography is used for replicating the elastomeric devices without costly capital equipment. To replicate the device, the master mold has to be fabricated before. The master mold by patterning photoresist on the rigid substrate oy by micromilling the thermoplastic directly. A brief description of the master mold fabrication, photolithography, is shown in figure 32. The process description can be found in the section of lithography in this review. After the master mold is well-fabricated, the PDMS is then cast onto the master mold to obtain the elastomeric microfluidic device. Basically, PDMS consists of 2 parts which are the pre-polymer and the curing agent. Usually, pre-polymer and curing agent are mixed with the ratio of 1:10. However, the ratio can be adjusted according to the rigidity of the desired device (242).
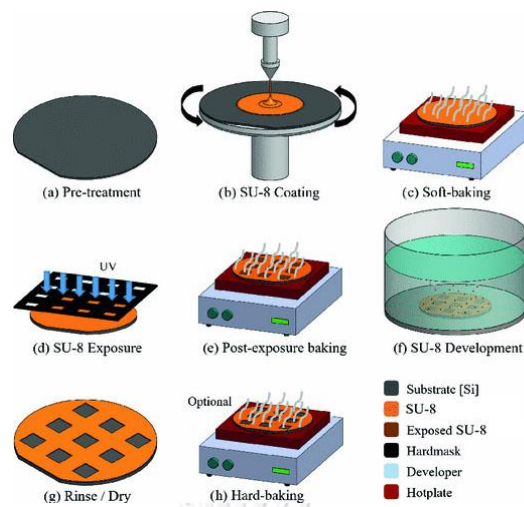
Figure 32 Master mold fabrication process for soft lithography technique

(The picture was modified from ref 242.)

2.5.2.2 Thermoplastics

Using thermoplastics in microfabrication technique eases the users because the clean room environment is not required. Thermoplastics has a low chemical absorption, biocompatibility, easy to use (245). However, thermoplastics can be dissolved in some organic solvents which can reduce the stiffness. Besides, thermoplastics can absorb the UV-light which inhibit their use in many applications. There are many techniques used in thermoplastic fabrication. In this review, we provide a brief example of some methods that are popular and/or has been used in this thesis.

3D printing allows researchers and normal people to be able to create many products and devices in-house. The technique is based on the design of desired device before converting to the code which can be transferred to 3D printer. The filaments that are commercially available is then installed to the 3D printer. When start the printer, it will heat the filaments while passing through the head of printer. The head of printer moves in XYZ axis, in order to create the 3D model without requiring the mold (242).

Injection molding is the high throughput fabrication technique which is currently used in the market. The technique consists of 5 steps including plastication, injection, packing, cooling, and mold resetting. In brief, the plastic is added in the machine before melted and injected into the mold cavity, containing the template for the features to be molded. Though this method can be used for fabricating many

devices in 1 time, it requires the tedious process of mold fabrication since the design has to be very precise (242).

Micromilling is another microfabrication technique that does not require master mold. The technique is based on the rotation of cutting tools to remove the bulk material from the workpiece. The machine works according to the computer numerical control or CNC which enables direct conversion of CAD. CNC could reduce the human error and allows the automation in the microfabrication process (242). The feature size replies on the size of mill tools which can be down to 50 microns. However, the fabrication might require many tools in 1 device which result in time-consuming.

2.6 *In vitro* cell invasion assay

Cancer, the deadliest disease nowadays, is influenced by multiple factors. To develop the therapeutic agents, understanding the cancer invasion mechanism is important. The crucial mechanism that leads to the malignant stage is metastasis. Cancer metastasis begins with cell adhesion, ECM proteolysis, and migration respectively (118). Once cancer cells invade through the ECM and migrate to various organs in the body, it can lead to a poor prognosis in patients. Thus, researchers have been focusing on the metastatic step to develop the treatment and understand the mechanism of cancer invasion. In order to understand the invasive mechanism of cancer cells, various *in vitro* methods have been developed to ease the study and improve the imitation to *in vivo* mechanism. In this review, we include the developed *in vitro* invasion assay both 2D and 3D cell culture, explained below.

2.6.1 Boyden chamber/Transwell assay

The transwell assay is the most conventional method used to assess the invasion activity of cells. Basically, transwell assay contains 2 chambers which are the upper and lower chambers. Both chambers are separated by the membrane which only allows the invasive cells to pass through. On the other hand, invasive cells can degrade ECM and pass through the bottom chamber. Invasive cells will then be analyzed by various methods such as stained and counted with a light microscope, or detached, stained and lysed using fluorimetric detection (17). However, transwell assay can only be used for the end-point assay. Invaded cells are also affected by pore size of membrane insert and gravity (18). Moreover, the commercial membrane

inserts are only available in fixed sizes and design which are not suitable for the customized device (Figure 33A).

2.6.2 Platypus invasion assay

The method is started by coating basal membrane extract (BME) at the bottom of 96 well plate. Accordingly, the stopper is placed in the middle of the well to separate the zone between 2 cell seeding zone (Figure 33B). Cells are then seeded and incubated until cells attach to the BME. Afterwards, the stopper is removed, which leave the area in the middle for adding ECM. After ECM is cured, cell invasion is then tracked overtime by a microscope or stop the measurement by cell fixation and perform immunofluorescent staining respectively. Though the method can be used for real-time tracking, this method has the same limitation as transwell assay, which the gradient of small molecules or chemoattractants cannot be formed (18).

2.6.3 3D cell tracking

As we discuss above, 2D cell culture could not reflect the *in vivo* like structure and cellular behavior due to the poor cell-cell contact. To overcome this problem, researchers have been developed 3D cell invasion assay by encapsulating cell in the ECM before placing into the culture well. Cell invasion can then be tracked either labeled and unlabeled cells by using wide field fluorescence, confocal or multiphoton microscopy as well as the contrast enhancing or digital holography microscopy (246). Since the invasion of cells is tracked by the path of cell movement, the only limited set of cells can be analyzed (Figure 33C) (18).

2.6.4 Gelatin degradation assay

Instead of study the invasion of whole cells, gelatin degradation assay allows researchers to study cell invasion in the sub-cellular level. This method leads to the understanding of cell invasion through the protusions as known as invadopodia formation (247). The assay is based on the use of fluorescent ECM. When cells are seeded on ECM and invade into the matrix, the invaded area will lack of fluorescent (Figure 33D) Though this method can be used for sub-cellular level, cells cannot form 3D structure due to the seeding step on top of ECM instead of encapsulation (18).

2.6.5 Vertical gel 3D invasion assay

The vertical gel 3D invasion assay was often reported in melanoma invasion study with or without the coculture condition (248-250). In this review, we provide the example of vertical gel 3D invasion assay of melanoma cells in the co-culture condition with fibroblast. In brief, fibroblast cells were encapsulated in collagen and placed in culture well. The collagen was then formed the thick layer of ECM. Subsequently, melanoma cells were seeded on top of collagen. Melanoma invasion can be quantified by immunohistochemical staining (251). This method can mimic the skin cancer similar to *in vivo*, in which heterotypic cell-cell interaction of epithelial cancer cell and fibroblast can be studied. The drawback of this method is labor-intensive and the requirement of special equipment such as embedding stations and microtomes (Figure 33E) (18).

2.6.6 Spheroid/monodispersed cell invasion assay

The multicellular cell aggregate or spheroid are the cluster that are formed *in vitro* to recapitulate *in vivo* tumor (252). The single cell invasion towards spheroid is the principle of this method. The aggregate formation can reflect the tumor environment in our body while the single cell can be used for study their invasiveness. The invasion of single cells can be tracked by confocal microscopy. Th invaded spheroid can be counted by flow cytometry (Figure 33F) (18).

2.6.7 Spheroid confrontation assay

The spheroid confrontation assay is based on the formation of 2 aggregates from a different cell type (253). The invasion between different cancer cell line can be studied. The invasive spheroids will start invading and fusing each other. While, the non-invasive ones will form a well-defined border. The use of 3D aggregate can reflect well-establish cell-cell interactions of different cell types. The quantification of invasive cells requires immunofluorescence and confocal microscopy. Therefore, this method requires the extensive post-experimental processing. Moreover, primary cells and some cell line that cannot form aggregate are not able to be used in this assay (Figure 33G) (18).

2.6.8 Spheroid gel invasion assays

Cellular invasion can be defined by cellular motility and their ability to degrade ECM. Instead of using 2D cell culture, the study of cellular ability to degrade ECM can also

be done by embedding spheroid in ECM. The non-invasive spheroid forms the well-defined edge in the ECM, while the invasive one invades the matrix, resulting in the astral outgrowth (Figure 33H) (253). Live cell imaging can be done to track cell invasion over time using photomicrographs (18).
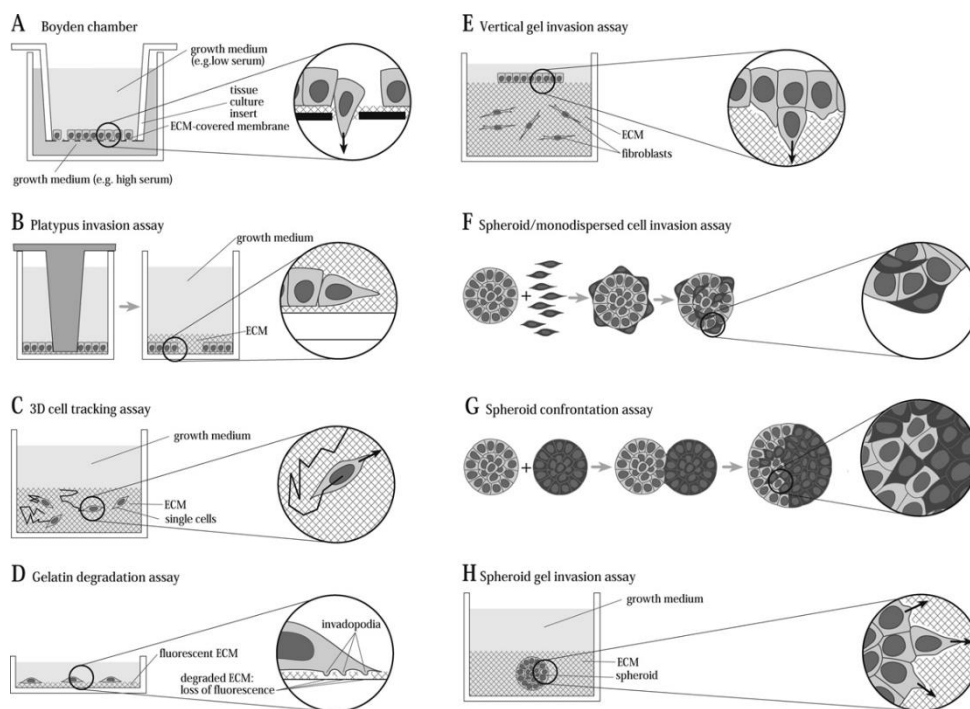
Figure 33 Schemes of commonly used invasion assays.

(A) Transwell invasion assay (Boyden chamber assay). (B) Platypus invasion assay. (C) 3D cell tracking assay. (D) Gelatin degradation assay. (E) Vertical gel invasion assay (F) Spheroid/monodispersed cell invasion assay. (G) Spheroid confrontation assay. (H) Spheroid gel invasion assay.

(The picture was taken from ref 18.)

2.7 Analytical techniques for estrogenic compound detection

Estrogenic compounds are one of the most harmful environmental contaminants due to their ability to mimic estrogen, causing various adverse effects to human and living organisms. In order to detect the estrogen in environmental contaminants, there are mainly two methods: chemical analysis, immunoassays and bioassays. Nevertheless, some methods might require the pre-treatment of the environmental sample such as solid-phase extraction (SPE), liquid-liquid extraction (LLE), solid-phase microextraction (SPME), and dispersive liquid-liquid microextraction (DLLME). The advantage of pre-treatment step is that it can reduce the unwanted adsorption of

other chemicals and increase the specificity of the assay. To perform the filtration of the environmental sample for enriching estrogenic compounds, various types of filter are available in the market including polyvinylidene fluoride (PVDF), nylon, and glass fiber. Currently, glass fiber is the most commonly used due to their ability to minimize the loss of estrogen (254, 255). To concentrate the estrogen from environmental sample, SPE is based on the affinity of filters to adsorp estrogen from the sample. On the other hand, LLE acquires the different partition coefficient between estrogen and the endogeneous interference to form a covalent bond with eluting solvent in two immiscible phases (256). Though both SPE and LLE has low operating cost, they are labor intensive and consume a lot of hazardous organic solvents (257). DLLME is currently high competitive due to the low sample and solvent consumption and provide high yields (258, 259).

2.7.1 Chemical analysis

Mostly, the chemical analysis is based on the coupling of chromatographic method chromatrography (GC) and liquid chromatrography (LC) with mass spectrometry (MS). Though GC-MS has an accuracy and environmental friendly due to the use of inert gas as an mobile phase (260, 261), LC-MS has a larger separation range and simple analysis method (262). Other than the coupling the analytical intruments with MS, Electrochemistry has been applied in many recent biosensors for estrogenic detection. The principle is based on the detection of 17ß-estradiol that has the irreversible oxidation properties when placing on the electrode (263). Li *et al*. have developed the electrochemical platform, based on estrogen receptor positive MCF-7 cells. The platform was applied for the detection of xanthine and hypoxanthine, which found to be correlated with the amount of intracellular estrogenic level (264). Though electrochemistry is simple and provide real-time detection, it has poor selectivity and does not provide information regarding the biological properties of estrogen (254). In present, various electrode has been developed to improve sensitivity and specificity to estrogen. For instance, graphene screen printed electrode was developed for estrone, 17ß-estradiol, and 17α-ethynylestradiol (synthetic estrogen) detection. This method shows a very low limit of detection (LOD) and the promising properties of graphene as an electrode for estrogenic detection (265). Recently, graphene has also been coupled with the use of aptamer

for 17β-estradiol. Due to the combination with aptamer, this method has an increased selectivity with the low LOD down to 50 fM (266).

2.7.2 Immunoassays

The principle of immunoassay is based on the binding of analytes of interest (estrogen) and the antibody. The most widely known assay is ELISA. ELISA has various types including, competitive, indirect, direct, sandwich, and multiple and portable ELISA. The assay is determined by the color after adding substrate to the enzyme conjugated antibody. The color has a direct correlation with the concentration of analytes (267). The on-chip sandwich immunoassay has been developed by Uraipong and colleagues (268). The assay is based on the treatment of ER positive MCF-7 cells, before adding the treated cells to the immobilized anti-MCF-7 cell platform. The amount of MCF-7 has a direct correlation with estrogen amount because their proliferation is based on the binding of estrogenic compounds. The enzyme conjugated secondary antibody was then added to the MCF-7 cells, providing color intensity that is correlated to the amount of estrogen (268).

2.7.3 Bioassays

Bioassays usually base on the whole cell or animals such as fish, birds, and insects. The use of *in vivo* experiment can provide the biological information of estrogen. However, the methods are not commonly used doe to the ethical concern, labor and cost intensive, and time consuming (254). One of the well-known *in vivo* assay is called Vitellogenin assay. Vitellogenin is the egg yolk, which is produced by fish after the exposure of estrogenic compounds (269). To overcome the drawbacks of *in vivo* experiments, three main *in vitro* bioassays have been developed: competitive ligand binding assays, E-screen assay, and yeast estrogen screen assay (YES).

- Competitive ligand-binding assays relies on the recombinant ER positive cell line, which can produce luciferase or fluorescence after the binding of estrogen on cell membrane. In addition, gold nanoparticles (AuNPs) have been developed for ligand-binding assays for estrogen detection. By incubating estrogen-specific aptamer in the sample, the bases of aptamer fail to absorb onto AuNPs, cause less fluorescence signal (270). However, this method could not determine the agonistic and antagonistic activity (271).

- E-screen assay is the method for screening estrogenic compounds, based on the binding of estrogen on ER of MCF-7 cells. The binding of estrogen later causes the increased of MCF-7 cell proliferation. MCF-7 cells are then fixed and stained for total protein measurement, which is correlated with the amount of treated estrogen (59). The E-screen is accurate, high throughput, and reproducible (272). Mitogen other than estrogen can also causes an increased MCF-7 cell proliferation, providing the possibility to detect xenoestrogenic compounds (Figure 34).
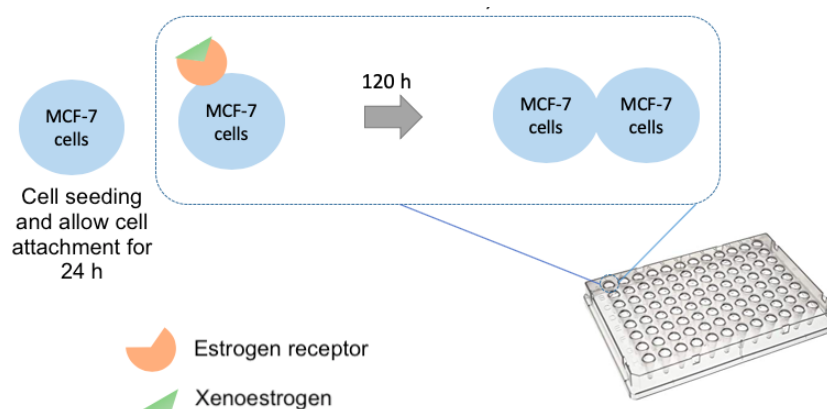
Figure 34 The concept of E-screen assay for the screening of xenoestrogen.

- YES assay is based on the ER positive genetically modified yeast, which provide the signal after the exposure of estrogen. Yeast cell wall can limit the penetration of lipophilic compounds, results in and increased specificity (273). Due to the use of recombinant yeast, YES assay could not provide the biological reaction represented in mammalian and human cell accurately (274).

Though various methods have been developed for estrogen detection, the assays are not perfect and shows various limitations as well as the different results when tested in the same compound. Thus, the advance biosensors are required these days. The ideal estrogenic detection should provide high sensitivity, specificity, eliminate pre-treatment step, low-cost, and user-friendly. At the same time, the estrogenic contaminants are increasing and resulting in various adverse effects in many living organisms, which is urgent for us to develop new technology to overcome these problems.

CHAPTER III MATERIALS AND METHODS

3.1 Laboratory instruments and equipment

-20°C freezer	Panasonic, Japan
-80°C deep freezer	Eppendorf, Germany
4°C refrigerator	Sharp, Japan
24-well cell culture plate	Biofil, China
96-well cell culture plate	Nest, China
Analytical balance	Mettler Toledo, Switzerland
Autoclave	Hirayama, Japan
Autopipette 0.2-2 µl	Mettler Toledo, Switzerland
Autopipette 2-20 µl	Mettler Toledo, Switzerland
Autopipette 20-200 µl	Mettler Toledo, Switzerland
Autopipette 100-1000 µl	Mettler Toledo, Switzerland
Beaker (50, 100, 250, 500 and 1000 ml)	Schott Duran, Germany
Cell culture flask (25 cm^3)	Nest, China
Cell culture flask (75 cm^3)	Nest, China
Centrifuge	Heraeus, Germany
Centrifuge tube (15 and 50 ml)	Nest, China
CO_2 incubator	Thermo Scientific, USA
Computer desktop for impedance analyzer	Dell, USA
Confocal microscope	Zeiss, USA
Cryovial tube 2 ml	Nest, China
Disposable serological pipette (5, 10, 25 ml)	Nest, China
Double-sided silicone adhesive tape (INT TA10)	Intertronics, UK
ECIS cell cultureware (8w20idf)	AppliedBiophysics, USA
ELISA plate reader	PerkinElmer, USA
Glass bottle (250, 500 and 1000 ml)	Schott Duran, Germany
Hemocytometer	Hausser Scientific, USA
Hot air oven	Memmert, Germany
Hot plate	IKA, Germany

Impedance analyzer	Palmsens, Netherlands
	Gamry, USA
	Solartron, USA
Interdigitated gold electrode (DRP-G-IDEAU10)	Metrohm Dropsens, Spain
Inverted light microscope	Olympus, Japan
Laminar flow	Airtech, USA
Laser cutter	Epilog Mini 18 Laser, USA
Light microscope	Olympus, Japan
Membrane insert (Polycarbonate) 24-well size	Corning, USA
Microcentrifuge	Eppendorf, Germany
Microcentrifuge tube 1.7 ml	Sorenson, USA
Micromilling machine	Minitech, USA
Microplate reader	TECAN, Switzerland
Multifunctional I/O device	National Instruments, USA
Petri dish (35 and 100 mm diameter)	Nest, China
Scanner	HP, USA
Scanning electron microscope	JEOL, Japan
Semiconductor wafer processing tape (SWT 20+R)	Nitto, Belgium
Sterile syringe filter 0.2 µl	Corning, USA
Syringe needle	Nipro, Thailand
Tip 10 µl	Corning, USA
Tip 200 µl	Corning, USA
Tip 1000 µl	Corning, USA
Vortex mixer	FINEPCR, Korea
Water bath	Memmert, Germany
Wax printer	XeroxColorcube, USA

3.2 Chemicals and reagents

17ß-Estradiol	Sigma-Aldrich, USA
4′,6-diamidino-2-phenylindole (DAPI)	Cell Signaling Technology, USA
α-Melanocyte stimulating hormone or α-MSH	Sigma-Aldrich, USA
Acetic acid	Sigma-Aldrich, USA
Anti-Glyceraldehyde 3-phosphate dehydrogenase antibody	Abcam, USA
Anti-rabbit IgG Alexa flour (R) 488	Cell Signaling Technology, USA
Arbutin	TCI, USA
Bisphenol-A	Sigma-Aldrich, USA
Bisphenol-AF	Sigma-Aldrich, USA
Bisphenol-F	Sigma-Aldrich, USA
Calcein-AM	Invitrogen, USA
Carbon sensor paste (Code no. C2030519P4)	SunChemical, USA
Charcoal stripped fetal bovine serum	Sigma-Aldrich, USA
Crystal violet	PanReac AppliChem, USA
Dulbecco's Modified Eagle Medium	Hyclone, USA
Dimethyl sulfoxide (Molecular grade)	Sigma-Aldrich, USA
Fetal bovine serum	Hyclone, USA
Insulin growth factor-1 (IGF-1)	Sigma-Aldrich, USA
Irgarol 1051	Sigma-Aldrich, USA
Kojic acid	Sigma-Aldrich, USA
L-glutamine	Sigma-Aldrich, USA
Matrigel	Corning, USA
Methanol	Merck, USA
Minimum Essential Medium (MEM)	Sigma-Aldrich, USA
Non-essential amino acid (NEAA)	Sigma-Aldrich, USA
Penicillin and streptomycin	Sigma-Aldrich, USA
Phenol red-free DMEM	Corning, USA
Phosphate buffer saline	Hyclone, USA
Polydimethylsiloxane	Sylgard, USA
Potassium ferri(III)cyanide	Sigma-Aldrich, USA

Potassium ferro(II)cyanide	Sigma-Aldrich, USA
Propidium iodide	Corning, USA
Paraformaldehyde	Merck, USA
Silver conductive glue	Epoxy Technology, USA
Sodium chloride	Merck, USA
Sodium hydroxide	Merck, USA
Sodium pyruvate	Sigma-Aldrich, USA
Sulforhodamine (SRB)	Sigma-Aldrich, USA
Trichloroacetic acid	Sigma-Aldrich, USA
Tritonx-100	PanReac AppliChem, USA
Trizma base	Sigma-Aldrich, USA
Trypan blue	Sigma-Aldrich, USA
Trypsin-EDTA	Cell Signaling Technology, USA
Paraformaldehyde	Merck, USA

3.3 Cell culture

B16 F10 mouse melanoma cells were purchased from the American Type Culture Collection (ATCC, USA). B16 melanoma 4A5 mouse melanoma cells, Mardin Darby Canine Kidney (MDCK) cells, and MCF-7 cells were purchased from the European Collection of Authenticated Cell Cultures (*ECACC*). B16F10, B16 melanoma 4A5, and MDCK cells were cultured in standard T75 cm^2 flasks and incubated in Dulbecco's Modified Eagle's medium or DMEM with 10% fetal bovine serum, 2 mM L-glutamine, 100 U mL^{-1} penicillin, and 100 U/ml streptomycin. MCF-7 cells were cultured in Minimum Essential Medium Eagle (MEM) with 10% fetal bovine serum, 1% Non-essential amino acid, 1mM Sodium pyruvate, 2 mM L-glutamine, 100 U/ml penicillin, and 100 U/ml streptomycin. Cells were incubated at 37 °C in a humidified incubator with a 5% CO$_2$ atmosphere.

Prior to seeding cells on the paper, cell suspensions were prepared by standard trypsinization using a trypsin-EDTA solution. Cells were centrifuged at 1500 rpm, 25 °C for 5 min. The cell number was determined by using a NucleoCounter NC-200 or a standard hemocytometer. The desired cell densities were prepared by diluting the initial cell suspension with the culture medium.

3.4 Design and fabrication of the paper-based scaffold for melanoma cell culture

The pattern of the paper-based scaffold was designed using Photoshop CS4 and 2020 software. Figure 35a shows a pattern of paper for anti-melanogenic screening. The paper contains 3 cell culture zones and 1 blank zone. Each zone has 5 mm diameter. Figure 35b shows a pattern of paper membrane insert for the invasion assay. The paper contains one circular 10 mm-cell culture zone in the middle. A paper has 45x45 mm size, which fits with the invasion device. Xerox ColorQube 8870 printer was used to print wax patterns onto one side of a sheet of cellulose filter paper. The papers were baked on a hot plate at 150 °C for 2 min to melt the wax through the thickness of papers. After cooling, the wax solidified in the paper and became a hydrophobic wall (90). Prior to cell seeding, the paper-based membrane insert was coated with 500 μg/ml Matrigel (Corning, NY, USA) in sterilized 0.7% NaCl (275) diluted Matrigel on the paper, and then cured at 37°C for 2 h. On the other hand, the paper for anti-melanogenic screening does not need gel coating before cell seeding step.
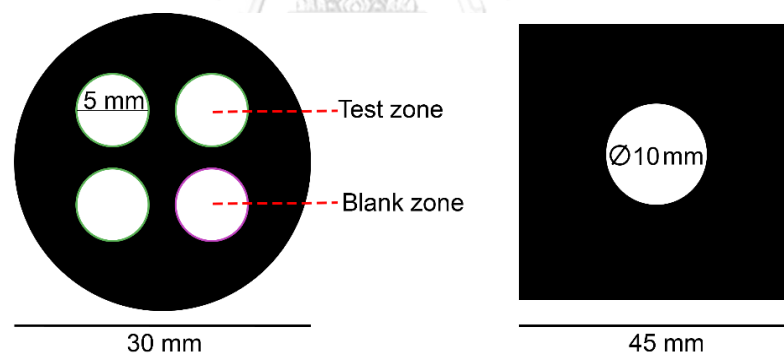
Figure 35 Patterns of the paper for a) anti-melanogenic screening and b) a membrane insert for the developed real-time invasion assay device.

3.5 Sterilization of papers

After paper fabrication, the wax printed paper was placed under UV lamp with the intensity of 40 μW/cm2 and the wavelength of 254 nm   on both the front and back sides of the paper for 15 min each before Matrigel coating step.

3.6 Sterilization of cell cultureware

Prior to cell seeding, the resusable cell culturewares including beakers, forceps, pipette tips, cryovials, and glass bottles were sterilized using autoclave at 15 psi, 121℃ for 30 min and air-dried at 65℃ overnight.

3.7 Optimization of cell culture conditions for melanoma cell culture on the paper and its application for melanin content screening

      3.7.1 Optimization of paper types, design, and incubation time

In order to find the most suitable type of paper for paper-based melanoma cell culture, 200,000 cells of the B16F10 cell line were suspended in Matrigel and seeded on the Whatman No. 1, Whatman No. 2, Whatman No. 4, CF4, LF1, and MF1. Next, cell-containing papers were incubated at 37 ℃ with 5% CO_2. After 48 h of culturing, papers were air-dried. The intensity of melanin on the paper was analyzed using ImageJ software. The same process was also performed without the use of Matrigel encapsulation. After that, the various cell concentrations were cultured on the paper to find the best concentration that fit with the test zone diameter. In brief, 100,000 200,000 400,000 and 800,000 cells of B16F10 in Matrigel were seeded on the paper with a test zone of 5 and 10 mm in diameter. Cell-containing papers were incubated at 37 ℃ with 5% CO_2. After 48 h of culturing, papers were air-dried. Next, the intensity of melanin on the paper was analyzed using ImageJ software. To find the least incubation time which is suitable for analyzing the melanin amount using ImageJ software, 200,000 cells of B16F10 in Matrigel were seeded on the paper. The cell containing paper was incubated at 37 ℃ with 5% CO_2. Next, melanin intensity on the paper was analyzed after 24, 48, 72, 96, and 120 h of incubation using ImageJ software.

      3.7.2 Confirmation of the cell morphology and cell viability on the Paper

B16F10 at a concentration of 200,000 cells were suspended in Matrigel and seeded onto Whatman No. 1 filter paper. The cell-containing paper was incubated at 37 ℃ with 5% CO_2. After 48 h of culturing, the paper was air-dried. To confirm 3D cell morphology, after sputter-coating with gold, the surface morphology of all samples was monitored with a scanning electron microscope (SEM).

To determine the biocompatibility of paper and viable cells, cell viability assay was performed after 24, 48, 72. 96, and 120 h of culturing. The paper was washed twice

using a phosphate buffer solution or PBS, and then fluorescently stained with a solution of calcein-AM (4 µg/ml in PBS) and propidium iodide (4 µg/ml in PBS) for 20 min at 37 °C in an environment of 5% CO_2. After that, the paper was washed with PBS twice before imaging with a confocal microscope (100-micron resolution images). The fluorescent images captured 5 fields before analyzing the intensity of calcein-AM and propidium iodide of each picture using ImageJ software. The average intensity of calcein-AM and propidium iodide of the 5 captured images was calculated as the mean intensity and converted to the percentage of cell viability from the ratio of living cells to total cells (living and dead cells).

3.7.3 Melanin content determination on the paper-based scaffold

The concentrated phenol red-free Matrigel (8.5 mg/ml protein concentration) was mixed with B16F10 cells with a ratio of 1:1. Afterwards, 5 µl of cell suspension was pipetted onto the test zone of the paper before placing in 2 ml of phenol red-free DMEM with 10% fetal calf serum, 4 mM L-glutamine 100 U/ml penicillin, or 100 U/ml streptomycin with or without α-MSH, Kojic acid, or Arbutin. Paper was incubated at 37 °C in a humidified incubator with a 5% CO_2 atmosphere. After incubation, paper was removed from the culture vial and air died. The dry paper was scanned by using a HP Deskjet F300 series scanner at a resolution of 600 dpi and the intensity was analyzed by using ImageJ software. After importing to ImageJ, the color RGB images were split and the blue channel image was used for analyzing the intensity of melanin on the paper (Figure 36).
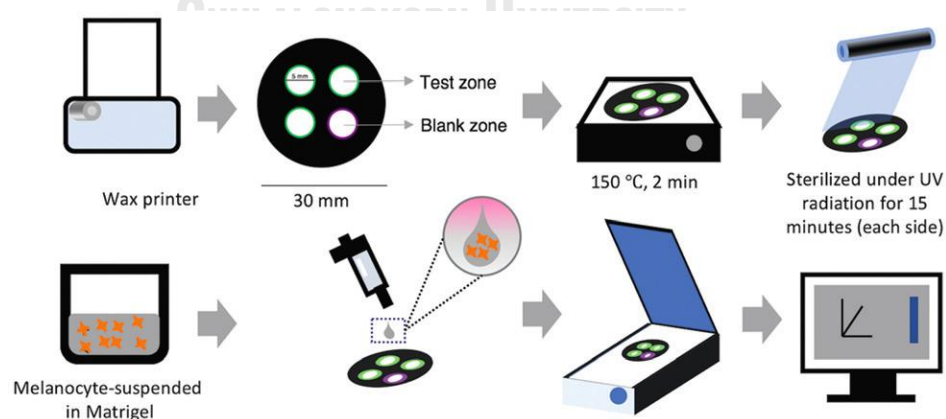
Figure 36 The experimental setup of paper-based 3D cell culture for screening melanin quantification

(Reproduced from ref. 111 by permission of The Royal Society of Chemistry)

3.7.4 Conventional melanin content analysis

B16F10 cells were seeded into the 6-well plate and allow to attach for 24 h. Next, cells were treated with α-melanocyte stimulating hormone or α-MSH or natural compounds (Kojic acid and Arbutin) for 48 h. α-MSH was used for confirming the melanin color on the paper. The suspension of cells and culture medium served as the negative control. After treatment, cells were washed twice with phosphate-buffered saline or PBS and trypsinized in 0.25 (% v/v) trypsin EDTA solutions. The collected cells were centrifuged at 13,000 g for 15 min. Cell pellets were dissolved in 1 N NaOH at 80 °C for 1 h. The relative melanin content was determined by measuring the absorbance at 475 nm on an ELISA plate reader (276).The percentage of produced melanin was determined using equation [4].

$$\frac{OD_{Test}}{OD_{Blank}} \times 100 = \% \text{ melanin production} \quad [4]$$

OD_{Test} represents the absorbance of produced melanin under the treatment of α-MSH (positive control) or natural compounds. OD_{Blank} represents the absorbance of produced melanin from untreated cells.

3.7.5 Detection of Glyceraldehyde-3-phosphate Dehydrogenase (GAPDH) of

B16F10 cells on the paper

B16F10 at a concentration of 200,000 cells were suspended in Matigel and seeded on the paper. The cell-containing paper was incubated at 37 °C with 5% CO_2 for 48 h. Afterwards, cells were fixed with 4% paraformaldehyde and permeated with 0.5% Tritonx-100. After that, cells were captured with anti-GAPDH antibody as a primary antibody and anti-rabbit IgG Alexa flour (R) 488 as a secondary antibody, respectively. The nucleus was stained with DAPI. The fluorescent image was then captured by using a confocal microscope.

3.8 The initial impedance characteristic study for cell culture and its application for real-time xenoestrogenic screening (Impedance-based E-screen assay)

3.8.1 Instrumentation and experimental setup

In order to characterize the sensitivity of the interdigitated electrode configurations, we applied 2 types of gold interdigitated electrode: 10 and 350 μm gaps. The 350 μm gap-electrodes were built-in with the cultureware (Figure 37a) while the 10 μm

gap-electrodes (Figure 37b) are bare. Therefore, the culture well had to be fabricated for 10 µm gap-electrode insertion. The cultureware was fabricated using micromilling machine, which consists of 8 wells (Figure 37c).

After cell seeding, the 350 µm gap-electrodes built-in cultureware was placed to the contact board for electrical connection. Cell proliferation was measured using Solartron 1260/Gain-Phase analyze. The measurement was performed automatically from well to well using digital I/O device as a multiplexer (Figure 37d). The 10 µm gap-electrodes containing device was connected to Palmsens4. The impedance measurement was performed automatically from well to well using the script setting in the PS trace software (Figure 37d). Both Palmsens4 and Solartron impedance analyzer are connected to one computer. AC applied potential of 5 mV was applied. Full spectra were acquired measuring 10 points over a frequency of 100 Hz to 1 MHz. Cells-seeded devices were incubated at 37 °C in a humidified incubator with a 5% CO_2 atmosphere throughout the experiment. The experiment was inspected remotely through mobile application, TeamViewer software.
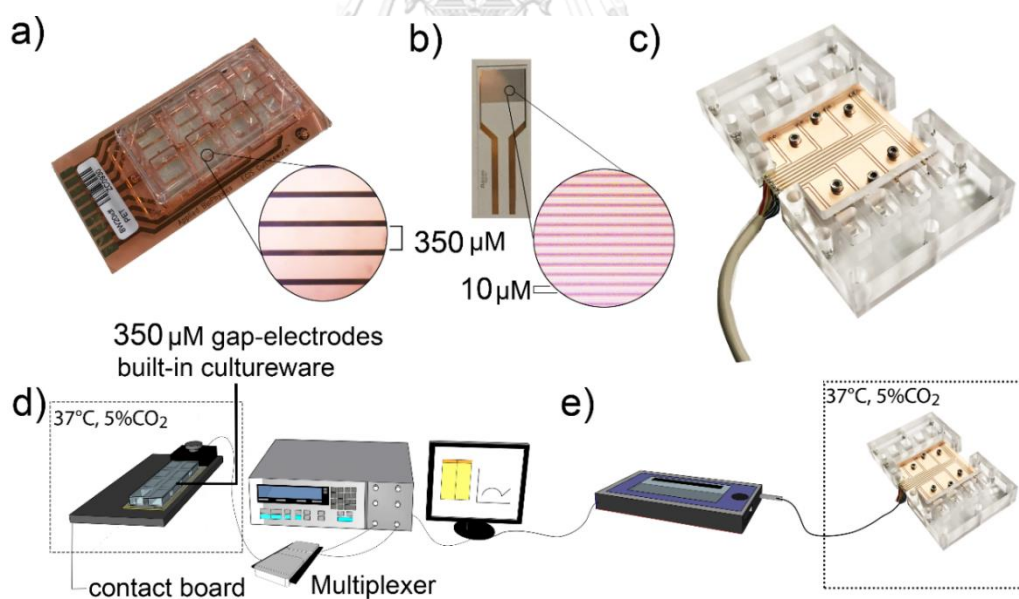
Figure 37 The choices of electrode used for primary impedance characteristic study. a) 350 µm gap-electrodes built-in cultureware b) the 10 µm gap-electrodes c) the integrated 10 µm gap-electrodes culture device d) the experimental setup of 350 µM gap-electrodes built-in cultureware e) the experimental setup of 10 µm gap-electrodes

In order to monitor cell proliferation over time, the impedance magnitude was converted to cell index (CI) using equation [5] (277),

$$\text{Cell index (CI)} = \max_{i=1,2,\dots,N} \frac{|Z\,(t,f_i)| - |Z\,(0,f_i)|}{|Z\,(0,f_i)|} \qquad [5]$$

where $|Z\,(t, f_i)|$ is the impedance magnitude at a specific frequency and time point and $|Z\,(0, f_i)|$ is the impedance magnitude at the same frequency at the time immediately after cell seeding. To determine the optimal frequency, at which the maximum value of CI was obtained, full impedance spectra were acquired at different time points and the relationship between normalized impedance magnitude (Equation 6) and log frequency was studied.

$$\text{Normalized impedance magnitude } (|Z|_{Norm}) = \frac{|Z\,(t,f_i)|}{|Z\,(0,f_i)|} \qquad [6]$$

3.8.2 Application of the primary impedance characteristic study for the impedance-based E-screen assay

To study the correlation between impedance signal and 17ß-Estradiol concentrations, cells were seeded onto the electrode using normal medium (MEM+10%FBS+Penicillin-Streptomycin). Cells were allowed to attach the electrode for 8 h before the treatment of 17ß-Estradiol or test compounds. After that, 17ß-Estradiol at the concentration of 0.001, 0.01, 0.1, 1, and 10 nM or Bisphenol-A (BPA) or Irgarol 1051 was diluted in the hormone free medium (Phenol red free DMEM+10% charcoal stripped FBS). The estrogenic effect of test substances was then monitored every hour for 144 h through the impedance measurement.

3.8.3 Conventional E-screen assay

MCF-7 cells at a concentration of 4,700 and 250,000 cells/cm^2 in normal medium were seeded in the 96 well plate. Cells were allowed to attach the well for 8 or 24 h. After that, the normal medium was replaced by the hormone-free medium supplemented with various concentrations of 17ß-Estradiol (0.001, 0.01, 0.1, 1, and 10 nM) or test compounds (BPA and Irgarol 1051). The experiment was stopped after 144 h of total incubation period (since cell seeding step). The total protein was then measured by SRB colorimetric assay (59).

In brief, cells were fixed with 10% (w/v) TCA at 4°C for 1 h. Because SRB can be solubilized in low concentration of chlorine, tap water was then used for washing the

plate after cell fixing for 4 times. After 96-well plate was air-dried, the total protein content of cells was stained with 4% SRB in 1% acetic acid for 30 min and washed with 1% acetic acid for 4 times. After the plate was air-dried, the stained total protein was dissolved in 10 mM Trizma base, and measured the absorbance at 492 nm (278). Afterwards, the xenoestrogenic effect was determined as proliferative effect (PE) using equation [7](279).

$$PE = \frac{\text{average cell number (test compound)}}{\text{average cell number (neg control)}} \quad [7]$$

3.8.4 Cell viability assay

MCF-7 cell at a concentration of 250,000 cells/cm^2 was seeded in 96 well plate using normal medium for 8 h. The medium was then replaced by 0, 0.001, 0.01, 0.1, 1, and 10 nM of 17 ß -estradiol in hormone-free medium. After 60 and 144 h of incubation, cells were stained with 2 µM calcein-AM and 2 µM of Ethidium homodimer-1 (LIVE/DEAD staining kit). Cells were incubated at 37 ℃ for 30 min before fluorescent imaging using Nikon spinning disc confocal microscope. The intensity of calcein-AM and ethidium homodimer-1 was measured using Fiji software and converted to the percentage of cell viability from the ratio of viable cells to total cells.

3.8.5 Statistical analysis

The results of all the experiments are expressed as the mean ± standard error of mean. The differences of MCF-7 cell seeding after 8 and 24 h was studied by paired T-test. P value of less than 0.01 was considered statistically significant (P ≤ 0.01). The xenoestrogenic effect of Irgarol using conventional E-screen assay was studied using one-way ANOVA analysis. P value of less than 0.05 was considered statistically significant (P ≤ 0.05).

3.9 Optimization of culture conditions and fabrication process of the integrated paper membrane insert for real-time invasion assay device

3.9.1 Invasion assay device and electrode fabrication

The invasion assay device consists of four layers, which are the stencil-printed electrode on polymethyl methacrylate (PMMA), a spacer between the working electrode (WE) and paper, a paper membrane insert, and a cell culture vial. Other than the stencil-printed electrode layer, every layer is 45x45 mm size. To limit the cell culture contamination, a culture vial was closed with a plastic lid made of

PMMA, which was specially fabricated for inserting the rod shape counter electrode (CE). The cell culture vial, spacer between WE and paper, and plastic lid were designed by using Autodesk Inventor Professional 2019. The designs were then converted to G-code using CimatronE 12.0 software and fabricated with a micromilling machine. Cell culture vial was made of PMMA, which was designed to have one central vial of 10-mm inner diameter, 30-mm outer diameter, and 8-mm thick cylindrical shape for adding the cell culture medium. Thus, the total volume of the cell culture vial was 628 µl. To create chamber for loading chemoattractants, a spacer between the WE and paper was designed to have one chamber of 10-mm diameter and 1.5-mm thick cylindrical shape in the center, made of PMMA. Next to the central chamber in the spacer, two microchannels were fabricated on each left and right side, connected to the chamber. One channel on the left was engraved from the top of the spacer with 1 mm depth. The channel on the right was engraved from below side of the spacer with 1 mm depth. The top channel on the left was placed by 1/32 microfluidic tube (outer diameter 0.8 mm, inner diameter 300 µm) to release the liquid tension within the lower chamber. The below channel was attached to the 1-ml syringe for medium or chemoattractant loading. Both the syringe needle (Nipro, no.21) and the microfluidic tube were glued with the channels by PDMS (1:100 Sylgard 184 curing agent: silicone elastomer base).

To fabricate the WE, we used a semiconductor wafer processing tape as a stencil. The stencil was then attached to the 100x100x1.5 mm thick PMMA. The printed carbon structure (designed using CorelDRAW X8) comprised a circular WE (Ø 10 mm) and a 43x4 mm2 rectangular part that served as a lead and contact pad. After attaching a stencil to PMMA, stencil was then cut to the electrode shape using a CO_2 laser cutter machine with 100% speed, 15% power, and frequency of 2500 Hz. We peeled off the cut stencil before spreading the carbon sensor paste on the PMMA by using a polydimethylsiloxane (PDMS)-made squeegee. The rest of the stencil was peeled off immediately after carbon ink spreading. The carbon was cured at room temperature (RT) for 72 h before being assembled with the rest of the device. To facilitate the connection of the WE with the impedance analyzer, the conductive wire was connected to the contact pad of the stencil-printed electrode by using a silver conductive glue. To assemble the device, the components of the device were assembled using double-sided silicone adhesive tape that was laser cut (15% power,

100% speed, and frequency of 2500 Hz) according to the dimensions of the device. A schematic view of the assembly is shown in Figure 38.
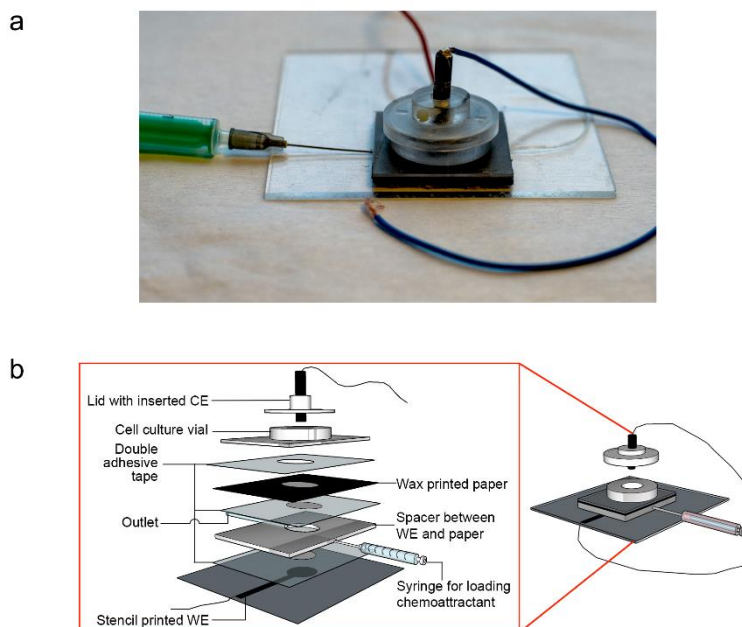
Figure 38 The image of fabricated invasion assay device and schematic diagram representing the layers of the fabricated invasion assay device (left) and the assembled device (right).

(This picture was modified from ref. 280.)

3.9.2 EIS characterization of the device

In order to characterize the different steps of device setup, EIS measurements were used applied. The steps of device optimization consist of (1) stencil printing of carbon WEs, (2) types of CE, (3) distance between the WE and CE, (4) choice of paper for the insert (Whatman filter paper No.1 and No.4 from GE healthcare), and (5) effect of Matrigel coating (from a 500 μg/ml solution in sterile 0.7% NaCl for 2 h at 37 °C) of the paper insert. The measurements were performed in PBS containing 10 mM potassium hexacyanoferrate(II/III) using a Palmsens 4. Impedance spectra were acquired by applying 10 mV$_{rms}$ sinusoidal potential over a frequency range of 100 Hz to 1 MHz (10 points per decade). Initially, for characterizing the performance of the stencil printed WEs, a gold coated silicon plate (10x25 mm^2) was used as the CE. During characterization of the paper inserts (before and after Matrigel coating) in an

assembled device, 450 μl and 150 μl of the potassium hexacyanoferrate solution was introduced in the upper and lower compartment, respectively.

3.9.3 Device preparation and the experimental setup for real-time invasion assay

After fabrication of the device components, the stencil printed WE, spacer, and cell culture vial were sterilized by soaking in 500 mM NaOH for 15 min followed by rinsing twice in PBS and sterile water. The sterilized components were air-dried prior to assembly. All the preparation steps, the UV sterilization of paper, and the device assembly (see section *3.8.3*) were done on a laminar flow bench. Prior to cell seeding, the paper insert was coated with 500 μg/ml Matrigel in sterilized 0.7% NaCl. Cell suspension in DMEM without FBS (450 μl) was placed in the cell culture vial (upper compartment). The lower compartment was filled with 150 μl of DMEM without FBS through the attached syringe. The device was closed with the lid containing the inserted glassy carbon (GC) CE. Cells were stabilized by incubating at 37 °C in a humidified incubator with 5% CO_2 atmosphere for 24 h. After that, the medium in the lower compartment was replaced by 150 μl of culture medium containing either IGF-1 (100 ng/ml) without FBS or only FBS. The cell-containing device was incubated at 37 °C in a humidified incubator with 5% CO_2 atmosphere throughout the experiment. EIS measurements (Palmsens 4 potentiostat) were performed using the same parameters as described in section 4. Cellular invasion through the paper was tracked by acquiring an impedance spectrum every 1 h for 47 h in total (Figure 39).
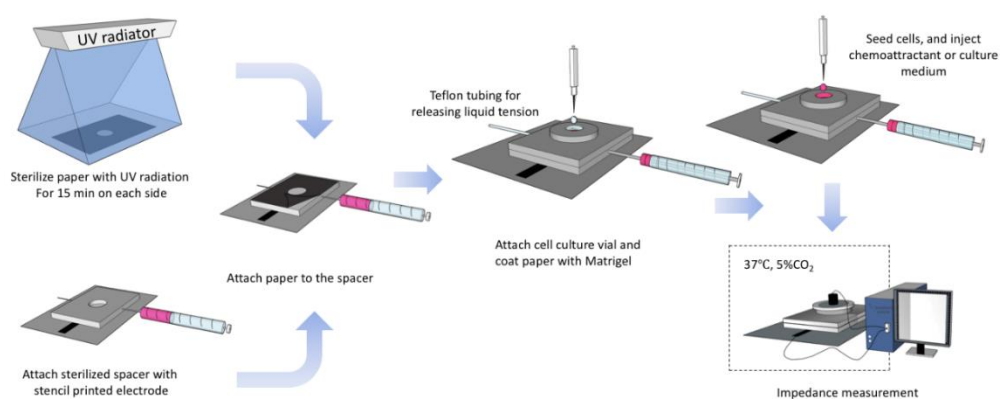
Figure 39 Experimental setup of the real-time invasion device for melanoma cells under IGF-1 treatment

(This picture was modified from ref. 280.)

3.9.4 Impedance data analysis

In order to monitor the invasion of cells through the thickness of paper over time, the change in the impedance magnitude was converted into cell index (CI) using equation [5]. To determine the frequency, at which the maximum value of CI was obtained, impedance spectra were acquired at different time points and the relationship between normalized impedance magnitude, calculated from equation [6] and log frequency was studied.

3.9.5 Biocompatibility testing of the invasion assay device and the confirmation of cell invasion using confocal microscopy

After the device was assembled, 800,000 cells of B16 melanoma 4A5 cells in culture medium (total volume 450 μl) were seeded on Matrigel-coated paper insert in the upper compartment and cultured as described above. The medium was changed every 24 h. After 4, 8, 12, 24, and 48 h of incubation, a solution containing calcein-AM and Propidium Iodide (PI) (both at 4 μg/ml in PBS) was added into the upper compartment and kept for 20 min at 37 °C in the incubator. The paper with the stained cells was then removed from the device with a scalpel and washed with PBS twice before imaging with confocal microscope. Fluorescent images were captured in five fields and the intensity of calcein-AM and PI in each image was analyzed using ImageJ software. The average intensity of calcein-AM and PI of the five captured images was calculated and converted to percentage of cell viability using the ratio of live cells to the total number of cells.

To confirm the invasion of cells through the paper, the Z-stack imaging was taken using confocal microscope (20 stacks, 160 μm thickness). The intensity of Calcein-AM on the top and through the thickness of the paper was compared between IGF-1, or FBS treatment with negative control (DMEM without FBS).

3.9.6 Scanning electron microscopy

In order to confirm cell invasion through the paper, B16 melanoma 4A5 at a concentration of 800,000 cells were seeded onto Matrigel-coated Whatman No. 1 filter paper. The cell-containing paper was incubated at 37 °C with 5% CO_2. After 47 h of real-time invasion assay, paper was cut out of the device using a scalpel and sputter-coated with gold. The surface morphology of all samples was monitored with a scanning electron microscope (SEM).

3.9.7 Conventional invasion assay

The 8-µm pore size polycarbonate membrane insert was coated with 500 µg/ml Matrigel in sterilized 0.7% NaCl. A membrane insert was then cured at 37°C for 2 h. The membrane insert was then placed in the 24-well plate. 5,000 B16 melanoma 4A5 cells in cell culture medium without FBS were then seeded on the Matrigel-coated membrane insert and incubated for 24 h to stabilize the experiment. After that, culture medium without FBS was removed. 500 µl of cell culture medium without or with 10% FBS or 100 ng/ml IGF-1 was then added under the membrane insert. 250 µl cell culture medium without FBS was added above the membrane insert. A well plate was incubated at 37 °C in a humidified incubator with a 5% CO_2 atmosphere for 24 h. Non-invading cells were then removed by cotton swab. Cells were fixed with 100% methanol and stained with crystal violet respectively. Invading cells were counted under the light microscope (281). The experiment was repeated 3 times.

CHAPTER IV RESULTS

Part I Paper-based melanoma culture for melanin content screening

In this thesis, author has divided the results into three parts. The first part is the initial optimization of paper for melanoma cell culture, which later was applied for screening anti-melanogenic substances through the visualization of melanin color on the paper. The second part is the primary study of impedance characteristic of cells. In the second part, author obtained the optimal impedance parameters, which are suitable for long term cell culture and can be applied for the third part of the PhD project. Also, those parameters were applied into the parallel project for the development of the impedance-based E-screen assay, which can be found in part II of chapter IV. The third part is the application of optimized conditions, obtained from part I and II to develop the paper-based real-time invasion assay device.

In part I, author aims to optimize various types of paper for culturing melanoma cells. However, there are plenty of melanoma cell lines in the market nowadays. In this thesis, we chose B16F10 as a primary choice of cells to optimize the culture conditions due to the well response to the anti-melanogenic treatment obtained by our colleague, Dr. Moragot Chatatikun (276). Since the optimized parameters from part I were further applied in part III, the compatibility of optimized conditions with B16 melanoma 4A5 cell line (used in the third project) was also considered and explained in this part. The detail of the optimized conditions can be found in detail below.

4.1. Culture conditions of melanoma cells on the paper-based scaffold

Currently, paper can be used as an alternative scaffold for 3D cell culture in various cell types. However, the reports of paper-based scaffold for cell culture are lack of the information regarding skin cell study. Since the work requires the visualization of melanin color on a paper directly, the paper types, design of cell culture zone, the modification of paper, the incubation period, and cell seeding number were studied.

4.2 Optimization of paper types

There are plenty of paper choices available in the market. However, to apply into the cell culture, the sterilization is a key. According to the literature search, Whatman filer paper has mostly been used for cell culture application due to the variability of

pore sizes, thickness, and cleanliness (282). In this work, we considered Whatman filter paper no.1, no.2, no.4, MF1, LF1, and CF4 due to the variability of pore size, thickness, and fiber type given below (Table 5).

Table 5 The comparison of paper properties used in this work (Whatman filter paper catalog).

Paper	Pore size (μm)	Thickness (μm)	Material
Whatman no. 1	11	180	Cellulose
Whatman no. 2	8	190	Cellulose
Whatman no. 4	20-25	205	Cellulose
MF1	≤ 2	367*	Glass fiber
LF1	≤ 2	-	Glass fiber
CF4	-	482*	Cellulose

* GE Healthcare catalog

In order to obtain the highest intensity of melanin color on the paper, melanoma cells should be able to attach on or in the paper scaffold after soaking in the culture medium. Matrigel has been used in paper-based 3D cell culture by Whitesides group. Cells were mixing with Matrigel before placing onto the paper. This technique is called Cells-in-Gel-in-Paper or CiGiP. The use of Matrigel provides the advantage of cell encapsulation due to the state transition based on the temperature. In brief, Matrigel is a liquid at 4°C and become solid at 37 °C. Thus, after mixing cells with Matrigel and placed on the paper at 4 °C, cell suspension was still in a liquid state. Afterwards, cell-containing paper was incubated in the 37 °C incubator, resulting in the solidified encapsulated cells in the paper. The solidified state of Matrigel can prevent cells from passing through the paper pores. We then compared the melanin intensity between with and without Matrigel encapsulation on the selected types of paper. To eliminate errors resulting from culture medium color, we used phenol red free DMEM medium when culturing on paper.

Figure 40 shows that the culture of cells on the paper without gel encapsulation caused the low intensity of the melanin on the paper when compared to the

Matrigel encapsulation. Due to the passing of cells through the pores of the paper, the low and unstable intensity of melanin on the paper were observed. The result of melanin intensity in gel encapsulation shows high dispersion among each type of paper. The differences in the mean values among the Matrigel encapsulation in each type of paper are greater than those would be expected by chance, which shows a statistically significant difference (P = 0.002) after analysis by one-way ANOVA, due to the various physiological properties of the paper, such as the thickness and pore size, which is explained in brief in the next paragraph.

Since melanoma cells used in this study, B16F10 (Figure 41a) and B16 melanoma 4A5 (Figure 41b, detail can be found in part III), are approximately the same size (10 μm), the optimization of paper type was initially studied using only B16 F10 cell line. The culture of cells on MF1, LF1, and Whatman No. 2 paper with or without gel encapsulation can cause high intensity of melanin on the paper because of the small pore size (MF1 and LF1 ≤2 μm; Whatman No. 2–8 μm; Table 5), which is smaller than the cell size (~10 μm; Figure 41). Therefore, cells attached on top of the paper without passing through the pores and behave as a 2D structure above the surface of the paper. Even though MF1, LF1, and Whatman No. 2 promoted high intensity of melanin on the papers, they are not suitable for 3D cell culture (131). Though the melanin intensity on MF1 and LF1 was high, the standard deviation in both types of the paper was large due to the difficulty in ensuring exact cell numbers on the small pore size paper, thus causing variation of melanin color on the paper. Due to the purpose of use in chromatography, CF4 is thick and stable when placed in the culture medium for a long time, but it has a high wettability property (GE Healthcare catalog); thus the paper took a very long time to dry, so it cannot decrease the duration of the conventional melanin content analysis. Moreover, the minus value of melanin intensity in CF4 was observed because the intensity of melanin on the CF4 paper was not seen when cultured with Matrigel encapsulation (Figure 40). This is due to the higher level of thickness of the CF4 paper (Table 5). As a result, a high cell number was required for the consistent distribution of cells under the culture area. In contrast, when cultured B16F10 cells on Whatman No. 1 and Whatman No. 4 filter paper with Matrigel encapsulation, the best intensity of melanin color and a statistically significant difference with CF4 paper was observed. (Figure 40), due to their suitable pore sizes, which are ~11 and ~25 μm in Whatman No. 1 and Whatman

No. 4, respectively (Whatman price catalog). Moreover, the viscous transitional property of Matrigel eases cell encapsulation and handling on the paper (283), which means that the total cells were encapsulated within the paper without passing through the pores of the paper. This result also supported that the use of paper can improve the handle and manipulation of the hydrogel for 3D cell support because the hydrogel alone has weak mechanical properties (92, 117). According to the result mentioned above, Whatman no.1 and no.4 were applied for the next experiment for B16F10 and in chapter IV, part III for B16 melanoma 4A5 cell culture.
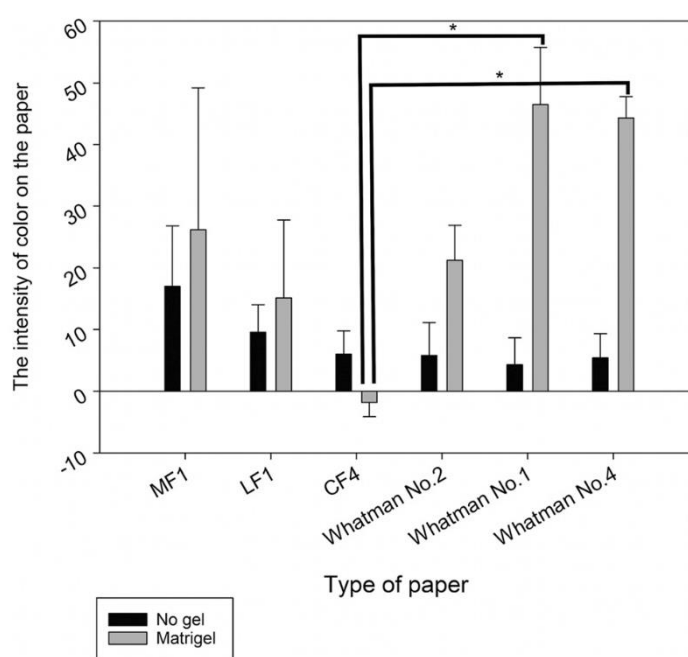
Figure 40 Optimization of paper for paper-based cell culture.

Data were analyzed by one-way ANOVA, followed by the Holm-Sidak test. Data are presented as the mean ± SD, n = 3 (*p < 0.05).

(Reproduced from ref. 111 by permission of The Royal Society of Chemistry)
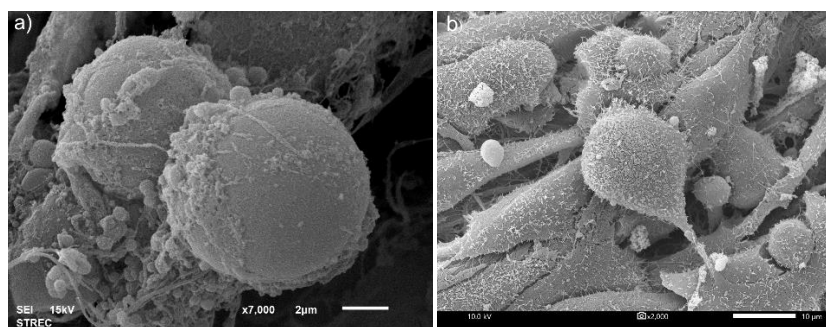
Figure 41 The scanning electrode microscope images of a) B16F10 and b) B16

melanoma 4A5 cell line in normal condition.

(Modified from ref.111 by permission of The Royal Society of Chemistry)

4.3 Optimization of paper design and cell seeding number

In order to apply paper for melanin content analysis and a membrane insert for invasion assay, the design of paper need to be compatible with the device design and contains a suitable area for melanin visualization. For melanin content analysis, we optimized B16F10 cell seeding number as well as the test zone size of the paper. In brief, Whatman No. 1 and Whatman No. 4 were used for culturing B16F10 cells in various concentrations which are 100,000 200,000 400,000 and 800,000 cells per test zone in designed paper with 5 mm and 10 mm test zone diameters. Figure 42 shows that the intensity of melanin has a direct variation with the cell number in both Whatman No. 1 and Whatman No. 4.
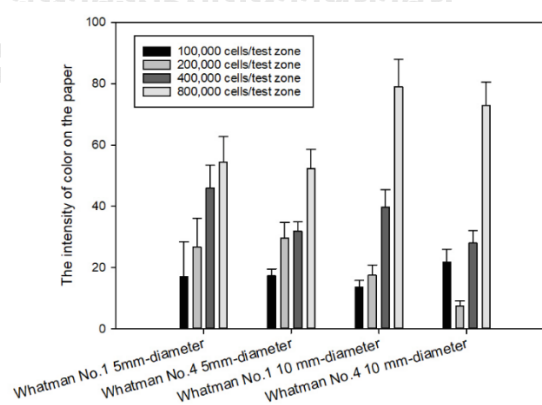
Figure 42 Optimization of cell number and test zone diameter.

Data is presented as the mean ± SD (n=3).

(Reproduced from ref. 111 by permission of The Royal Society of Chemistry)

However, the test zone with 10 mm diameter was excessive in every cell concentration and caused inconsistent distribution of melanin on the paper. The melanin color were only observed in the middle of the test zone because of the viscosity of cell-containing hydrogel. In brief, hydrogel slowly absorbed into the paper and become solidified before dissolving throughout the paper area. This leads to the mark of cells on the area where they were pipetted. In contrast, 5 mm diameter paper showed consistent distribution of melanin throughout the paper surface in cell concentrations of 200,000 400,000 and 800,000 cells per test zone (Figure 42). However, the melanin intensity on the paper was higher in Whatman No. 1, due to the 11 μm pore size (Table 5), which better fits the B16F10 cell size (~10 μm; Figure 41). Therefore, Whatman No. 1 was the most suitable paper for this work. Nonetheless, the cell concentration of 100,000 cells per test zone is too low for screening the effect of a whitening substance on melanin production (Figure 43). Thus, the lowest amount of cells which can be used for screening the effects of natural compounds on melanin production is 200,000 cells per test zone with the encapsulation of Matrigel. Although the required cell amount was around 2 times higher than conventional melanin content analysis, which normally requires 100,000 cells per well of the 6-well plate, the total volume of cells suspended in Matrigel (5 μl) was very low compared to conventional melanin content analysis.

Figure 43 Example of paper after seeding cells in various concentrations on Whatman

No. 1 and Whatman No. 4 with a test zone diameter of 5 and 10 mm

(Reproduced from ref. 111 by permission of The Royal Society of Chemistry)

4.4 Optimization of the incubation time for melanin content analysis

In the conventional method, melanoma cells were incubated approximately 48 h accessing melanin amount by the absorbance measurement (13, 14). However, the incubation time can be varied according to the treatment and cell line types. In this work, we aim to minimize the analytical time of melanin content analytical process. Thus, we optimized the most suitable incubation time for screening the melanin intensity on the paper, in order to obtain the least incubation time required for stimuli and anti-melanogenic screening. Whatman no.1 with 5 mm test zone was applied for 200,000 cells of B16F10 cell culture and incubated for 24, 48, 72, 96, and 120 h. The result showed that after culturing for 48 h, B16F10 cells produced suitable amounts of melanin that can be observed with the naked eye (Figure 43). Moreover, the intensity of melanin on the paper increased with incubation time, showing the ability of cells to produce melanin for at least 120 h during the culturing on the paper (Figure 44). According to this experiment, paper is beneficial for melanin visualization that was easily observed with the naked eye due to the contrast of the white color of the paper and the dark color of melanin. Moreover, by scanning the paper and analyzing the intensity with ImageJ software, the total analysis time took only 20 min, which is very quick compared to conventional melanin content analysis, which takes about 1 hour and 30 min (15 min to centrifuge melanoma cells, 1 hour to solubilize melanin in NaOH, and another 10 min to perform the absorbance measurement) (11).
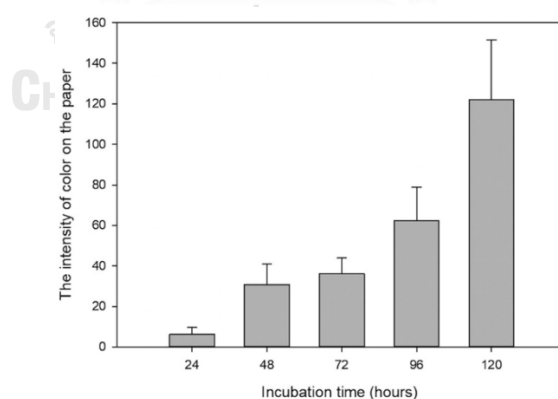
Figure 44 Optimization of the incubation time.

Data are presented as the mean ± SD (n = 3)

(Reproduced from ref. 111 by permission of The Royal Society of Chemistry)

4.5 Identification of melanoma cell morphology on the paper-based scaffold

In order to confirm whether B16F10 could behave similar to the *in vivo* structure inside the paper, we used scanning electron microscopy to access their structure inside the paper. In brief, B16F10 cells were encapsulated with Matrigel, pipetted onto Whatman No. 1 paper and incubated at 37 ℃ with 5% CO_2 for 48 h before obtaining images. Figure 45a shows the structure of naked Whatman No. 1 paper which contains fibrous pores which are suitable to be a scaffold for cell support. Figure 45b shows the 3D structure of B16F10 cells that tended to form clusters. Figure 45c shows B16F10 cells in a 3D shape surrounded by produced melanin on the paper fiber. Thus, the 3D architecture of Whatman No. 1 paper was able to provide the 3D cell culture condition. In addition, the use of Matrigel encapsulation can provide the native extracellular matrix which enables cells to behave similar to those seen *in vivo*.
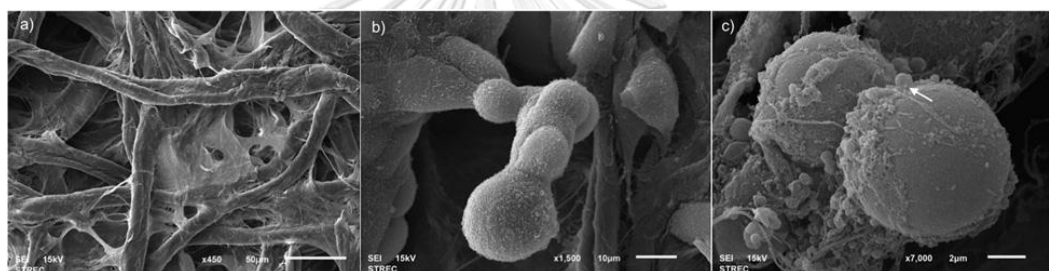
Figure 45 SEM images of microarchitecture of a) bare paper, b) melanoma tumor and c) 3D melanoma cells

(Reproduced from ref. 111 by permission of The Royal Society of Chemistry)

4.6 Identification of melanoma cell viability under paper-based cell culture

In order to perform melanin content analysis on the paper, B16 F10 should be able to survive on the paper for at least 48 h due to the optimized incubation time that melanin can be visualized. Moreover, for B16 melanoma 4A5 cell culture, the cells-containing paper had to be integrated with the newly fabricated invasion assay device which consisted of various materials. Therefore, the biocompatibility is crucial (Chapter IV, part III). To test the biocompatibility of the paper-based cell culture system and their suitability for long term cell culture, LIVE/DEAD staining was performed after culturing B16F10 cells on paper for 24, 48, 72, 96, and 144 h without changing the culture medium. After that, calcein-AM and propidium iodide (PI) were added in culture well. In brief, calcein-AM can be converted to green fluorescence after

acetoxymethyl ester hydrolysis by esterase in living cells (284). Propidium iodide (PI) binds to the double strand DNA of dead cells with the intact plasma membrane (285). Figure 46f shows that during the first 72 h the percentage of cell viability was high. At 96 and 120 h, percent cell viability decreased due to the high cell number and the limited culture medium. However, the high number of cells seen in figure 46d and e confirmed their ability to proliferate under the paper-based cell culture for up to 120 h. The result shows single viable cells in the paper after 24 h of culturing. After 48 h of culturing, cells started proliferating and forming clusters of cells. After 72 and 96 h, cell numbers were higher than after 24 and 48 h of incubation with some dead cells shown in red color. After 120 h, the cells continued forming clusters, covering almost the entire area of paper thus indicating cell proliferation (Figure 46a-e).
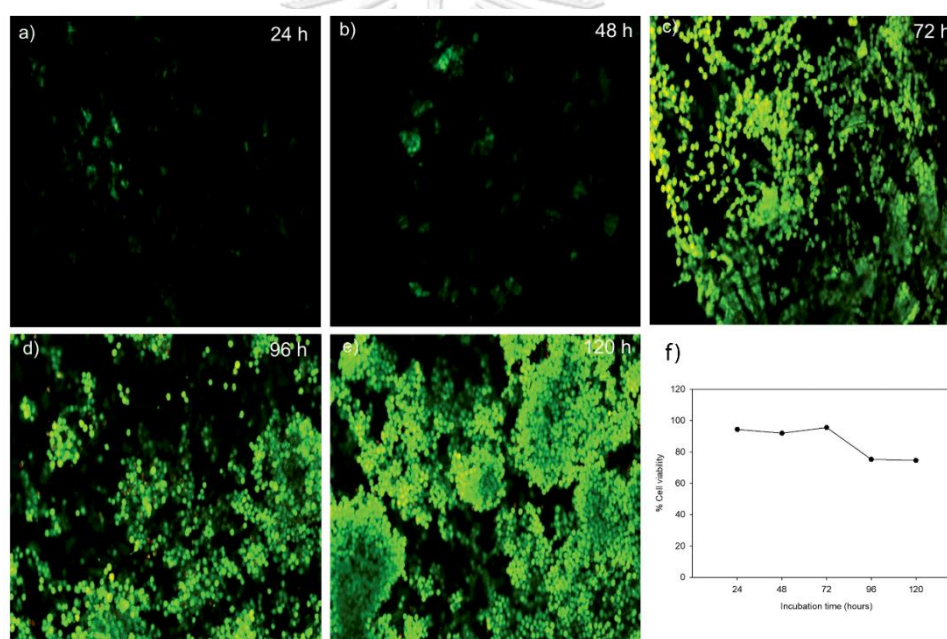
Figure 46. Confocal images of B16F10 cells and % cell viability after culturing for various incubation time.
(Green – GAPDH; Red – Propidium iodide; 100-micron resolution images)
(Modified from ref.111 by permission of The Royal Society of Chemistry)

4.7 Confirmation of melanin color on the paper-based scaffold

α-Melanocyte stimulating hormone or α-MSH is known as a melanotropic hormone and a major physiologic stimulus for murine pigmentation (286-288). Therefore, we applied α-MSH in B16F10 cell culture on the paper, in order to confirm that the color seen in the

paper was from the produced melanin. **α**-MSH at a concentration of 0, 0.1, 1, and 10 μM was suspended in the culture medium after placing paper in culture well. The conventional absorbance measurement was performed to confirm the percentage of melanin production under **α**-MSH treatment. Figure 47 shows the direct correlation between **α**-MSH and the intensity of color on the paper. Intensity of melanin at 0 μM **α**-MSH can be observed because initial seeded melanoma cells naturally produce melanin without **α**-MSH stimulation. Above each bar of figure 47 is shown an example of increased color on the paper with higher concentrations of **α**-MSH, confirming that the color on the paper was a produced melanin from B16F10 cells.
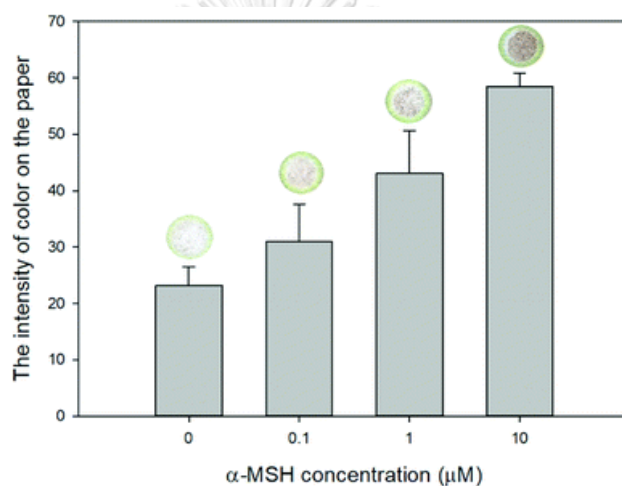
*Figure 47 The intensity of melanin on the paper under **α**-MSH treatment at various concentrations.*
Data are presented as the mean ± SD (n = 3)

(Reproduced from ref. 111 by permission of The Royal Society of Chemistry)

Next, we confirm the existence of the living cells by using immunofluorescence staining of Glyceraldehyde 3-phosphate dehydrogenase or GAPDH. GAPDH served as the internal control of the experiments due to the constant expression of the GAPDH gene, which can be found in the cells (289) (represented in green color in figure 47). Also, nuclei were stained by DAPI, a DNA-specific probe, allowing the fluorescent imaging of nuclei (represented in blue color of figure 47) (290). Figure 48 shows the immunofluorescent image of GAPDH of B16F10 on the paper-based scaffold. Some stained cells were unclear due to the obstruction of fibers in the paper. Therefore, this image can confirm that the paper-based scaffold contains living B16F10 cells.
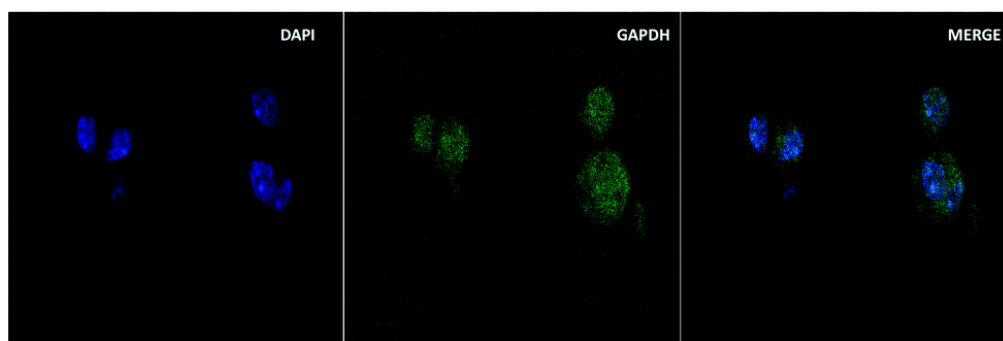
Figure 48 GAPDH staining of B16F10 cells on the paper

(green – GAPDH; blue – DAPI; 1000-micron resolution images)

(Reproduced from ref. 111 by permission of The Royal Society of Chemistry)

4.8 Comparison between the percentage of melanin production with the conventional method (Absorbance Measurement) and melanin intensity on the paper-based scaffold

To compare the melanin production between the conventional assay and paper-based scaffold, B16F10 at the concentration of 200,000 cells were seeded in a 6-well plate and paper-based scaffold. Cells were then treated with α-MSH at a concentration of 0.1, 1, and 10 μM. The percentage of melanin production in the conventional method was found to be increased by the higher α-MSH concentrations. Moreover, percentage of melanin production showed a direct proportion with the intensity of melanin on the paper when treated with the same concentration of α-MSH with the conventional method (Figure 49). This result confirmed that the intensity of melanin on the paper was consistent with the percentage of melanin production in the conventional assay.
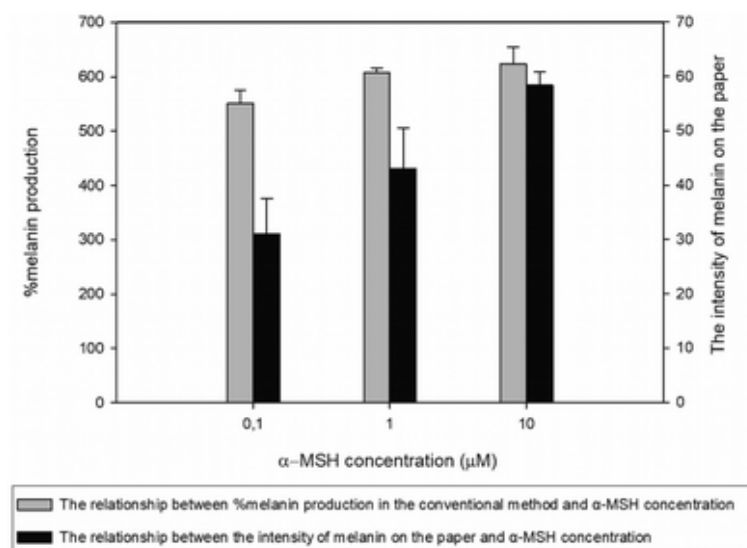
Figure 49 Bar graph shows the relationship between % melanin production in the

*conventional method and the intensity of melanin on the paper with **α**-MSH at a*

concentration of 0.1, 1, and 10 µM.

Data are presented as the mean ± SD (n = 3).

(Reproduced from ref. 111 by permission of The Royal Society of Chemistry)

Several studies have used paper as a scaffold for cell culture. Yet, there is no evidence on paper-based melanoma cell culture for the melanin study. In this work, we first applied a paper-based scaffold for melanoma cell culture for screening the effect of natural compounds on melanin production. We confirmed that the melanin color on the paper can reflect the effect of treated substances on melanin production by treating with α-MSH which is generally known as a stimulant for melanin production. The color of melanin on the paper was consistent with the amount of melanin in conventional assay after the treatment of α-MSH which can also confirm that the visible color on the paper was melanin.

4.9 The use of the paper-based scaffold for screening the effects of natural compounds on melanin production

Kojic acid and Arbutin are known as tyrosinase inhibitors, a crucial enzyme in synthesizing melanin through melanogenesis (291-293). To validate the ability of the paper-based scaffold to detect the effect of natural compounds on melanin production, we applied our developed paper-based melanoma cell culture for screening the anti-melanogenic

effect of Kojic and Arbutin. In brief, 200,000 cells of B16F10 encapsulated in Matrigel were placed in Whatman no.1. Afterwards, paper was placed in natural compounds containing medium. Cells were treated with Kojic acid at a concentration of 0, 0.2, 0.4, 0.8, and 1.6 mM, and Arbutin at a concentration of 0, 0.1, 0.2, 0.4, and 0.8 mM. The suspension of cells was then seeded on the paper and incubated at 37 °C with 5% CO_2. The suspension of the cells and hydrogel alone served as the negative control. The intensity on the paper was then analyzed using ImageJ software. Furthermore, the conventional melanin content analysis was performed on both non-treatment and natural compound treatments to confirm the effect on melanin production.

Figure 50 shows the inverse correlation between melanin intensity of on the paper and the concentration of Kojic acid and Arbutin in a dose dependent manner. These results confirm the whitening effect of Kojic acid and Arbutin on melanin production as well as the ability of paper-based melanoma cell culture to detect the effects of whitening substances on melanin production. Nevertheless, the paper-based scaffold was only used with low concentrations of whitening substances because of the limitation of melanin color on the paper, which required a longer incubation time for increasing melanin production, before perceiving the effect of high concentration of whitening substances on melanin production.
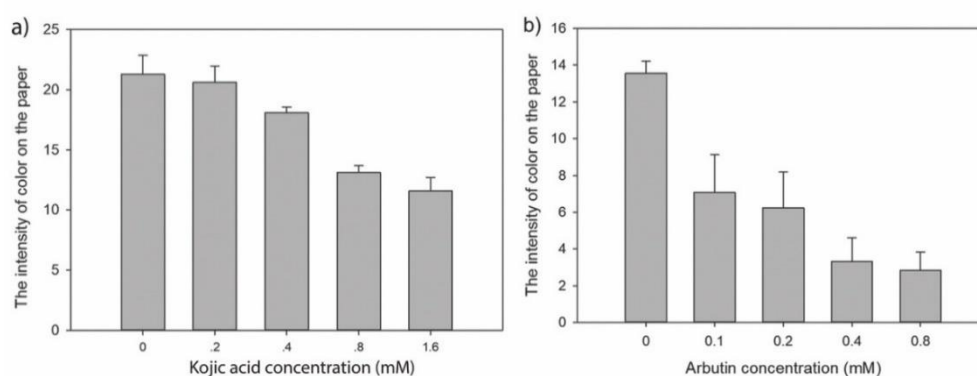
Figure 50 The intensity of melanin on the paper under (a) Kojic acid (b) Arbutin

treatment at various concentrations.

Data are presented as the mean ± SD (n = 3).

(Reproduced from ref. 111 by permission of The Royal Society of Chemistry)

In this part, author has obtained the optimal parameters for culturing B16F10 cells. These parameters were applied for the anti-melanogenic screening 2 substances,

Kojic acid and Arbutin. By using the advantage of existing white color of the paper substrate, the black color of melanin complexion can be easily observed after 48 h of culture. Furthermore, the treatment of natural compounds can be performed with the seeding step of cells in the paper, which is faster than the conventional 2D cell culture that needs at least 4 h for cell attachment before natural compound treatment. The analysis of the effects of natural compounds can be easily analyzed by scanning the paper and measuring the intensity of melanin with ImageJ software and comparing with the untreated paper. In addition, the paper-based scaffold was able to culture B16F10 cells in 3D conditions where cells can similarly behave to *in vivo* structures. Besides, fluorescent staining can be performed directly on the paper. This work guides the future trend for high throughput anti-melanogenic screening by just fabricating several cell culturing zones on the paper. Though this part provides the information regarding optimal conditions for B16F10 cell culture on the paper, it leads to the future development of novel paper-based cell culture as membrane insert for the melanoma invasion assay device (can be found in chapter IV part III). In the third part, readers can find the application of parameters obtained in this part for B16 melanoma 4A5 cell line, which has similar properties to B16F10 but more invasive.

Part II Initial impedance characteristic study for cell culture system and its application for Impedance-based E-screen assay

Before moving to the application of paper-based cell culture for real-time invasion assay device, author has primarily studied the impedance characteristics of cells using commercial electrode. The use of commercial electrodes provides the opportunity to compare the results to the newly developed electrode, which was used in part III. Moreover, the commercial electrodes used in this part are well known and were applied in various cell culture applications before (The information can be found in biophysics.com and dropsens.com). Other than application of impedance characteristic of cells for invasion assay (Chapter IV, part II), author has applied the obtained conditions for the Impedance-based E-screen assay as a parallel project. The principle of the work was based on ER on MCF-7 breast cancer cells. The binding of estrogen on ER-positive MCF-7 cells resulted in the increased cell proliferation. Fortunately, when cells attach on the electrode surface, they act as an insulator. Their insulating membrane can impede the current flow on the electrode, causing high impedance signal. Therefore, the more cell proliferates, the higher impedance signal can be obtained.

4.10 Primary impedance characteristic study using MDCK cells

In the impedance experiment, the optimal potential is applied. The applied potential in this work is a crucial part due to the application in cell culture. In brief, the Electrochemical Impedance Spectroscopy (EIS) is the measurement of resistance from the applied AC voltage to input current between two electrodes (294). Therefore, the increased applied potential can generate high input current. This can cause excessive electrical stimulation to cells, resulted in cell death. Specially, in this work, we perform the impedance measurement based on 2D cell culture. Therefore, cells directly contact to the electrode surface and expose to the applied potential. The applied potential need to be carefully optimized and should be as low as possible.

However, the applied potential could not be too low in some experiments due to various limitations such as electrode configuration, redox probe, and the capacity of the impedance analyzer. In our case, we first optimize the applied potential using 8W20idf cell cultureware from AppliedBiophysics company (Figure 37). Based on the previous report (295), Solartron analyzer was applied in cell-based analysis with the

applied potential at 10 mV. Therefore, in this work, we aim to minimize the applied potential for long tern cell culture. We then chose to optimize whether 10 mV (applied in previous report) and the lower potential, 5 mV, would work in our experiments.

Though the final goal of this part is to develop the impedance-based E-screen, which relied on the estrogen receptor (ER) on MCF-7 cells, we chose to study the primary impedance characteristics using MDCK cells instead of MCF-7 cells. Due to the colony-like formation of MCF-7 cell, the impedance characteristics might not reflect the whole population of cells due to the inconsistent cell distribution on electrode surface (Figure 51a). On the other hand, MDCK cells form the 2D monolayer with a consistent distribution on the electrode surface (Figure 51b). Thus, the optimal parameters for applying in the cultureware could be obtained. After seeding MDCK cells at a concentration of 250,000 cells/cm^2 in the cultureware using normal medium, we applied AC potential at 5 and 10 mV with the frequency at the range of 10 Hz to 1 MHz. In order to obtain the maximum impedance magnitude at the optimal frequency, the relationship between log(frequency) and the normalized impedance magnitude was studied.

The relationship between log(frequency) and the normalized impedance magnitude shows the highest impedance magnitude at 4, 5, and 10 kHz at the different time points in both 5 and 10 mV (figure 51c and d). Therefore, the impedance magnitude at the frequency of 4, 5, and 10 kHz was collected and calculated into cell index using equation [4]. Impedance was then performed every 1 h for 48 h. Figure 51e and f show the cell index after applying 5 and 10 mV potential respectively. After 10 mV potential was applied, the cell index was continuously increased due to cell attachment on the electrode surface as well as cell proliferation. Nevertheless, cell index was decreasing after 24 h, indicating cell death due to high applied potential. On the other hand, after 5 mV potential was applied, cell index was continuously increasing over 48 at every frequency, indicating the optimal potential for applying for the long-term culture.
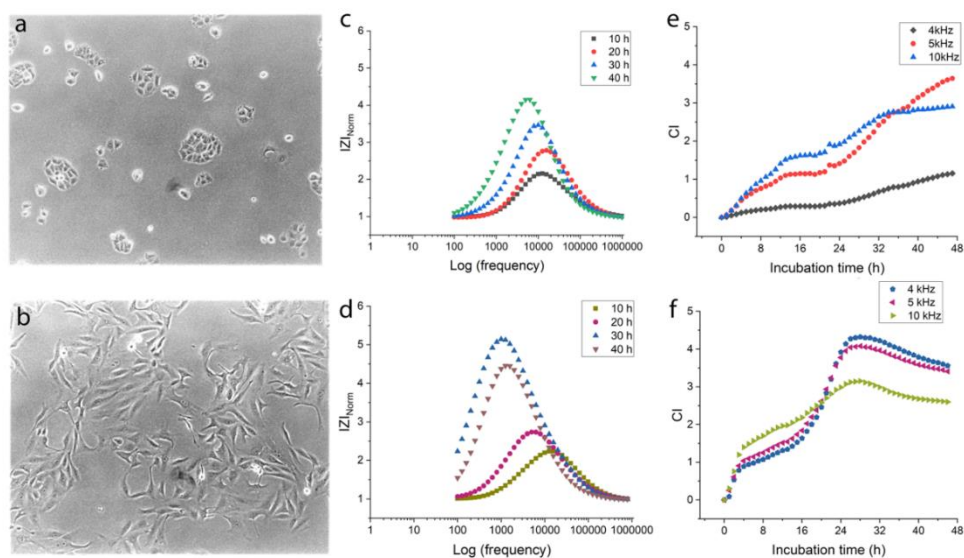
Figure 51 Primary impedance characteristic study using MDCK cells

The comparison between a) the colony-like formation of MCF-7 cells and b) the flat shape monolayer of MDCK cells. The primary impedance characteristic study using MDCK cells representing the obtained highest impedance magnitude at the frequency of 4, 5, and 10 kHz after applying c) 5 and d) 10 mV potential. The impedance magnitude was then converted to cell index representing cell proliferation over time after applying e) 5 and f) 10 mV potential respectively.

4.11 Impedance characteristics of MCF-7 cells in 10 and 350 μm gap electrode cultureware

After acquiring the optimal potential for applying in MDCK cell culture, we applied 5 mV potential for MCF-7 cell culture. In order to compare the effect of gap of interdigitated gold electrode, MCF-7 cells were cultured on two electrode types with relatively large different gaps at 10 and 350 μm.

For 10 μm electrode cultureware, MCF-7 cells at a concentration of 4,700 cells/cm^2 were seeded due to the concentration used in conventional assay. Impedance measurement was performed at 5, 10, 15, 20, 30, 40, 50 h of incubation. The relationship between normalized impedance magnitude and log(frequency) was studied to obtain the optimal frequency that could give highest impedance magnitude. Figure 52a shows that the highest impedance magnitude was obtained at approximate 10kHz frequency at every time point. We therefore applied the frequency of 10 kHz to study the influence of cell seeding number on CI value. MCF-7 cells at the concentration of 4,700 9,400 50,000 and 100,000 cells/cm^2 were

seeded in the culture wells. Impedance measurement was performed every 1 h for 40 h. Figure 52b shows that CI increased with the direct correlation with cell seeding number over time. However, in order to obtain the dramatic increase of CI, the cell seeding concentration of 100,000 cells/cm^2 was required.

Due to the larger well bottom area (0.25 and 0.8 cm^2 in 10 and 350 μm gap electrode cultureware respectively), we increased cell seeding number for the optimization of frequencies in 350 μm gap electrode cultureware. In brief, MCF-7 cells at the concentration of 15,500 cells/cm^2 was seeded. The impedance measurement was performed every 10 h for 70 h of the total incubation. Figure 52c shows that the normalized impedance magnitude was increasing by the increased incubation time indicating cell survival. Moreover, the highest impedance magnitude can be found at the frequency of 6,309 Hz at every time point. Thus, the impedance magnitude was collected at the frequency of 6,309 Hz for the rest of the experiments.

Next, we optimized the optimal cell seeding number for the impedance measurement. In brief, MCF-7 cells at the concentration of 125,000 187,500 250,000 312,500 cells/cm^2 were seeded on 350 μm gap electrode cultureware before performing the impedance measurement every 1 h for 42 h of the incubation. Figure 52d shows that at the cell concentration of 125,000 cells/cm^2 was only slightly increasing of cell index over 42 h, indicating low cell density which resulted in the longer incubation period for determining the cell proliferation. Meanwhile, at the cell concentration of 312,500 cells/cm^2, cell index was dramatically increasing within 42 h of the incubation. However, the rapid proliferation rate was caused by the high cell concentration, which might result in the reach the plateau phase due to the full coverage of cells on the electrode surface. Furthermore, the treatment of xenoestrogenic compounds could not possibly be observed because the cell number was beyond the limit of detection. The cell concentration of 187,500 and 250,000 cells/cm^2 show the optimal growth curve with the similar cell index value throughout the incubation. In order to observe the estrogenic effect on cell proliferation faster, the concentration of 250,000 cells/cm^2 was more suitable due to the higher cell concentration.

In conclusion, the optimal cell seeding number for 10 and 350 μm gap electrode cultureware was 100,000 and 250,000 cells/cm^2 respectively. The use of 10 μm gap

electrode was found to be more sensitive to cell seeding number, due to their capability to detect the change of CI at the low cell seeding concentration. Nevertheless, the small gap interdigitated electrode could possibly be too sensitive to cell distribution (296). Therefore, the further study regarding cell seeding number and culture conditions still need to be performed for the improvement of assay sensitivity (The discussion and outlook was also provided in Chapter VI). Therefore, 350 µm gap electrode was primarily chosen for performing experiments.
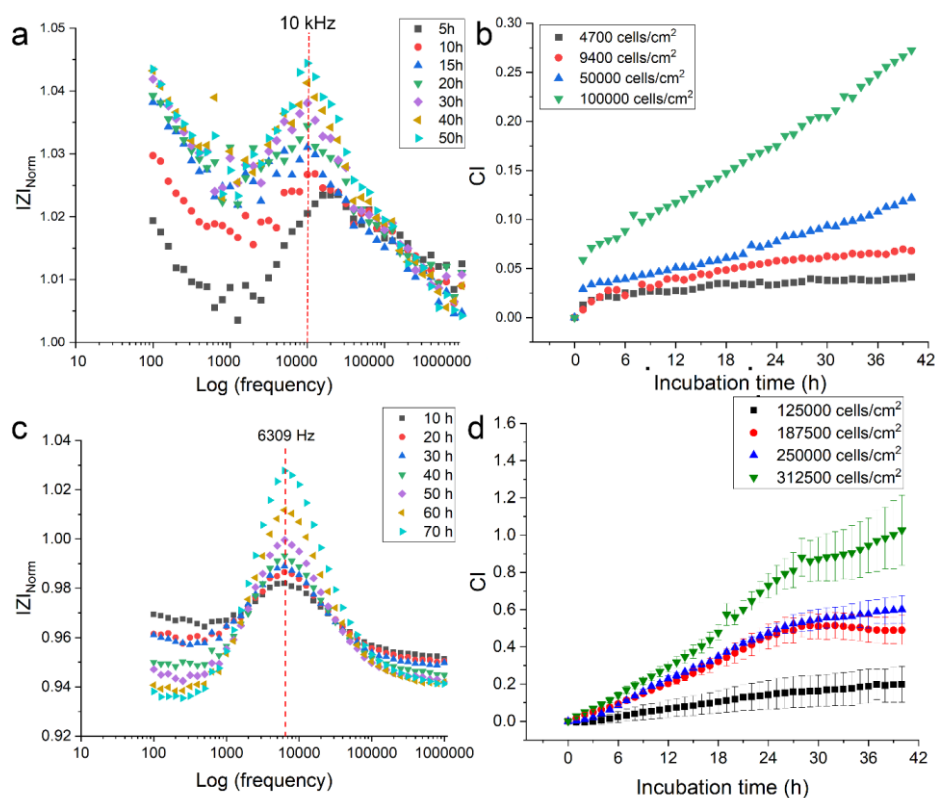
Figure 52 Impedance characteristics of MCF-7 cells when cultured in 10 and 350 µm gap electrode.
The highest impedance magnitude was obtained at a) 10 kHz and c) 6309 Hz when cultured in 10 and 350 µm gap electrode respectively. The relationship between CI and incubation time was studied to access the effect of various cell seeding numbers in b) 10 and d) 350 µM gap electrode. Data in figure d are represented at the mean ± s.e.m. (n=3).

4.12 The reduction of cell attachment time

In the conventional E-screen assay, MCF-7 cells were seeded using normal medium and allow to attach the bottom of well plate for 24 h before replacing with test

compound diluted in hormone-free medium. In our work, we aim to provide rapid E-screen method. Therefore, we optimized whether the cell attachment time could be reduced to 8 h. MCF-7 cells were seeded at a concentration of 4,700 *(same as conventional E-screen assay)* and 250,000 cells/cm^2 *(optimized cell number for the Impedance-based E-screen assay)* using normal medium. Cells were incubated for 8 and 24 h before fixed and stained with SRB. Figure 53 shows the total cell number after incubating for 8 and 24 h. The results show no significant difference when allowed cell attachment step for 8 and 24 h. Therefore, we applied 8 h incubation time for cell attachment in the next experiment.
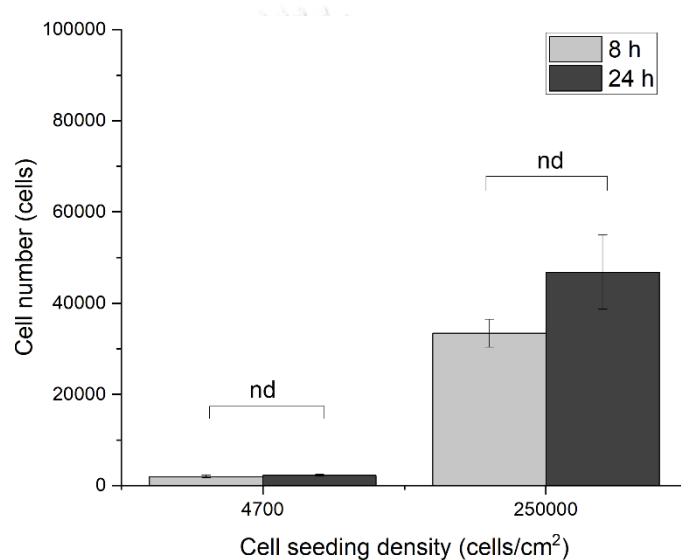
Figure 53 The comparison between MCF-7 cell attachment with 8 and 24 h

incubation shows no statistical difference (pair t-test p<0.01)

nd= no statistically difference

4.13 Treatment of 17β-estradiol and ER antagonist in the impedance-based E-screen assay

In order to study the kinetic of MCF-7 cell proliferation after 17β-estradiol treatment, MCF-7 cells at a concentration of 250,000 cells/cm^2 were seeded using normal medium and allowed cell attachment for 8 h. Afterwards, we added 0, 0.001, 0.01, 0.1, 1, and 10 nM 17β-estradiol in hormone-free medium. The impedance measurement was performed every 2 h for 144 h, which was the same total incubation period applied in conventional E-screen assay. We found that even though the treatment of hormone-free medium alone can also cause cell

proliferation, the growth rate was relatively slow throughout 144 h of the incubation. Besides, the exponential growth of MCF-7 can be observed between 24-120 h depending on the concentration of 17ß-estradiol (Figure 54a). We observed that cell proliferation reached the plateau phase after 120, 118, 118, 106, and 94 h when treated with 17ß-estradiol at the concentration of 0.001, 0.01, 0.1, 1, and 10 nM respectively (Figure 54b-f). The period of exponential growth shows the inverse correlation with the concentrations of 17ß-estradiol because of cell clumping when exposed to high concentrations of 17ß-estradiol. In brief, when treated MCF-7 cells with 0.001, 0.01, and 0.1 nM 17ß-estradiol, cells tend to grow slower and spread themselves throughout the electrode surface, caused the increased CI for over 106-120 h before reaching plateau phase. In contrast, when treated MCF-7 cells with 1 and 10 nM 17ß-estradiol, cells started to quickly clump together. Thus, the coverage of cells on the electrode surface was less, resulted in low CI and early reach plateau phase. Moreover, the decrease of cell index during the late incubation time could be found sooner in 10 nM when compared with 1 nM. These caused by the higher rate of cell clumping when treated with high concentrations of 17ß-estradiol (Figure 54e and f).

In order to confirm the binding of 17ß-estradiol on ER of MCF-7, ER antagonist (5 nM ICI182780) was co-treated with 17ß-estradiol at the concentration of 0.001, 0.01, 0.1, 1, and 10 nM. Figure 54b, c, and d shows the decreased cell index throughout 144 h of the incubation, indicating the antagonistic effect of ICI 182780. Co-treatment of 1 and 10 nM 17ß-estradiol with 5 nM ICI 182780 show the increase of CI over time due to the high concentration of 17ß-estradiol (Figure 54e and f). According to the effect of ER antagonist, cells were partially inhibited growth after the treatment of 1 and 10 nM 17ß-estradiol. These results correlated with the conventional E-screen assay, which shows PE less than 1 when co-treated ICI182780 with 0.001, 0.01, and 0.1 nM 17ß-estradiol and slightly more than 1 when co-treated ICI 182780 with 1 and 10 nM 17ß-estradiol (Figure 55a). Therefore, cell clumping was not observed when co-treated with ER antagonist but rather the spread of cells throughout the surface of culture well (Figure 55e and f).
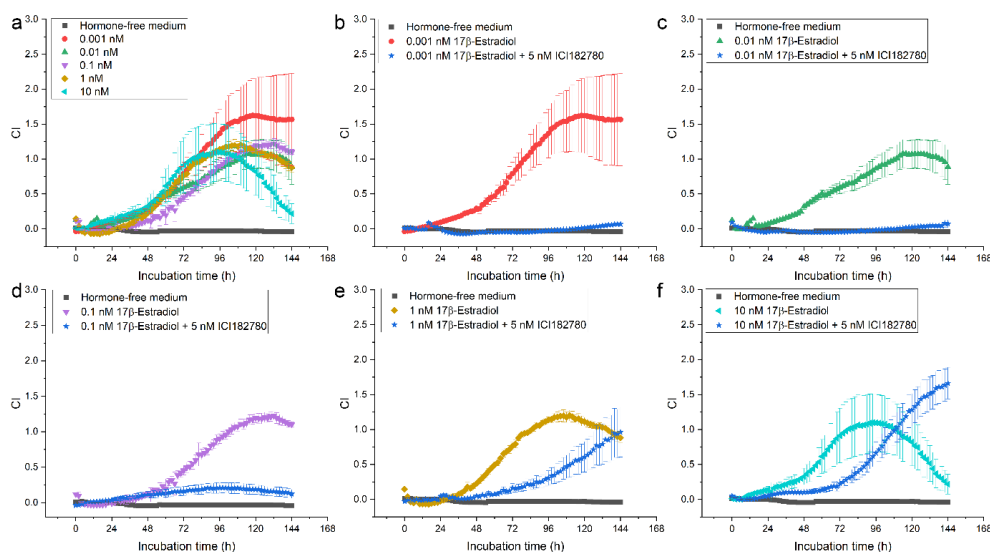
Figure 54 The kinetics of cell proliferation under 17beta-Estradiol treatment with and without ER antagonist

a) The relationship between cell index (CI) and incubation time after cell attachment step using normal medium (first 8h) and the treatment of 17ß-estradiol 0, 0.001, 0.01, 0.1, 1, and 10 nM 17ß-estradiol in hormone-free medium (8-144 h) and the comparison between co-treatment of ER antagonist (5 nM ICI182780) with 17ß - estradiol and the pure treatment of 17ß-estradiol at the concentration of b) 0.001, c) 0.01, d) 0.1, e) 1, and f) 10 nM

Other than the high concentration of 17ß-estradiol, we found that the high initial cell seeding number also contributed to cell clumping. In conventional method, cell seeding number is 4,700 cells/cm^2 while our experiment requires 250,000 cell/cm^2 due to large gap of the interdigitated electrode. Therefore, high cell seeding density was required for sensing cells. When performed conventional E-screen assay with 4,700 cells/cm^2 seeding concentration, PE shows direct correlation with 17ß-estradiol concentration after 144 h incubation (Figure 55a). In contrast, when performed conventional E-screen assay with 250,000 cells/cm^2 seeding concentration, PE shows direct correlation with 17ß-estradiol at a concentration of 0.001, 0.01, and 0.1 nM. Meanwhile, 17ß-estradiol at the concentration of 1 and 10 nM show slight and dramatic decrease of PE respectively (Figure 55b). The decrease of PE when treated with high concentrations of 17ß-estradiol was caused by the high cell seeding number, which contributed to the clump of cells. Cell clumps were observed after fixing cells with TCA and can easily detach from well bottom, caused false interpretation of low absorbance and PE. Unlike conventional method, our system does not require cell fixation. Cell clumping caused by high cell seeding

concentration could not affect the interpretation of estrogenic effect. Besides, CI value could provide the information regarding cell pattern after the treatment of estrogenic compounds e.g. the monolayer coverage of cells on electrode or cell clumping.
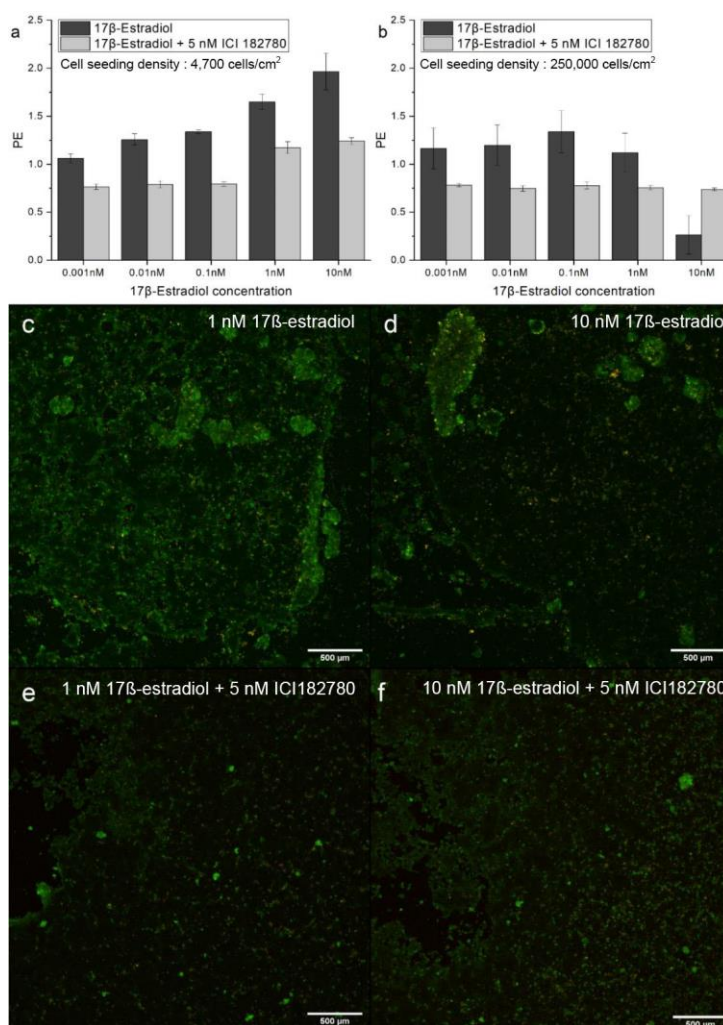
Figure 55 A comparison of proliferative effect of 17ß-estradiol and its cotreatment with ICI182780 and confocal images of cell clumping after estrogen treatment

4.14 Cell viability assay and the confirmation of the effect of cell clumping on CI value

In another perspective, the decrease of cell index after the treatment of 17ß-estradiol could be caused by cell death due to the high concentrations of 17ß-estradiol or the detachment of cells due to the full coverage of cells on the electrode surface. Afterwards, we confirmed the cell viability at the exponential growth phase and the end of the experiment after 60 and 144 h of the incubation

respectively. Figure 56a and c shows the LIVE/DEAD staining of MCF-7 cells in 350 μm gap electrode cultureware after 60 and 144 h respectively. % Cell viability during the exponential growth phase was up to approx. 90% (Figure 56b) and drop to approx. 70% after 144 h of the incubation at every concentration of 17ß -estradiol (Figure 56d). Since all the treated concentrations of 17ß -estradiol resulted in slightly decreased % cell viability at 144, this result does not correlate with cell index, which was much lower number in the high concentrations of 17ß -estradiol. Moreover, the morphology of MCF-7 cells tend to show cell clumping and less cell number when treated with the high concentrations of 17ß -estradiol. These results confirm that the decrease of cell index in the late incubation period of the treatment 17ß-estradiol caused by the clumping due to the rapid proliferation rate and not cell death.
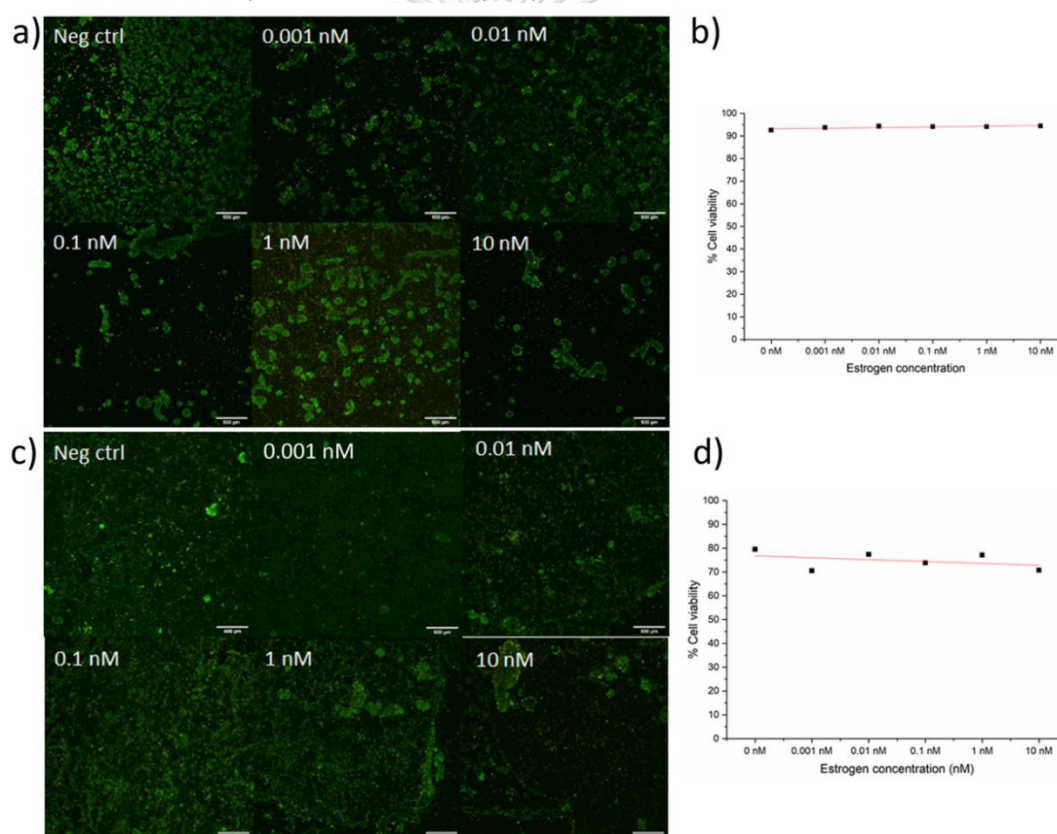
Figure 56 LIVE/DEAD staining of MCF-7 cells and %cell viability
after a) 60 and b) 144 h incubation of 0.001, 0.01, 0.1, 1, 10 nM 17ß-estradiol
treatment and their % cell viability at b) 60 and d) 144 h respectively.

4.15 Application of impedance-based E-screen assay for screen estrogenic effect of Bisphenol-A and Irgarol 1051

BPA is one of the harmful EDC due to their ability to mimic estrogenic effect (297). In this work, we applied our developed Impedance-based E-screen assay to detect their

estrogenic effect as well as study the kinetic of cell proliferation after BPA exposure. Based on previous report, BPA shows a agonistic activity to ER at a concentration down to 1 nM (42). We then applied the same concentration of BPA to our system. Figure 57a shows that BPA resulted in the increased of cell proliferation over time. The exponential growth can be observed during 72–136 h of incubation, which was relatively similar to the treatment of 0.001 nM 17ß-Estradiol. To confirm the estrogenic effect of BPA, we co-treated 1 nM BPA with 5 nM ICI182780. We found that CI remained low and stable throughout incubation time. This result confirms that BPA can bind to ER, resulted in the increased cell proliferation. Besides, when co-treated with ER antagonist, BPA cannot bind to ER, resulted in no cell proliferation (Figure 57a). The results were correlated with the conventional E-screen assay (Figure 57c).

Another environmental concerning substance is Irgarol 1051, due to its use on ship paint that directly contact to the seawater. The estrogenic effect of Irgarol 1051 has also been studied. However, the results were inconclusive among various methods (47, 48). In this work, we first demonstrated the estrogenic effect of Irgarol 1051 using the conventional and impedance-based E-screen assay. After the treatment of 30 µg/L Irgarol 1051 and cotreatment with ICI 182780, CI shows low value throughout the experiment. The drop of CI was observed in the beginning of co-treatment of Irgarol with ICI182780 due to the slow cell attachment (Figure 57b). Therefore, Irgarol 1051 shows no estrogenic effect when using our developed system. The result also shows the same effect in the conventional E-screen assay (Figure 57c).
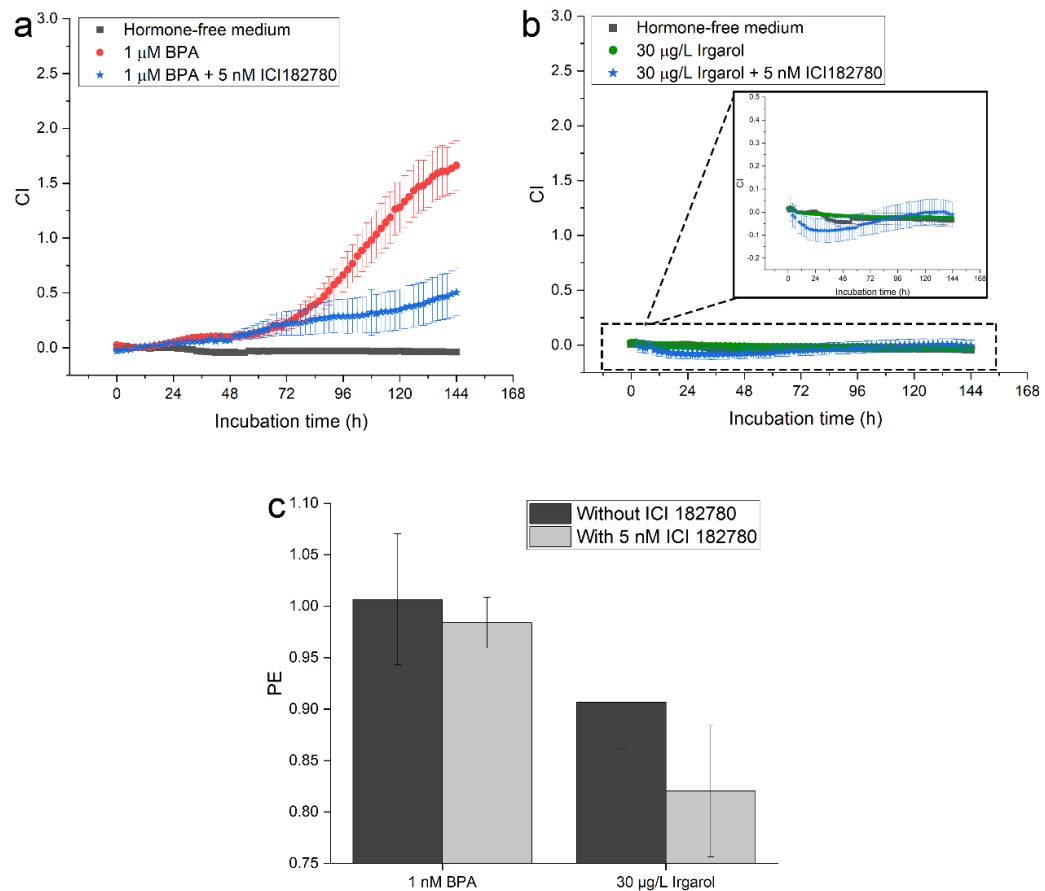
Figure 57 The estrogenic screening of a) BPA and b) Irgarol 1051 using Impedance-based E-screen assay and c) conventional E-screen assay

In this work, author has obtained the optimal parameter used for cell-based impedance measurement. These parameters were applied for the parallel study, the impedance-based E-screen assay. The impedance-based E-screen assay was successfully developed for real-time estrogenic screening. The method was validated by the estrogenic screening of BPA and Irgarol 1051. Both estrogenic effect of BPA and non-estrogenic effect of Irgarol 1051 were correlated with conventional E-screen assay.

Part III Paper-based cell culture as a membrane insert for real-time invasion assay

In this part, author aims to demonstrate novel application of paper-based cell culture as a membrane insert for invasion assay. Because filter papers are available in various pore sizes, thickness, and type of fiber composition. Moreover, filter papers are clean and biocompatible, which are compatible with cell culture. Instead of relying on the commercial plastic insert, we demonstrate the more accessible invasion assay device, which can be built in-house without relying on commercial device with the low cost, as well as provide another perspective of paper-based cell culture application.

4.16 Stencil printed carbon electrodes on PMMA substrate

Stencil printed electrode was chosen as a working electrode in this work, due to their ease of fabrication process and low cost. Pellitero *et al*. have pioneered the accessible electrode fabrication process, called stencil-printed electrode. Though the screen-printed electrodes are commercialized nowadays, in some laboratories still are lack of access to order or find the right match of electrode to their work. Stencil printed electrodes are great option to fabricate and optimize electrodes in your own laboratories (298). Unlike screen printed electrode, stencil printed electrode does not require the tedious alignment of mask onto substrate. In this work, the adhesive tape was attached directly to PMMA substrate before cutting with laser ablation at the defined electrode position and spreading with carbon ink respectively. Usually, after spreading carbon ink on polymer or paper substrate, the ink was cured at ca. 60°c for 30 min (299, 300). However, this protocol does not fit with the PMMA due to their rigidity, causing the crack and shrink of carbon paste when incubated at the high temperature. We here demonstrated that curing carbon paste on PMMA at room temperature (RT) for 72 h shows a well functioned electrode (Figure 58). Moreover, we found that the step of removing adhesive stencil affects the charge transfer resistance (R_{ct}) of the electrode. In brief, we divided experiment into two groups: the first group had an immediate stencil removal right after spreading carbon ink. While the second group, the carbon ink was cured at RT for 24 h before stencil removal. Both of experimental groups of electrodes were then cured at RT for 72 h in total before EIS characterization.

Figure 58 shows lower R_{ct} in the immediate stencil removal group than the electrodes that we allowed to undergo 24 h precuring. The scanning electron microscope images of the electrode surface also show similar structure as a previous report (Figure 58b-d) (298). Furthermore, the solution and possible contact resistance were higher in 24 h precuring group (can be observed from the high frequencies of the starting point of Nyquist plot). The exact R_{ct} numbers are represented in table 6.

Table 6 R_{ct} of the optimization of the fabrication process when the screen-printing electrode after mask removal. The result was obtained from the Nyquist curve fitting to the equivalent circuit.

Process	Charge transfer resistance $(R_{ct})/\Omega$
Immediate mask removal after screen printing 1	61.78
Immediate mask removal after screen printing 2	50.74
Mask removal 24 after screen printing 1	88.87
Mask removal 24 after screen printing 2	89.79

จุฬาลงกรณ์มหาวิทยาลัย

CHULALONGKORN UNIVERSITY
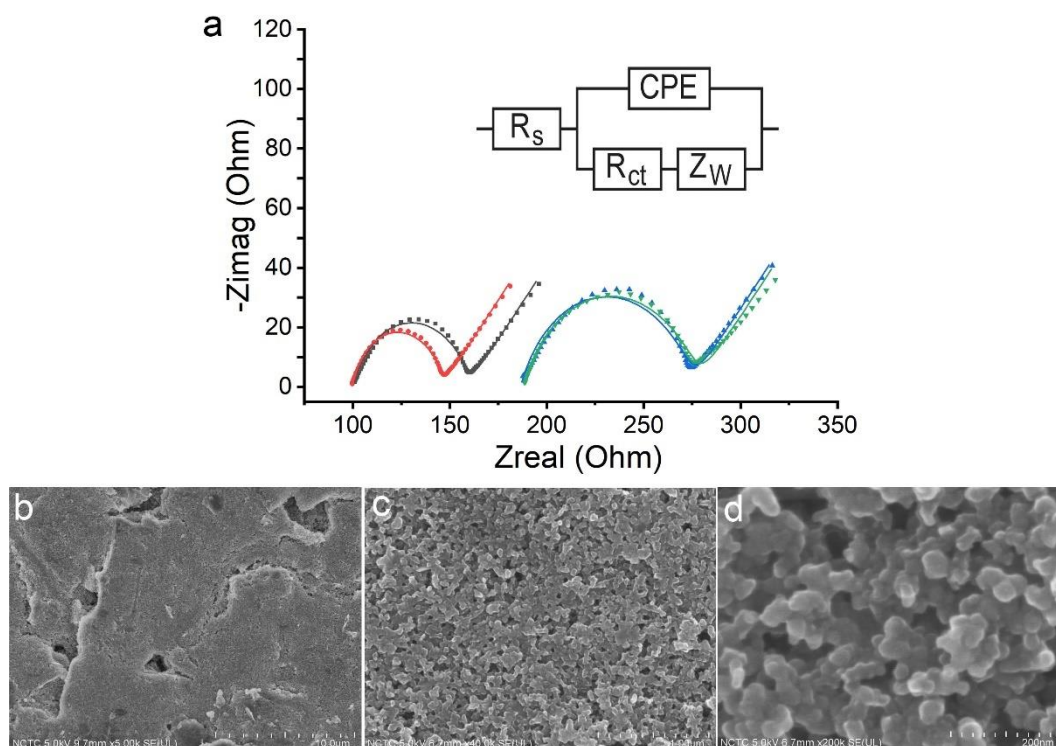
Figure 58 The impedance characteristics of stencil-printed electrode and its surface morphology represented in scanning electron microscope images.

a) Nyquist plots representing the comparison of fabrication of stencil printed electrode between the immediate (red and black represent 2 repetitive identical tests) and 24 h (blue and green represent 2 repetitive identical tests) precuring removal of stencil after spreading carbon ink (n=2) and SEM images of electrode surface at b) 5000x c) 40,000x, and d) 200,000x
The solid lines represent curve fitting to the equivalent circuit in the inset.

(This picture was taken from ref. 280.)

4.17 Choice of counter electrode and its placement in the device

In general, gold is the most conductive material which is used in an electrode fabrication. However, in this work, the available gold electrode in our laboratory was not compatible with our fabricated device. The gold on silicon plate (a 10x25x05 mm rectangular shape) has the flat shape and therefore cannot be inserted and soaked at the desired depth in our device. To find another suitable CE type fitting the device geometry, we investigated whether a platinum wire, a stainless-steel wire, or a glassy carbon rod would give the best electrical characteristics compared to the gold on silicon plate used above. We chose platinum, stainless steel, and glassy carbon according to rod shape. The advantage of the rod shape of the CE is a large surface

area and it can be soaked into the culture medium at our desired depth. Hence, we can acquire the impedance signal from the whole device. In brief, the plastic lid was designed to have a hole that fits the platinum, stainless steel wire, and glassy carbon. The platinum wire, the stainless-steel wire, or the glassy carbon rod was inserted into the plastic lid. The platinum wire has a 0.785 mm^2 surface area and a 26 mm long cylindrical shape. The stainless-steel wire has a 0.64 mm^2 surface area and 23.38 mm long cylindrical shape. The glassy carbon rod has a 19.625 mm^2 surface area and 22.5 mm long cylindrical shape. After the device assembly, the various CEs were inserted and adjusted to have a 2.5 mm gap between the WE and the CE. A 10 mM ferricyanide:10mM ferrocyanide solution was then inserted into the cell culture vial. The device was then connected to the impedance analyzer before performing the impedance measurement.

Figure 59 shows that stainless steel gives a huge R_{ct}, which is not compatible with our system. On the other hand, the glassy carbon gives the lowest R_{ct} while gold on the silicon plate gives a slightly higher R_{ct}. Additionally, the Nyquist plot of glassy carbon results in a lower electrode resistance and internal resistance than the platinum wire (301) (Table 7). Thus, glassy carbon was the most suitable material for constructing the CE to be used in our system due to its rod shape, which fits with our customized lid and gives a low R_{ct} when combined with our screen-printed electrode (WE). Moreover, the surface at the bottom of glassy carbon is flat and wide which is suitable for mapping the cell movement within the whole device.

Table 7 R_{ct} of each CE type when applied in the device. The result was obtained from the Nyquist curve fitting to the equivalent circuit.

Counter electrode	Charge transfer resistance (R_{ct})/Ω
Stainless steel	>1200000
Gold on silicon plate	145.7
Platinum wire	185.8
Glassy carbon	126.9
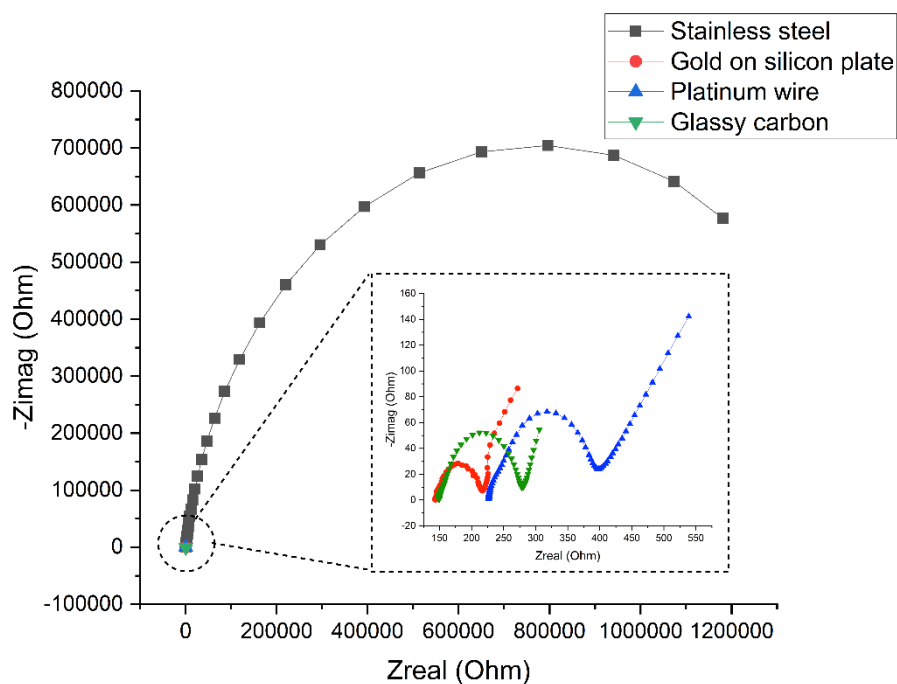
Figure 59 Nyquist plot after using gold on silicon plate, platinum wire, stainless steel, and glassy carbon as a counter electrode (CE) with carbon screen printed electrode as a working electrode (WE).

Afterwards, we optimized the placement of GC rod in the invasion assay device. According to our lid design, GC rod can be adjusted up and down by loosening 2 screws on the lid (Figure 60a). This aids the adjustment of the medium soaking level of GC rod as well as the distance between WE and CE. In order to optimize the distance between CE and WE, GC rod was adjusted at a distance of 2.5, 3.5, 4.5, and 5.5 mm from WE. Figure 60b shows the Nyquist plots after adjusting the GC rod apart from WE at different levels. The 3 different device assemblies were then used for optimizing the distance between WE and CE (Figure 60c). The results show that when CE was closer to WE, the R_{ct} was decreased. However, the least distance that CE can be apart from WE is 2.5 mm due to the insertion of paper membrane and the avoidance of cell exposure.
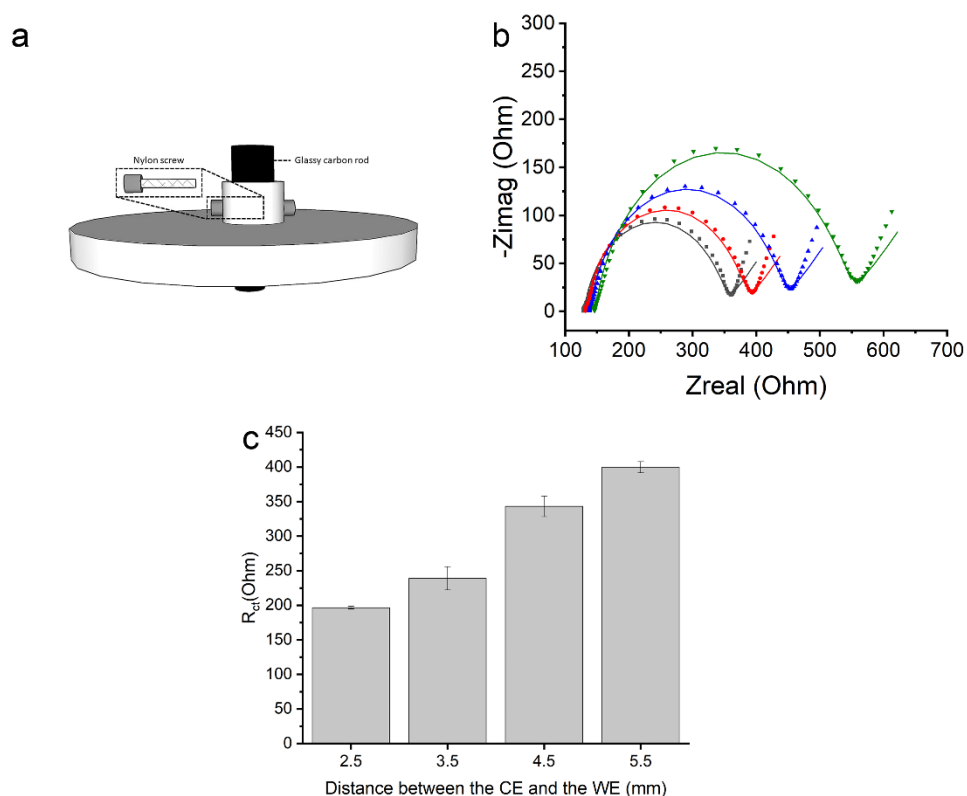
Figure 60 a) Schematic of the lid with an inserted glassy carbon (GC) electrode. The length of medium soaked GC rod, can be adjusted by losing the nylon screw, b) Nyquist plots acquired at different distance between the CE and the WE and c) their average R_{ct} when characterized in 3 different device assemblies.

The solid lines represent curve fitting to the equivalent circuit in the inset of Figure 58. Data is figure c are presented as mean ± SD (n=3).

(This picture was modified from ref. 280.)

4.18 Choice of paper for the membrane insert

According to the optimized paper types from Chapter IV part I, we found that Whatman filter paper No.1 and 4 fit with B16F10 melanoma cell culture. The SEM also proofs that B16F10 and B16 melanoma 4A5 (used in this part) have similar size, approximately 10 μm. Therefore, Whatman No.1 and 4 could also be good candidates for this work. We then optimized the impedance characteristic of the papers by inserting bare Whatman No.1 and 4 and assembled the invasion assay device using double adhesive tape. In order to determine invasiveness of the cells, cells should represent their motility and ability to invade through the extracellular matrix (ECM) (118). Hence, membrane insert is needed to be coated with ECM. In this

work, we used Matrigel due to state transition. In brief. Matrigel is liquid at 4°C and become solid at 37 °C (302). Therefore, when incubating Matrigel coated paper, Matrigel will be solidified, which can prevent the passing of gel through the thickness of paper. We then optimized the impedance characteristic of Matrigel coated Whatman no.1 and 4.

Figure 61a shows that bare Whatman no.4 shows lower R_{ct} than bare Whatman no.1 due to larger pore size, which allow the better current flow (Table 5). When Matrigel was coated on both papers, Whatman no.4 shows higher R_{ct} due to the higher filtration rate than Whatman no.1. Therefore, Matrigel can pass through the thickness of the paper faster Whatman no.1, resulted in the clog of paper pores, and impeded the current flow. Since we need to coat Matrigel on the paper for invasion assay, Whatman no.1 is more suitable than Whatman no.4 due to the lower R_{ct}. The results were confirmed by optimizing in 3 different device assemblies (Figure 61b).
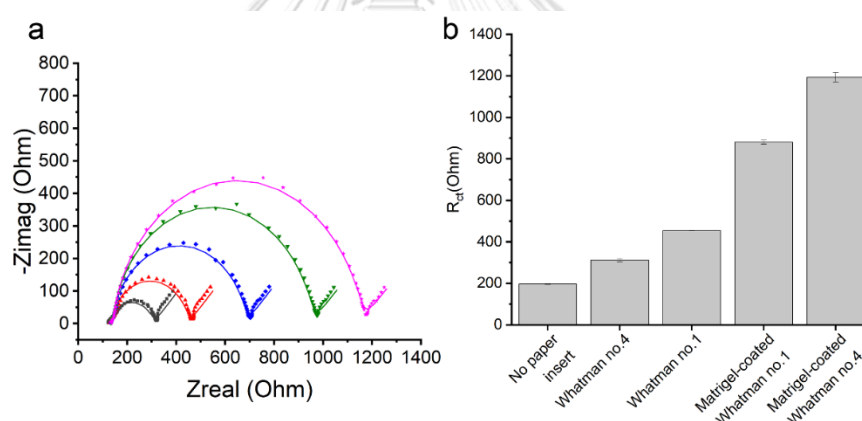
Figure 61 Nyquist plots acquired for the optimization of paper types for inserting as a membrane insert in the invasion assay devices and b) their average R_{ct} when characterized in 3 different device assemblies.
The solid lines in figure a represent curve fitting to the equivalent circuit in the inset of Figure 58. Data is figure b are presented as mean ± SD (n=3).

(This picture was modified from ref. 280.)

4.19 Cell viability and morphology assessment of the paper insert

Since the invasion assay device consists of many parts, the biocompatibility has to be determined. After device assembly, 800,000 cells of B16 melanoma 4A5 cells were

seeded on Matrigel-coated Whatman no. 1. LIVE/DEAD staining was then performed after 4, 8, 12, 24, and 48 h of incubation.

Figure 62f represents high cell viability over 48 h. Confocal images also confirm the high cell viability at 4, 8, 12, 24, and 48 h (Figure 62a-e). Moreover, at 4, 8, and 12 h, cells were not fully attached to the paper (can be observed with circular shape of cells) and were washed out when LIVE/DEAD stain was added. On the other hand, at 24 h, cells were more flatted and expanded on top the paper, representing full cell attachment. This can be applied for the stabilization of the experiment before adding chemoattractant to the device. According to the use of medium with 10% FBS, cells started to penetrate to the thickness of the paper at 48 h due to the chemoattractive properties of FBS (Figure 63b), causing less cell number on the surface of the paper and representing more cells in the paper pores (Figure 62e).
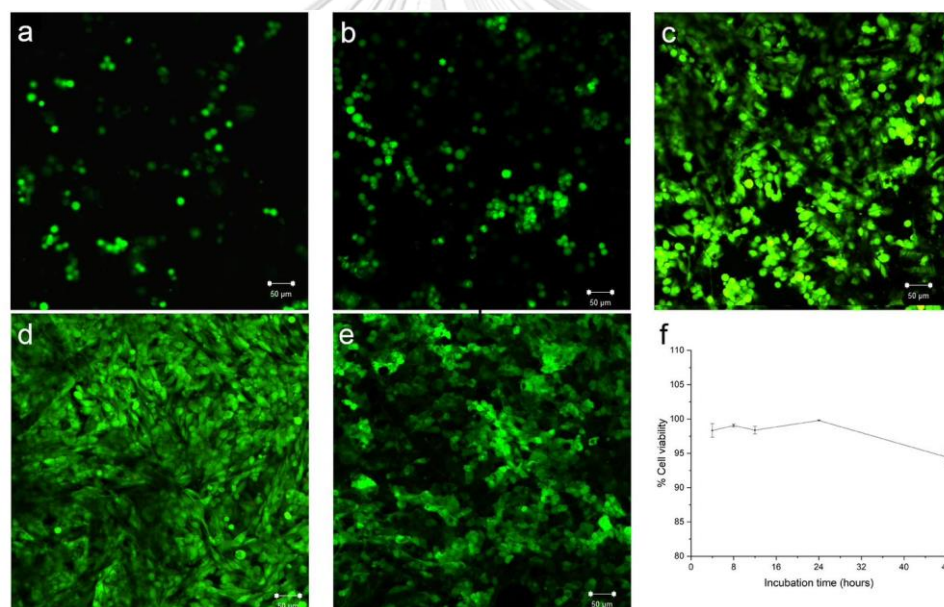
Figure 62 LIVE/DEAD staining of B16 melanoma 4A5 melanoma cells in the invasion assay device at a) 4, b) 8, c) 12, d) 24, and e) 48 h and f) their % cell viability at each time point

(green − Calcein-AM; red − Propidium iodide; scale bars: 50 μm) Data are presented as the mean ± SD (n = 3).

(This picture was taken from ref. 280.)

4.20 Impedance characteristics of the device in the presence of cells

According to the optimization of applied potential in the cell-based system from part II, we found that 5 mV is not harmful for cells. We then applied the potential of 5 mV in this work after 800,000 B16 melanoma 4A5 cell seeding in the assembled device using normal medium. Afterwards, impedance was performed every hour for 12 h. Figure 63a shows the normalized impedance magnitude (Equation [5]) as a function of log frequency based on the impedance spectra acquired after 3, 6, 9, and 12 h incubation. The result indicates that the highest impedance magnitude is obtained at approximately 100 kHz, which was then chosen for the subsequent experiments.

In the cell-based impedance measurement, the optimization of cell number is required due to the necessity of baseline impedance value, which later applied for evaluating cell response to drugs or chemical treatments (303). In order to optimize cell seeding number for this work, B16 melanoma 4A5 cell line at a concentration of 25,000 50,000 500,000 and 1,000,000 cells/cm^2 in normal medium was added in the assembled invasion assay device. Subsequently, impedance spectra were acquired every hour for 12 h. Figure 63b shows that cell concentration of 25,000 cells/cm^2 has no increasing impedance value over 12 h. Therefore, the cell density of 25,000 cells/cm^2 is below the limit of detection. Meanwhile, the concentration of 50,000 500,000 and 1,000,000 cells/cm^2 show the increased impedance value over time. For 1,000,000 cells/cm^2, the impedance value 0 h was higher than that at 1 h due to the turbulence in the medium containing high cell seeding number. Moreover, the determined impedance at 1,000,000 cells/cm^2 was the highest, reaching a plateau, which provided a clear initial baseline prior to introduction of the chemoattractant. In order to obtain the signal of cellular invasion rapidly with high sensitivity, cell density of 1,000,000 cells/cm^2 is an optimal cell seeding concentration for the subsequent experiments.
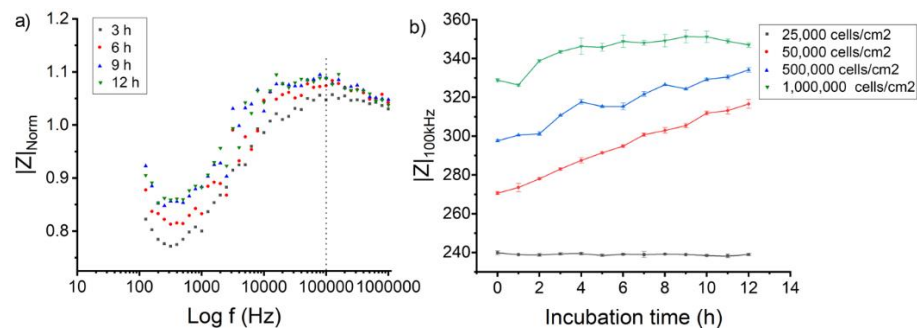
Figure 63 Impedance characteristics of the invasion assay device in the presence of

B16 melanoma 4A5 cells

a) *the relationship between normalized impedance magnitude ($|Z|_{Norm}$) and log*

frequency after 3 ,6, 9, and 12 h of incubation, showing a maximum at 100

kHz for each time point, and b) the impedance magnitude at 100 kHz

($|Z|_{100kHz}$) over time after seeding 25,000 50,000 500,000 and 1,000,000

cells/cm^2. Data are presented as the mean ± SD (n = 3).

(This picture was modified from ref. 280.)

4.21 Invasion assay of B16 melanoma 4A5 cells

Insulin growth factor-1 (IGF) is known as the chemoattractant which increase the metastasis of cancer, specially melanoma cells (6). In this work, we applied IGF-1 as a chemoattractant to validate our invasion assay device. The result was compared with the treatment of normal medium with and without FBS (negative control). After cell seeding and stabilizing for 24 h, the 100 ng/ml IGF-1, and normal medium with and without were added into lower compartment of the device. The impedance was performed every hour throughout 48 h of the incubation. Figure 64a shows that after the first 24 h of incubation, the cells had a rather similar CI baseline. During this period, the CI slightly increased due to cell adhesion on the paper insert. After 24 h, the lower compartment was filled with medium without FBS (negative control) shows no increase cell index, indicating absence of cell invasion. Meanwhile, the treatment of normal medium with 10%FBS shows increasing cell index during 25-29 h before reaching plateau until 48 h of the incubation. This result suggests the induced invasion effect of FBS, which correlates with the conventional transwell assay (Figure 64b). When IGF-1 was introduced, a 3-fold increase in CI could be observed. This chemoattractant-induced increase in CI is probably attributed to the penetration of cells into the pores of the paper, which results in an additional impediment of current flow within the system. Thus, the more extensive the observed cell invasion

is, the more obstruction to the current is caused by the cells penetrating within the pores of paper, concomitantly increasing the measured impedance. This phenomenon was similar to the filtration of Matrigel through the pore of paper, resulted in an increased impedance signal. Additionally, the invasion of B16 melanoma 4A5 under the treatment of FBS and IGF-7 could be distinguished from negative after 7h of the incubation. Since our developed assay required such rapid incubation time to observed cellular invasion, the cell index value was less likely to be influenced by cell proliferation. The confocal image of B16 melanoma 4A5 with the treatment of medium without FBS (Figure 64c left) also shows more fluorescent intensity of cells on the surface of the paper than the treatment of IGF-1 (Figure 63c right). Besides, through the thickness of the paper, the treatment of medium without FBS shows less fluorescent intensity than the treatment of IGF-1, indicating more invasion of cells into the pore of papers (Figure 64c). SEM images also confirms the invasion of cells when observed from the top of the paper. In brief, when treated with normal medium without FBS, cells form the multi layers with the flatten shape, indicates their inability to penetrate ECM coated on the paper (Figure 64d). On the other hand, when treated with IGF-1, cells form 3D structure and penetrate through the pore of the paper, confirming the invasion of cells towards the treatment of IGF-1. The invasion results obtained from our developed invasion assay device also correlated with the transwell assay (Figure 64b), confirming the validity of our invasion assay device for melanoma cells.
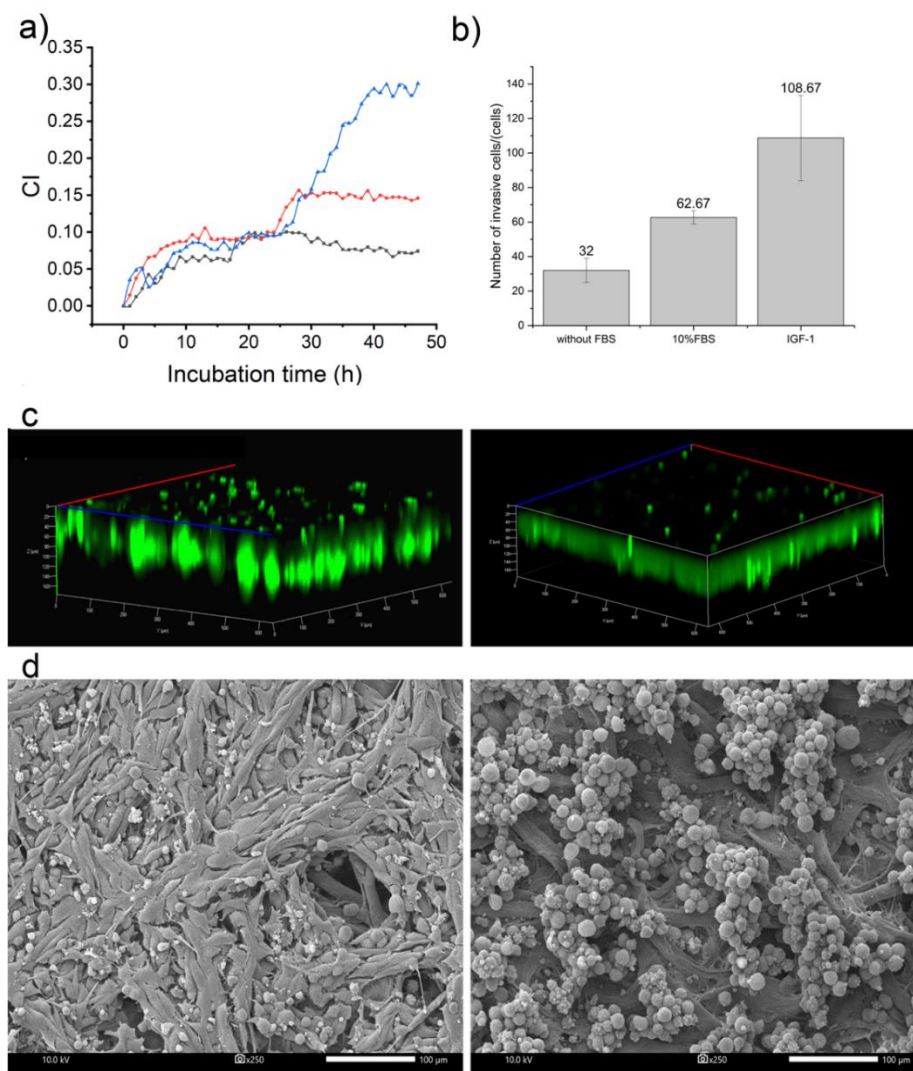
Figure 64 The real-time invasion study of B14 melanoma 4A5 cells using the developed device

a) CI vs. incubation time for B16 melanoma 4A5 cells (initial cell seeding density of 1000,000 cells/cm^2), showing a stable baseline when cells were maintained in culture medium without FBS, the negative control for the first 24 h, and an increase in CI (from 25 to 47 h) when the medium in the lower compartment was replaced by DMEM with 10% FBS or 100 ng/ml IGF-1. b) Results was confirmed by conventional transwell assay. c) Confocal microscope and d) SEM images showing B16 melanoma 4A5 cell behavior on paper insert in the absence (left) and presence (right) of IGF-1 (green – Calcein-AM; red – Propidium iodide).

(This picture was taken from ref. 280.)

In this part, the paper-based cell culture has shown their potential application as a membrane insert for real-time invasion assay. Based on the pore size of the paper, invasive cells were able to break the ECM coated on the paper and penetrate into the pores. Cell penetration inside paper pores impede the current flow in the device, related in the increased impedance signal. During the invasion, cells were able to penetrate into the pores of paper based on their 3D formation. Therefore, cells could behave similarly to *in vivo* conditions. Besides, our developed device makes real-time invasion assay more accessible, since each part of the device can be fabricated in-lab without relying on the commercial products. The preliminary result of the melanoma invasion under IGF-1 provides the possibility to develop our device for the high throughput experiments in the future.

CHAPTER V CONCLUSIONS

In this thesis, author describes the novel applications of paper-based 3D cell culture for melanoma study and the real-time biosensing applications. The final goal of this thesis is to improve the *in vitro* experimental procedure regarding cost, analysis time, and reliability. The project started by developing paper-based scaffold for 3D formation of melanoma cells, which was later applied for anti-melanogenic screening. This model was then further developed for real-time biosensing applications based on the so-called Electrochemical Impedance Spectroscopy (EIS). In order to obtain the parameters for cell-based impedance measurement, author have begun with the pilot study based on MDCK and MCF-7 cells before applying to melanoma cells. The parameters obtained from this pilot study were then applied for the development of real-time estrogenic effect screening as a parallel project.

As describe in the introduction, to access melanoma mechanism, the analysis of melanin production and understanding its metastatic mechanism are the key. Other than the low cost, we found that papers could support 3D formation of melanoma cells. This contributes to the advancement of melanoma study based on 3D cell culture, which could reflect cellular behavior closer to *in vivo* conditions.

In order to develop the *in vitro* method to access the amount of melanin production, paper has an advantage of their existing white color that ease the detection of the black color of melanin complexion. The combination of high cell seeding density with Matrigel encapsulation and the use of paper allowed rapid melanin color detection within 48 h after cell seeding step. In order to limit cell culture zone, paper was easily fabricated using wax printing technique. Unlike the conventional melanin content analysis, the treatment of natural compounds can be performed together with the seeding step of cells in the paper without the need of cell attachment step for 4-24 h before. Analysis of the effects of natural compounds as well as stimuli can be easily analyzed by scanning the paper and measuring the intensity of melanin with ImageJ software and comparing with the untreated paper. Accordingly, we improve the conventional melanin content analysis using absorbance measurement by eliminating the cell centrifugation (takes 15 min), melanin solubilization (takes 1 h), and absorbance measurement (takes 5-10 min). Due to the permanent melanin color on the paper after air-dried, the melanin

intensity was analyzed by ImageJ within 20 min. In order to confirm cell markers or determine their viability, paper allows the direct fluorescent staining without initial cell lysing step. The developed paper-based scaffold was validated by using as a screening device for anti-melanogenic effects in Kojic acid and Arbutin, which confirmed that the paper-based melanoma cell culture can serve as the platform for a quick and *in situ* screening of the effects of compounds of interest on melanin production and provides great opportunities for developing further high-throughput platforms i.e. 96-well paper devices that could be used for quantitative melanin content analysis with more efficacy and accuracy (Table 10).

Table 8 The comparison between paper-based 3D cell culture and conventional absorbance measurement for screening anti-melanogenic activity

	Paper-based devices	Conventional method
Limit of detection	10,183 cells per mm^2 of paper culture area	Not performed in the B16F10 cell line so far [a]
Preparation step	Cells can be treated with anti-melanogenic substance directly after seeding on the paper	Treatment can be performed only after cells attach to the bottom of well (which requires at least 4 h)
Analysis time	20 min	120 minutes

[a] Fernandes *et al*. have reported that the detection limit of absorbance measurement was 310000 cells per ml in the SK-MEL-1 cell line and 630000 cells/ml in the SK-MEL-23 cell line (14).

(Reproduced from ref.111 by permission of Royal Society of Chemistry)

After we successfully developed and optimized the proper conditions for melanoma cell culture on the paper, we then applied the paper-based scaffold for invasion assay. In this work, we made the real-time invasion assay more accessible by demonstrating the in-house invasion assay device. Most of the device compositions can be made within the lab except the glassy carbon rod counter electrode. The membrane insert was made of filter paper, which is cost effective and available in every scientific laboratory. Besides, the use of paper could ease the establishment of invasion assay device because it can be easily cut and allows easy customization to fit different cell culture devices. Device was assembled by simple adhesive tape. Other than cost reduction, we combined the assay with Electrochemical Impedance

Spectroscopy, which is the tool for real-time cellular behavior study. By using real-time EIS measurements, invasion of cells through the pores of paper showed the direct correlation with impedance signal due to the blockage of current flow within the device. The insulin growth factor-1 (IGF-1) induced invasion of B16 melanoma 4A5 cells on the paper could be distinguished from a negative control faster than using a conventional transwell assay. Hence, the invasion study was less influenced by cell proliferation. The pore size of filter paper was a crucial factor in determining the suitable paper for the EIS based invasion assay. Filter paper with intermediary pore size (~11 μm) comparable to the size of melanoma cells resulted in lower background impedance upon Matrigel coating, allowing more sensitive detection of the impedance changes caused by cell invasion into the pores of the paper. Moreover, paper-based scaffold could provide the invasion study of cells based on 3D formation (Figure 64C right). Therefore, the invasion performed in this developed assay could exhibit similar conditions to *in vivo*. Our developed device has guided the user towards the self-made real-time invasion assay device based on 3D cell culture.

As a parallel project, author has applied the knowledge in cell-based impedance measurement to develop the real-time impedance-based E-screen assay. The assay was inspired by the conventional E-screen assay, which is based on the binding of xenoestrogenic compounds on ER of MCF-7 cells, results in the increased of cell proliferation. In our work, instead of incubating for 144 h, we reduced analysis time to 48-120 h by applying EIS for detecting cell proliferation. After the treatment of xenoestrogenic compounds, the kinetic of cell proliferation can be monitored in real time. The effect of estrogen and co-treatment with ER antagonist on cell proliferation can be observed by comparing cell index with negative control (MCF-7 cell culture using hormone-free medium). Our developed impedance-based E-screen assay could be used for detecting estrogenic effect with the limit of detection up to 0.1 nM 17β-estradiol. Besides, we found that cell attachment step can be reduced to 8 h before the treatment of compounds of interest. The well-known estrogenic compound, BPA, was applied for our developed assay validation. The results show the increased cell index over incubation time and can be distinguished from negative control during 72-120 h of the incubation. Additionally, we firstly tested the estrogenic effect of Irgarol 1051, the antifouling agent, by the impedance-based and conventional E-screen assay and found no estrogenic effect in both assays. Our developed impedance-based E-screen assay does not only improve the analysis time, but also provides the

kinetic information regarding cell proliferation and their spreading behavior during the estrogen treatment.

Together with all projects, author has demonstrated the assay development for 3 aspects: melanin content analysis, invasion assay, and estrogenic screening. Every project could improve analysis time, provide easy experimental setup, and cost reduction. Since the reliable scientific results could only come from accurate and well-developed assays, author hopes that this thesis will guide readers towards the enhancement of scientific methods for life science research.

จุฬาลงกรณ์มหาวิทยาลัย

CHULALONGKORN UNIVERSITY

CHAPTER VI DISCUSSION

Though the developed paper for melanoma cell culture could be represented as a cost-effective material for 3D cell culture, the combination of paper-based scaffold with extracellular matrix is still a crucial part. In this work, we applied Matrigel as an extracellular matrix to support cells on the paper due to its ability to convert between solid and liquid state based on the temperature. Hereby, the cost can be further reduced by using an alternative hydrogel that could provide cell support on the paper. For example, Polyethylene glycol (PEG) has been known as a blank state hydrogel with a low cost. PEG allows users to modify its material to present adhesive ligands for a better cell encapsulation. Besides, the modification of the paper could improve cell attachment such as the use of iCVD or plasma treatment (see the literature review). However, the 3D cell morphology needs to be confirmed because the modification might force cells to attach differently on the paper. In this work, we were able to demonstrate the semi-quantitative melanin content analytical method. In order to provide the in-dept information for further study, the quantitative measurement of melanin amount is desirable. Technically, by using ImageJ software for analyzing melanin content on the paper, we could demonstrate the intensity of melanin in quantitative result. In figure 49, we represent the correlation between melanin intensity on the paper and melanin content obtained from conventional method. Nevertheless, this result could not exhibit the significant correlation between the two conditions yet. Therefore, our developed method could only exhibit the semi-quantitative results of melanin content. This was due to the instability of melanin color, caused by the inconsistent dispersion of cells in the paper. Regarding the internal control, the existence of cells in the paper was confirmed by staining GAPDH, which is a house keeping gene of cells. This result could be improved further to narrow down the specific marker of melanin-producing cells. Tyrosinase enzyme is responsible for a rate limiting step of melanin production. Hence, the staining of T_4-Tyrosinase gene could confirm not only the existence of living cells, but more specific to melanin-producing cells (304). The validation of our developed paper-based scaffold was performed in the whitening substance, which could be used in melanoma treatment as well as supplements in cosmetic products. The application could also be further developed for screening the agonist on

melanogenesis, in order to improve the effect of whitening substance for melanoma treatment.

Due to the lack of standard whitening compounds, we validated our paper-based devices by the treatment of the well-known whitening compounds, Kojic acid and Arbutin. To improve this experiment, the calibrator is required for anti-melanogenic assessment. The possible way to calibrate the melanin content on the paper is the use of synthetic melanin from *Sepia Officinalis* (305). By varying synthetic melanin amount and seeding on paper-based scaffold, the standard curve between melanin amount and intensity on a paper could be used a device calibrator.

For further development, our developed paper-based scaffold has a potential to apply for melanin content analysis in other melanin-producing cells. For instance, the quantification of neuromelanin, produced by neuron, which has the efficacy on the treatment neurodegenerative disease e.g. Parkinson's disease (306). Other than the improvement of paper-based melanoma cell culture for quantitatively measurement of melanin content, the paper was easy to scalable to be used for a high throughput measurement. For example, paper could be designed to contain 96 cell culture zones by just increase the paper size and well design. The anti-melanogenic screening could then be performed simultaneously. The paper could be coupled with the sterile plastic holder to ease medium adding step, reduce solution usage, and limit the testing area for the treatment of different whitening compounds in different culture zones. Regarding the analyzing technique used in this work, we chose ImageJ because it is user-friendly, well-accepted in scientific community due to its functions, and available for free download. However, other software could also be used for measuring melanin intensity on the paper such as Photoshop or Meazure. In the future, the developed mobile application could ease this step by just taking a picture of papers and automatically measuring the intensity via ImageJ-inspired applications. This could also ease the analyzing step for high throughput measurement.

For the impedance-based E-screen assay, author observed the clumping of MCF-7 cells when cultured in 1 and 10 nM 17ß-estradiol. Cell clumping resulted in the low impedance signal due to the free electrode surface, allowed the current to flow better. Cell clumping was mainly caused by the high cell seeding density together

with the nature of MCF-7 cells, which usually form a colony like structure instead of monolayer. Therefore, the impedance signal obtained in the later exponential growth might cause false understanding to the cell death. In order to improve the assay, the higher sensitivity electrode is required. Because of the 350 µM gap-electrodes, high cell seeding number was required due to a very small size of MCF-7 cells. Since MCF-7 cell is ~ 10 µm size, the smaller gap-electrodes could possibly be suitable because the chance of cell exposing to the electrode surface is higher. Figure 52 shows the potential use of 10 µm gap electrode, which could detect cell proliferation with low cell seeding density. To confirm 10 µm gap electrode function on the improvement of assay sensitivity, the repetition of the experiment in figure 52b is required. However, as discuss in chapter IV part II, the use of small-gap electrode must be careful optimized because of the inconsistent cell distribution after cell seeding. Accordingly, the various gap sizes should be further studied before applying to MCF-7 cells. Cell clumping not only lead to the false understanding in the impedance-based setup, but also the conventional method. When cell seeding concentration was too high (250,000 cells/cm^2), cell clumping was also observed in 96 well plate when treated with 10 nM 17β-estradiol. This phenomenon could be observed with naked eye after fixing cells with TCA at 4° C. Cell clumps were easily removed when plate was washed multiple times and stained with SRB, resulted in low cell number when performed absorbance measurement. Another possible way to avoid cell clumping is to use the ER positive monolayer cells. The use of mammalian cells will provide the biological information as well as the toxicity of the test compounds. However, the validation of molecular cell functions should be measured before the assay development.

For the developed invasion assay device, the paper was further developed as a membrane insert for invasion assay. The study was performed in melanoma cells using the optimized conditions, obtained from the first project. In order to represent the invasiveness, cells should be motile and able to invade through the extracellular matrix. In this work, we coated Matrigel on top of the paper. Matrigel consists of collagen, various structural proteins such as laminin, and growth factors that could promote cell proliferation. Hence, the invasion assay should perform as quick as possible, to avoid the effect of cell proliferation on the increased impedance magnitude. In this work, we used EIS to detect cell invasion through the thickness of

the paper, which can detect melanoma invasion within 7 h after the treatment of IGF-1. However, the further validation should be performed using various types for chemoattractants. Regarding the sterilization of the device, paper and micromilled components had to be sterilized separately using the different protocols. The paper could only be sterilized using UV while the micromilled components were sterilized using NaOH. Both micromilled components and paper could not use the same sterilization technique because paper should not be soaked in a strong NaOH in a long period, to avoid paper dissolution. On the other hand, the micromilled components were made of PMMA, which could potentially form a toxic component after exposing to UV radiation multiple times. The sterilization could not be done after the device assembly. Therefore, the careful handling during the device assembly was required.

Regarding the possible development of the invasion assay device, there are many perspectives to improve the device including the design and fabrication process. In this work, the invasion assay was developed as a prototype with one culture well. The repetition of experiments could only be performed in the different device assemblies. Therefore, the high throughput devices should be further developed. Currently, we chose micromilling as a fabrication tool. Micromilling provides a smooth surface of the fabricated device and the possibility to fabricate such a small structure. However, micromilling gives low throughput, requires a tedious work, and deliberate design. Besides, a tool changing during the fabrication process is time consuming. To improve the fabrication process, stereolithography and 3D printing could potentially be used for device fabrication. Nevertheless, the available materials are not biocompatible and expensive. In the future, if there are alternative materials, which are biocompatible and low cost, stereolithography could be used as a high throughput method for the device fabrication. Regarding the design of the device, in our work, we developed only one well device, which allows only one experiment to be performed at a time. However, the high throughput device could be further developed by easily adjusting the design. Paper could be designed to have as many well as we need. However, the multiplexing capacity of the impedance analyzer should be considered.

While the current published works have been focusing on the development of gradient of chemoattractants in the invasion assay device, we developed the pilot

work using the paper as a membrane insert. The formation of the gradient of chemoattractants is still desirable, in order to mimic the *in vivo* conditions. However, this is the first step of the use of paper as a membrane insert for real-time invasion assay, which could be used as a prototype for further development to mimic the *in vivo* cancer metastasis as much as possible.

REFERENCES

1. Chen KG, Gottesman MM. How Melanoma Cells Evade Chemotherapy. From Melanocytes to Melanoma: Springer; 2006. p. 591-603.

2. Geller AC, Annas GD, editors. Epidemiology of melanoma and nonmelanoma skin cancer. Seminars in oncology nursing; 2003: Elsevier.

3. Haridas P, Penington CJ, McGovern JA, McElwain DS, Simpson MJ. Quantifying rates of cell migration and cell proliferation in co-culture barrier assays reveals how skin and melanoma cells interact during melanoma spreading and invasion. Journal of theoretical biology. 2017;423:13-25.

4. Erdei E, Torres SM. A new understanding in the epidemiology of melanoma. Expert review of anticancer therapy. 2010;10(11):1811-23.

5. Thompson JF, Scolyer RA, Kefford RF. Cutaneous melanoma. The Lancet. 2005;365(9460):687-701.

6. Shain AH, Bastian BC. From melanocytes to melanomas. nature reviews Cancer. 2016;16(6):345.

7. Arrangoiz R, Dorantes J, Cordera F, Juarez MM, Paquentin EM, de León EL. Melanoma review: Epidemiology, risk factors, diagnosis and staging. Journal of Cancer Treatment and Research. 2016;4(1):1-15.

8. Davey RJ, van der Westhuizen A, Bowden NA. Metastatic melanoma treatment: combining old and new therapies. Critical reviews in oncology/hematology. 2016;98:242-53.

9. Chinembiri TN, Du Plessis LH, Gerber M, Hamman JH, Du Plessis J. Review of natural compounds for potential skin cancer treatment. Molecules. 2014;19(8):11679-721.

10. Wakamatsu K, Ito S. Advanced chemical methods in melanin determination. Pigment Cell Research. 2002;15(3):174-83.

11. Watanabe T, Tamura A, Yoshimura Y, Nakazawa H. Determination of melanin in human hair by photoacoustic spectroscopy. Analytical biochemistry. 1997;254(2):267-71.

12. Ito S. High-performance liquid chromatography (HPLC) analysis of eu-and pheomelanin in melanogenesis control. Journal of Investigative Dermatology. 1993;100(2):S166-S71.

13. Rosenthal MH, Kreider JW, Shiman R. Quantitative assay of melanin in melanoma cells in culture and in tumors. Analytical biochemistry. 1973;56(1):91-9.

14. Fernandes B, Matamá T, Guimarães D, Gomes A, Cavaco-Paulo A. Fluorescent quantification of melanin. Pigment cell & melanoma research. 2016;29(6):707-12.

15. Chen H-C. Boyden chamber assay. Cell migration: Springer; 2005. p. 15-22.

16. Albini A, Benelli R. The chemoinvasion assay: a method to assess tumor and endothelial cell invasion and its modulation. Nature protocols. 2007;2(3):504.

17. Marshall J. Transwell® invasion assays. Cell Migration: Springer; 2011. p. 97-110.

18. Kramer N, Walzl A, Unger C, Rosner M, Krupitza G, Hengstschläger M, et al. In vitro cell migration and invasion assays. Mutation Research/Reviews in Mutation Research. 2013;752(1):10-24.

19. Keese CR, Bhawe K, Wegener J, Giaever I. Real-time impedance assay to follow the invasive activities of metastatic cells in culture. Biotechniques. 2002;33(4):842-50.

20. Wegener J, Keese CR, Giaever I. Electric cell–substrate impedance sensing (ECIS) as a noninvasive means to monitor the kinetics of cell spreading to artificial surfaces. Experimental cell research. 2000;259(1):158-66.

21. Chollangi T, Clabault H, Thibeault A-AH, Yong HE, Narula S, Menkhorst E, et al. An electrical impedance-based assay to examine functions of various placental cell types in vitro. Preeclampsia: Springer; 2018. p. 267-76.

22. Gharaei M, Xue Y, Mustafa K, Lie S, Fristad I. Human dental pulp stromal cell conditioned medium alters endothelial cell behavior. Stem cell research & therapy. 2018;9(1):69.

23. Primiceri E, Chiriacò MS, Dioguardi F, Monteduro AG, D'Amone E, Rinaldi R, et al. Automatic transwell assay by an EIS cell chip to monitor cell migration. Lab on a Chip. 2011;11(23):4081-6.

24. Derda R, Tang SK, Laromaine A, Mosadegh B, Hong E, Mwangi M, et al. Multizone paper platform for 3D cell cultures. PloS one. 2011;6(5):e18940.

25. Derda R, Laromaine A, Mammoto A, Tang SK, Mammoto T, Ingber DE, et al. Paper supported 3D cell culture for tissue-based bioassays. Proceedings of the National Academy of Sciences. 2009;106(44):18457-62.

26. Mosadegh B, Dabiri BE, Lockett MR, Derda R, Campbell P, Parker KK, et al. Three-dimensional paper-based model for cardiac ischemia. Advanced healthcare materials. 2014;3(7):1036-43.

27. Min SK, Kim CR, Kim SH, Shin HS. Assessment of morphology, activity, and infiltration of astrocytes on marine EPS-imbedded electrospun PCL nanofiber. Journal of Nanomaterials. 2014;2014.

28. Kim Y, Uhm S, Gupta M, Yang J, Lim J-G, Das Z, et al. Successful vitrification of bovine blastocysts on paper container. Theriogenology. 2012;78(5):1085-93.

29. Lee K-H, Sun J-C, Chuang C-k, Guo S-F, Tu C-F, Ju J-C. An efficient and mass reproducible method for vitrifying mouse embryos on a paper in cryotubes. Cryobiology. 2013;66(3):311-7.

30. Mosadegh B, Lockett MR, Minn KT, Simon KA, Gilbert K, Hillier S, et al. A paper-based invasion assay: Assessing chemotaxis of cancer cells in gradients of oxygen. Biomaterials. 2015;52:262-71.

31. Lei KF, Huang C-H, Tsang N-M. Impedimetric quantification of cells encapsulated in hydrogel cultured in a paper-based microchamber. Talanta. 2016;147:628-33.

32. Safe S, Jutooru I, Jin U-H, Chadalapaka G. Estrogenic endocrine disruptors: molecular characteristics and human impacts. 2018.

33. Singleton DW, Khan SA. Xenoestrogen exposure and mechanisms of endocrine disruption. Front Biosci. 2003;8:s110-s8.

34. Xia W, Li Y, Wan Y, Chen T, Wei J, Lin Y, et al. Electrochemical biosensor for estrogenic substance using lipid bilayers modified by Au nanoparticles. Biosensors and Bioelectronics. 2010;25(10):2253-8.

35. Inadera H. The immune system as a target for environmental chemicals: xenoestrogens and other compounds. Toxicology Letters. 2006;164(3):191-206.

36. Scognamiglio V, Antonacci A, Patrolecco L, Lambreva MD, Litescu SC, Ghuge SA, et al. Analytical tools monitoring endocrine disrupting chemicals. TrAC Trends in Analytical Chemistry. 2016;80:555-67.

37. Ijaz S, Ullah A, Shaheen G, Jahan S. Exposure of BPA and its alternatives like BPB, BPF, and BPS impair subsequent reproductive potentials in adult female Sprague Dawley rats. Toxicology mechanisms and methods. 2020;30(1):60-72.

38. Saleh A. The effects of BPA and BPS on anti-Müllerian hormone and its receptor during early embryonic development 2020 [PhD Thesis].

39. Chen D, Kannan K, Tan H, Zheng Z, Feng Y-L, Wu Y, et al. Bisphenol analogues other than BPA: environmental occurrence, human exposure, and toxicity□ a review. Environmental science & technology. 2016;50(11):5438-53.

40. Final report for the review of literature and data on Bisphenol A: Food and Drug Administration; 2014. Available from: https://www.fda.gov/media/90546/download [Accessed 13 May 2020].

41. Moon MK. Concern about the safety of bisphenol A substitutes. Diabetes & metabolism journal. 2019;43(1):46-8.

42. Kojima H, Takeuchi S, Sanoh S, Okuda K, Kitamura S, Uramaru N, et al. Profiling of bisphenol A and eight its analogues on transcriptional activity via human nuclear receptors. Toxicology. 2019;413:48-55.

43. Mesnage R, Phedonos A, Arno M, Balu S, Corton JC, Antoniou MN. Editor's highlight: transcriptome profiling reveals bisphenol A alternatives activate estrogen receptor alpha in human breast cancer cells. Toxicological Sciences. 2017;158(2):431-43.

44. Ying G-G, Kookana RS. Degradation of five selected endocrine-disrupting chemicals in seawater and marine sediment. Environmental Science & Technology. 2003;37(7):1256-60.

45. Readman JW. Development, occurrence and regulationof antifouling paint biocides: historical review and future trends. Antifouling paint biocides: Springer; 2006. p. 1-15.

46. Zhang AQ, Zhou G-J, Lam MH, Leung KM. Toxicities of the degraded mixture of Irgarol 1051 to marine organisms. Chemosphere. 2019;225:565-73.

47. Noguerol T-N, Boronat S, Casado M, Raldúa D, Barceló D, Piña B. Evaluating the interactions of vertebrate receptors with persistent pollutants and antifouling pesticides using recombinant yeast assays. Analytical and bioanalytical chemistry. 2006;385(6):1012-9.

48. Park K, Jo H, Kim D-K, Kwak I-S. Environmental Pollutants Impair Transcriptional Regulation of the Vitellogenin Gene in the Burrowing Mud Crab (Macrophthalmus Japonicus). Applied Sciences. 2019;9(7):1401.

49. Zhang Z, Wang J, Pan Z, Zhang Y, Zhang X, Tian H, et al. Distribution of vitellogenin in Japanese flounder (Paralichthys olivaceus) for biomarker analysis of marine environmental estrogens. Aquatic Toxicology. 2019;216:105321.

50. He P, Matich EK, Yonkos LT, Friedman AE, Atilla-Gokcumen GE, Aga DS. Mass spectrometry based detection of common vitellogenin peptides across fish species for assessing exposure to estrogenic compounds in aquatic environments. Science of The Total Environment. 2019;646:400-8.

51. Wright P, Pinnegar J, Fox C. Impacts of climate change on fish, relevant to the coastal and marine environment around the UK. MCCIP Science Review 2020. 2020:354-81.

52. Legler J, Broekhof JL, Brouwer A, Lanser PH, Murk AJ, van der Saag PT, et al. A novel in vivo bioassay for (xeno-) estrogens using transgenic zebrafish. Environmental science & technology. 2000;34(20):4439-44.

53. Barreto K, Geyer CR. Screening combinatorial libraries of cyclic peptides using the yeast two-hybrid assay. Yeast Protocols: Springer; 2014. p. 273-309.

54. Chini A. Application of yeast-two hybrid assay to chemical genomic screens: a high-throughput system to identify novel molecules modulating plant hormone receptor complexes. Plant Chemical Genomics: Springer; 2014. p. 35-43.

55. Ramirez T, Buechse A, Dammann M, Melching-Kollmuß S, Woitkowiak C, van Ravenzwaay B. Effect of estrogenic binary mixtures in the yeast estrogen screen (YES). Regulatory Toxicology and Pharmacology. 2014;70(1):286-96.

56. Rainina E, Efremenco E, Varfolomeyev S, Simonian A, Wild J. The development of a new biosensor based on recombinant E. coli for the direct detection of organophosphorus neurotoxins. Biosensors and Bioelectronics. 1996;11(10):991-1000.

57. Jarque S, Bittner M, Blaha L, Hilscherova K. Yeast biosensors for detection of environmental pollutants: current state and limitations. Trends in biotechnology. 2016;34(5):408-19.

58. Peng Y, Wang J, Wu C. Determination of Endocrine Disruption Potential of Bisphenol A Alternatives in Food Contact Materials Using In Vitro Assays: State of the Art and Future Challenges. Journal of agricultural and food chemistry. 2019;67(46):12613-25.

59. Soto AM, Sonnenschein C, Chung KL, Fernandez MF, Olea N, Serrano FO. The E-SCREEN assay as a tool to identify estrogens: an update on estrogenic environmental pollutants. Environmental health perspectives. 1995;103(suppl 7):113-22.

60. Fang TY, Praveena SM, deBurbure C, Aris AZ, Ismail SNS, Rasdi I. Analytical techniques for steroid estrogens in water samples-A review. Chemosphere. 2016;165:358-68.

61. Rodriguez-Mozaz S, Marco M-P, de Alda MJL, Barceló D. Biosensors for environmental monitoring of endocrine disruptors: a review article. Analytical and bioanalytical chemistry. 2004;378(3):588-98.

62. Granek V, Rishpon J. Detecting endocrine-disrupting compounds by fast impedance measurements. Environmental science & technology. 2002;36(7):1574-8.

63. Giaever I, Keese CR. Monitoring fibroblast behavior in tissue culture with an applied electric field. Proceedings of the National Academy of Sciences. 1984;81(12):3761-4.

64. Rath A, Eichhorn M, Träger K, Paulsen F, Hampel U. In vitro effects of benzalkonium chloride and prostaglandins on human meibomian gland epithelial cells. Annals of Anatomy-Anatomischer Anzeiger. 2019;222:129-38.

65. Chiu S-P, Lee Y-W, Wu L-Y, Tung T-H, Gomez S, Lo C-M, et al. Application of ECIS to Assess FCCP-Induced Changes of MSC Micromotion and Wound Healing Migration. Sensors. 2019;19(14):3210.

66. Bogunovic N, Meekel JP, Micha D, Blankensteijn JD, Hordijk PL, Yeung KK. Impaired smooth muscle cell contractility as a novel concept of abdominal aortic aneurysm pathophysiology. Scientific reports. 2019;9(1):1-14.

67. Furst AL, Hoepker AC, Francis MB. Quantifying hormone disruptors with an engineered bacterial biosensor. ACS central science. 2017;3(2):110-6.

68. Kenney RM, Boyce MW, Truong AS, Bagnell CR, Lockett MR. Real-time imaging of cancer cell chemotaxis in paper-based scaffolds. Analyst. 2016;141(2):661-8.

69. Collins SJ, Gallo RC, Gallagher RE. Continuous growth and differentiation of human myeloid leukaemic cells in suspension culture. Nature. 1977;270(5635):347.

70. Wu J, King G, Daugulis A, Faulkner P, Bone D, Goosen M. Engineering aspects of insect cell suspension culture: a review. Applied microbiology and biotechnology. 1989;32(3):249-55.

71. Chu L, Robinson DK. Industrial choices for protein production by large-scale cell culture. Current opinion in biotechnology. 2001;12(2):180-7.

72. Parker RC. Methods of tissue culture. Methods of tissue culture. 1950(Edn 2).

73. Castiaux AD, Spence DM, Martin RS. Review of 3D cell culture with analysis in microfluidic systems. Analytical Methods. 2019;11(33):4220-32.

74. Wu H-W, Hsiao Y-H, Chen C-C, Yet S-F, Hsu C-H. A PDMS-based microfluidic hanging drop chip for embryoid body formation. Molecules. 2016;21(7):882.

75. Frey O, Misun PM, Fluri DA, Hengstler JG, Hierlemann A. Reconfigurable microfluidic hanging drop network for multi-tissue interaction and analysis. Nature communications. 2014;5:4250.

76. Caliari SR, Burdick JA. A practical guide to hydrogels for cell culture. Nature methods. 2016;13(5):405.

77. Chirani N, Gritsch L, Motta FL, Fare S. History and applications of hydrogels. Journal of biomedical sciences. 2015;4(2).

78. Tibbitt MW, Anseth KS. Hydrogels as extracellular matrix mimics for 3D cell culture. Biotechnology and bioengineering. 2009;103(4):655-63.

79. Meyvantsson I, Warrick JW, Hayes S, Skoien A, Beebe DJ. Automated cell culture in high density tubeless microfluidic device arrays. Lab on a Chip. 2008;8(5):717-24.

80. Walker GM, Beebe DJ. A passive pumping method for microfluidic devices. Lab on a Chip. 2002;2(3):131-4.

81. Young EW, Beebe DJ. Fundamentals of microfluidic cell culture in controlled microenvironments. Chemical Society Reviews. 2010;39(3):1036-48.

82. Bauer M, Su G, Beebe DJ, Friedl A. 3D microchannel co-culture: method and biological validation. Integrative Biology. 2010;2(7-8):371-8.

83. Nehls V, Drenckhahn D. A novel, microcarrier-based in vitro assay for rapid and reliable quantification of three-dimensional cell migration and angiogenesis. Microvascular research. 1995;50(3):311-22.

84. Qiu Y, Brown AC, Myers DR, Sakurai Y, Mannino RG, Tran R, et al. Platelet mechanosensing of substrate stiffness during clot formation mediates adhesion, spreading, and activation. Proceedings of the National Academy of Sciences. 2014;111(40):14430-5.

85. Lutolf M, Lauer-Fields J, Schmoekel H, Metters AT, Weber F, Fields G, et al. Synthetic matrix metalloproteinase-sensitive hydrogels for the conduction of tissue regeneration: engineering cell-invasion characteristics. Proceedings of the National Academy of Sciences. 2003;100(9):5413-8.

86. Karajanagi SS, Yoganathan R, Mammucari R, Park H, Cox J, Zeitels SM, et al. Application of a dense gas technique for sterilizing soft biomaterials. Biotechnology and bioengineering. 2011;108(7):1716-25.

87. Huebsch N, Gilbert M, Healy KE. Analysis of sterilization protocols for peptide-modified hydrogels. Journal of Biomedical Materials Research Part B: Applied Biomaterials: An Official Journal of The Society for Biomaterials, The Japanese Society for Biomaterials, and The Australian Society for Biomaterials and the Korean Society for Biomaterials. 2005;74(1):440-7.

88. Lee DW, Choi WS, Byun MW, Park HJ, Yu Y-M, Lee CM. Effect of γ-irradiation on degradation of alginate. Journal of agricultural and food chemistry. 2003;51(16):4819-23.

89. Park H-J, Yu SJ, Yang K, Jin Y, Cho A-N, Kim J, et al. Paper-based bioactive scaffolds for stem cell-mediated bone tissue engineering. Biomaterials. 2014;35(37):9811-23.

90. Carrilho E, Martinez AW, Whitesides GM. Understanding wax printing: a simple micropatterning process for paper-based microfluidics. Analytical chemistry. 2009;81(16):7091-5.

91. Camci-Unal G, Laromaine A, Hong E, Derda R, Whitesides GM. Biomineralization guided by paper templates. Scientific reports. 2016;6:27693.

92. Wu X, Suvarnapathaki S, Walsh K, Camci-Unal G. Paper as a scaffold for cell cultures: Teaching an old material new tricks. MRS Communications. 2018;8(1):1-14.

93. Camci-Unal G, Newsome D, Eustace BK, Whitesides GM. Fibroblasts enhance migration of human lung cancer cells in a paper-based coculture system. Advanced healthcare materials. 2015.

94. Feinberg AW, Wilkerson WR, Seegert CA, Gibson AL, Hoipkemeier-Wilson L, Brennan AB. Systematic variation of microtopography, surface chemistry and elastic modulus and the state dependent effect on endothelial cell alignment. Journal of Biomedical Materials Research Part A: An Official Journal of The Society for Biomaterials, The Japanese Society for Biomaterials, and The Australian Society for Biomaterials and the Korean Society for Biomaterials. 2008;86(2):522-34.

95. Juvonen H, Määttänen A, Laurén P, Ihalainen P, Urtti A, Yliperttula M, et al. Biocompatibility of printed paper-based arrays for 2-D cell cultures. Acta biomaterialia. 2013;9(5):6704-10.

96. Chen Y-H, Kuo Z-K, Cheng C-M. Paper–a potential platform in pharmaceutical development. Trends in biotechnology. 2015;33(1):4-9.

97. Gleason K. iCVD: G-Lab at MIT. Available from: http://web.mit.edu/gleason-lab/iCVD.html [Accessed 24 October 2019].

98. Faustel. Corona Treating for Coating Applications: Faustel. Available from: https://www.faustel.com/technical-library/corona-treating-for-coating-applications/ [Accessed 13 May 2020].

99. Rahimi R, Ochoa M, Donaldson A, Parupudi T, Dokmeci MR, Khademhosseini A, et al. A Janus-paper PDMS platform for air–liquid interface cell culture applications. Journal of Micromechanics and Microengineering. 2015;25(5):055015.

100. Arima Y, Iwata H. Effect of wettability and surface functional groups on protein adsorption and cell adhesion using well-defined mixed self-assembled monolayers. Biomaterials. 2007;28(20):3074-82.

101. Haynes CA, Norde W. Structures and stabilities of adsorbed proteins. Journal of Colloid and Interface Science. 1995;169(2):313-28.

102. Silva-Bermudez P, Rodil S, Muhl S. Albumin adsorption on oxide thin films studied by spectroscopic ellipsometry. Applied Surface Science. 2011;258(5):1711-8.

103. Vogler EA. Structure and reactivity of water at biomaterial surfaces. Advances in colloid and interface science. 1998;74(1-3):69-117.

104. Baharloo B, Textor M, Brunette D. Substratum roughness alters the growth, area, and focal adhesions of epithelial cells, and their proximity to titanium surfaces. Journal of Biomedical Materials Research Part A: An Official Journal of The Society for Biomaterials, The Japanese Society for Biomaterials, and The Australian Society for Biomaterials and the Korean Society for Biomaterials. 2005;74(1):12-22.

105. Wang L, Carrier RL. Biomimetic topography: bioinspired cell culture substrates and scaffolds. Advances in biomimetics. 2011;21:454-72.

106. Stevens MM. Biomaterials for bone tissue engineering. Materials today. 2008;11(5):18-25.

107. Tse J, Engler A. Current Protocols in Cell Biology. 2010. Unit.10:1-16.

108. Deiss Fdr, Mazzeo A, Hong E, Ingber DE, Derda R, Whitesides GM. Platform for high-throughput testing of the effect of soluble compounds on 3D cell cultures. Analytical chemistry. 2013;85(17):8085-94.

109. Deiss F, Matochko WL, Govindasamy N, Lin EY, Derda R. Flow-through synthesis on teflon-patterned paper to produce peptide arrays for cell-based assays. Angewandte Chemie International Edition. 2014;53(25):6374-7.

110. Frimat J-P, Menne H, Michels A, Kittel S, Kettler R, Borgmann S, et al. Plasma stencilling methods for cell patterning. Analytical and bioanalytical chemistry. 2009;395(3):601-9.

111. Pupinyo N, Chatatikun M, Chiabchalard A, Laiwattanapaisal W. In situ paper-based 3D cell culture for rapid screening of the anti-melanogenic activity. Analyst. 2019;144(1):290-8.

112. Biaglow JE. The effects of ionizing radiation on mammalian cells. ACS Publications; 1981.

113. Billiet T, Vandenhaute M, Schelfhout J, Van Vlierberghe S, Dubruel P. A review of trends and limitations in hydrogel-rapid prototyping for tissue engineering. Biomaterials. 2012;33(26):6020-41.

114. Hutmacher DW. Scaffolds in tissue engineering bone and cartilage. The biomaterials: Silver jubilee compendium: Elsevier; 2000. p. 175-89.

115. Ryan G, Pandit A, Apatsidis DP. Fabrication methods of porous metals for use in orthopaedic applications. Biomaterials. 2006;27(13):2651-70.

116. Sáenz A, Rivera E, Brostow W, Castaño VM. Ceramic biomaterials: an introductory overview. Journal of Materials Education. 1999;21(5/6):267-76.

117. Lantigua D, Kelly YN, Unal B, Camci-Unal G. Engineered paper-based cell culture platforms. Advanced healthcare materials. 2017;6(22):1700619.

118. Hanahan D, Weinberg RA. Hallmarks of cancer: the next generation. cell. 2011;144(5):646-74.

119. Boyce MW, Kenney RM, Truong AS, Lockett MR. Quantifying oxygen in paper-based cell cultures with luminescent thin film sensors. Analytical and bioanalytical chemistry. 2016;408(11):2985-92.

120. Hong B, Xue P, Wu Y, Bao J, Chuah YJ, Kang Y. A concentration gradient generator on a paper-based microfluidic chip coupled with cell culture microarray for high-throughput drug screening. Biomedical microdevices. 2016;18(1):21.

121. Simon KA, Mosadegh B, Minn KT, Lockett MR, Mohammady MR, Boucher DM, et al. Metabolic response of lung cancer cells to radiation in a paper-based 3D cell culture system. Biomaterials. 2016;95:47-59.

122. Aikawa E, Whittaker P, Farber M, Mendelson K, Padera RF, Aikawa M, et al. Human semilunar cardiac valve remodeling by activated cells from fetus to adult: implications for postnatal adaptation, pathology, and tissue engineering. Circulation. 2006;113(10):1344-52.

123. Dreger SA, Thomas P, Sachlos E, Chester AH, Czernuszka JT, Taylor PM, et al. Potential for synthesis and degradation of extracellular matrix proteins by valve interstitial cells seeded onto collagen scaffolds. Tissue engineering. 2006;12(9):2533-40.

124. Sapp MC, Fares HJ, Estrada AC, Grande-Allen KJ. Multilayer three-dimensional filter paper constructs for the culture and analysis of aortic valvular interstitial cells. Acta biomaterialia. 2015;13:199-206.

125. Park T-E, Mustafaoglu N, Herland A, Hasselkus R, Mannix R, FitzGerald EA, et al. Hypoxia-enhanced Blood-Brain Barrier Chip recapitulates human barrier function and shuttling of drugs and antibodies. Nature communications. 2019;10(1):2621.

126. Wang L, Xu C, Zhu Y, Yu Y, Sun N, Zhang X, et al. Human induced pluripotent stem cell-derived beating cardiac tissues on paper. Lab on a Chip. 2015;15(22):4283-90.

127. Bhattacharya I, Ghayor C, Weber FE. The use of adipose tissue-derived progenitors in bone tissue engineering-a review. Transfusion Medicine and Hemotherapy. 2016;43(5):336-43.

128. Whatman filter paper: GE lifesciences. Available from: https://www.gelifesciences.com/ [Accessed 13 May 2020].

129. Liu F, Ge S, Yu J, Yan M, Song X. Electrochemical device based on a Pt nanosphere-paper working electrode for in situ and real-time determination of

the flux of H 2 O 2 releasing from SK-BR-3 cancer cells. Chemical Communications. 2014;50(71):10315-8.

130. Kim YJ, Kim JE, Ryu SY, Ogunjobi KO, editors. UV irradiance monitoring and effects of aerosol optical depth on the ground-based measurement of ultraviolet irradiance at Kwangju, Korea. Ultraviolet Ground-and Space-based Measurements, Models, and Effects II; 2003: International Society for Optics and Photonics.

131. Wei Y, ZHANG Q, Bin C, LIANG G-T, Wei-Xuan L, Xiao-Mian Z, et al. Study on microenvironment acidification by microfluidic chip with multilayer-paper supported breast cancer tissue. Chinese Journal of Analytical Chemistry. 2013;41(6):822-7.

132. Zelada-Guillén GA, Tweed-Kent A, Niemann M, Göringer HU, Riu J, Rius FX. Ultrasensitive and real-time detection of proteins in blood using a potentiometric carbon-nanotube aptasensor. Biosensors and Bioelectronics. 2013;41:366-71.

133. Ahmed A, Rushworth JV, Hirst NA, Millner PA. Biosensors for whole-cell bacterial detection. Clinical microbiology reviews. 2014;27(3):631-46.

134. Liu M-M, Guo Z-Z, Liu H, Li S-H, Chen Y, Zhong Y, et al. Paper-based 3D culture device integrated with electrochemical sensor for the on-line cell viability evaluation of amyloid-beta peptide induced damage in PC12 cells. Biosensors and Bioelectronics. 2019;144:111686.

135. Khairy M, Choudry NA, Ouasti M, Kampouris DK, Kadara RO, Banks CE. Gold nanoparticle ensembles allow mechanistic insights into electrochemical processes. ChemPhysChem. 2010;11(4):875-9.

136. Shi Z, Wu X, Gao L, Tian Y, Yu L. Electrodes/paper sandwich devices for in situ sensing of hydrogen peroxide secretion from cells growing in gels-in-paper 3-dimensional matrix. Analytical Methods. 2014;6(12):4446-54.

137. Ge S, Zhang L, Zhang Y, Liu H, Huang J, Yan M, et al. Electrochemical K-562 cells sensor based on origami paper device for point-of-care testing. Talanta. 2015;145:12-9.

138. Jiang D, Ge P, Wang L, Jiang H, Yang M, Yuan L, et al. A novel electrochemical mast cell-based paper biosensor for the rapid detection of milk allergen casein. Biosensors and Bioelectronics. 2019;130:299-306.

139. Su M, Ge L, Ge S, Li N, Yu J, Yan M, et al. Paper-based electrochemical cyto-device for sensitive detection of cancer cells and in situ anticancer drug screening. Analytica chimica acta. 2014;847:1-9.

140. Su M, Ge L, Kong Q, Zheng X, Ge S, Li N, et al. Cyto-sensing in electrochemical lab-on-paper cyto-device for in-situ evaluation of multi-glycan expressions on cancer cells. Biosensors and Bioelectronics. 2015;63:232-9.

141. Cai H. Hydrogen peroxide regulation of endothelial function: origins, mechanisms, and consequences. Cardiovascular research. 2005;68(1):26-36.

142. Accetta R, Damiano S, Morano A, Mondola P, Paternò R, Avvedimento EV, et al. Reactive oxygen species derived from NOX3 and NOX5 drive differentiation of human oligodendrocytes. Frontiers in cellular neuroscience. 2016;10:146.

143. Roy S, Noda Y, Eckert V, Traber MG, Mori A, Liburdy R, et al. The phorbol 12-myristate 13-acetate (PMA)-induced oxidative burst in rat peritoneal neutrophils is increased by a 0.1 mT (60 Hz) magnetic field. FEBS letters. 1995;376(3):164-6.

144. Riss TL, Moravec RA, Niles AL, Duellman S, Benink HA, Worzella TJ, et al. Cell viability assays. Assay Guidance Manual [Internet]: Eli Lilly & Company and the National Center for Advancing Translational Sciences; 2016.

145. Stoddart MJ. Cell viability assays: introduction. Mammalian cell viability: Springer; 2011. p. 1-6.

146. Jiang L, Lu Y, Dai Z, Xie M, Lin B. Mini-electrochemical detector for microchip electrophoresis. Lab on a Chip. 2005;5(9):930-4.

147. Lin S, Kemmner W, Grigull S, Schlag PM. Cell surface α2, 6-sialylation affects adhesion of breast carcinoma cells. Experimental cell research. 2002;276(1):101-10.

148. Giaever I, Keese CR. A morphological biosensor for mammalian cells. Nature. 1993;366(6455):591-2.

149. Tiruppathi C, Malik AB, Del Vecchio PJ, Keese CR, Giaever I. Electrical method for detection of endothelial cell shape change in real time: assessment of endothelial barrier function. Proceedings of the National Academy of Sciences. 1992;89(17):7919-23.

150. Brenner M, Hearing VJ. The protective role of melanin against UV damage in human skin. Photochemistry and photobiology. 2008;84(3):539-49.

151. Coelho SG, Zhou Y, Bushar HF, Miller SA, Zmudzka BZ, Hearing VJ, et al. Long-Lasting Pigmentation (LLP) of Human Skin, a New Look at an Overlooked Response to UV. Pigment cell & melanoma research. 2009;22(2):238.

152. Kobayashi N, Nakagawa A, Muramatsu T, Yamashina Y, Shirai T, Hashimoto MW, et al. Supranuclear melanin caps reduce ultraviolet induced DNA photoproducts in human epidermis. Journal of Investigative Dermatology. 1998;110(5):806-10.

153. d'Ischia M, Wakamatsu K, Cicoira F, Di Mauro E, Garcia‐Borron JC, Commo S, et al. Melanins and melanogenesis: from pigment cells to human health and technological applications. Pigment cell & melanoma research. 2015;28(5):520-44.

154. Ito S, Nakanishi Y, Valenzuela RK, Brilliant MH, Kolbe L, Wakamatsu K. Usefulness of alkaline hydrogen peroxide oxidation to analyze eumelanin and pheomelanin in various tissue samples: application to chemical analysis of human hair melanins. Pigment cell & melanoma research. 2011;24(4):605-13.

155. Chedekel MR, Smith SK, Post PW, Pokora A, Vessell DL. Photodestruction of pheomelanin: role of oxygen. Proceedings of the National Academy of Sciences. 1978;75(11):5395-9.

156. Felix C, Hyde J, Sarna T, Sealy R. Melanin photoreactions in aerated media: electron spin resonance evidence for production of superoxide and hydrogen peroxide. Biochemical and biophysical research communications. 1978;84(2):335-41.

157. Simon JD, Peles DN. The red and the black. Accounts of chemical research. 2010;43(11):1452-60.

158. Harsanyl Z, Post P, Brinkmann JP, Chedekel M, Deibel RM. Mutagenicity of melanin from human red hair. Experientia. 1980;36(3):291-2.

159. Mitra D, Luo X, Morgan A, Wang J, Hoang MP, Lo J, et al. An ultraviolet-radiation-independent pathway to melanoma carcinogenesis in the red hair/fair skin background. Nature. 2012;491(7424):449.

160. Robbins LS, Nadeau JH, Johnson KR, Kelly MA, Roselli-Rehfuss L, Baack E, et al. Pigmentation phenotypes of variant extension locus alleles result from point mutations that alter MSH receptor function. Cell. 1993;72(6):827-34.

161. Valverde P, Healy E, Jackson I, Rees JL, Thody AJ. Variants of the melanocyte–stimulating hormone receptor gene are associated with red hair and fair skin in humans. Nature genetics. 1995;11(3):328.

162. Cheli Y, Luciani F, Khaled M, Beuret L, Bille K, Gounon P, et al. αMSH and cyclic AMP elevating agents control melanosome pH through a protein kinase A-independent mechanism. Journal of Biological Chemistry. 2009;284(28):18699-706.

163. Abdel-Malek Z, Swope VB, Suzuki I, Akcali C, Harriger MD, Boyce ST, et al. Mitogenic and melanogenic stimulation of normal human melanocytes by melanotropic peptides. Proceedings of the National Academy of Sciences. 1995;92(5):1789-93.

164. Videira IFdS, Moura DFL, Magina S. Mechanisms regulating melanogenesis. Anais brasileiros de dermatologia. 2013;88(1):76-83.

165. Park H, Kosmadaki M, Yaar M, Gilchrest B. Cellular mechanisms regulating human melanogenesis. Cellular and molecular life sciences. 2009;66(9):1493-506.

166. Slominski A, Tobin DJ, Shibahara S, Wortsman J. Melanin pigmentation in mammalian skin and its hormonal regulation. Physiological reviews. 2004;84(4):1155-228.

167. Ito S, Wakamatsu K. Chemistry of mixed melanogenesis—pivotal roles of dopaquinone. Photochemistry and photobiology. 2008;84(3):582-92.

168. Edge R, d'Ischia M, Land E, Napolitano A, Navaratnam S, Panzella L, et al. Dopaquinone redox exchange with dihydroxyindole and dihydroxyindole carboxylic acid. Pigment cell research. 2006;19(5):443-50.

169. Grando SA, Pittelkow MR, Schallreuter KU. Adrenergic and cholinergic control in the biology of epidermis: physiological and clinical significance. Journal of Investigative Dermatology. 2006;126(9):1948-65.

170. Costin G-E, Hearing VJ. Human skin pigmentation: melanocytes modulate skin color in response to stress. The FASEB journal. 2007;21(4):976-94.

171. Schiaffino MV. Signaling pathways in melanosome biogenesis and pathology. The international journal of biochemistry & cell biology. 2010;42(7):1094-104.

172. Thody AJ, Graham A. Does α-MSH have a role in regulating skin pigmentation in humans? Pigment cell research. 1998;11(5):265-74.

173. Tadokoro T, Yamaguchi Y, Batzer J, Coelho SG, Zmudzka BZ, Miller SA, et al. Mechanisms of skin tanning in different racial/ethnic groups in response to ultraviolet radiation. Journal of Investigative Dermatology. 2005;124(6):1326-32.

174. Godechal Q, Mignion L, Karroum O, Magat J, Danhier P, Morandini R, et al. Influence of paramagnetic melanin on the MRI contrast in melanoma: a combined high-field (11.7 T) MRI and EPR study. Contrast media & molecular imaging. 2014;9(2):154-60.

175. Godechal Q, Ghanem GE, Cook MG, Gallez B. Electron paramagnetic resonance spectrometry and imaging in melanomas: comparison between pigmented and nonpigmented human malignant melanomas. Molecular imaging. 2013;12(4):7290.2012. 00037.

176. Grabacka M, Wieczorek J, Michalczyk-Wetula D, Malinowski M, Wolan N, Wojcik K, et al. Peroxisome proliferator-activated receptor α (PPARα) contributes to control of melanogenesis in B16 F10 melanoma cells. Archives of dermatological research. 2017;309(3):141-57.

177. Matsunaka H, Yamamoto Y, Furukawa F. Non-invasive quantification of melanin in the stratum corneum: a novel indicator of skin lesions in pigmentation diseases. Skin Research and Technology. 2017;23(1):104-11.

178. Hu DN. Methodology for evaluation of melanin content and production of pigment cells in vitro. Photochemistry and photobiology. 2008;84(3):645-9.

179. Kim MJ, Jung TK, Park H-C, Yoon K-S. Effect of Hoechunyangkyeok-San extract on melanogenesis. Journal of Cosmetics, Dermatological Sciences and Applications. 2016;6(3).

180. Chung S, Lim GJ, Lee JY. Quantitative analysis of melanin content in a three-dimensional melanoma cell culture. Scientific reports. 2019;9(1):780.

181. Hu D-N, McCormick SA, Orlow SJ, Rosemblat S, Lin AY, Wo K. Melanogenesis by human uveal melanocytes in vitro. Investigative ophthalmology & visual science. 1995;36(5):931-8.

182. LIN A, HU D, ORLOW S, WO K, MCCORMICK S, editors. Melanogenesis in cultured human uveal melanocytes. Investigative Ophthalmology & Visual Science; 1994: LIPPINCOTT-RAVEN PUBL 227 EAST WASHINGTON SQ, PHILADELPHIA, PA 19106.

183. Ito S, Wakamatsu K. Chemistry of melanins. The Pigmentary System Physiology and Pathophysiology. 2006;2:282-310.

184. Prince S, Wiggins T, Hulley P, Kidson S. Stimulation of melanogenesis by tetradecanoylphorbol 13-acetate (TPA) in mouse melanocytes and neural crest cells. Pigment cell research. 2003;16(1):26-34.

185. Lassalle MW, Igarashi S, Sasaki M, Wakamatsu K, Ito S, Horikoshi T. Effects of melanogenesis-inducing nitric oxide and histamine on the production of eumelanin and pheomelanin in cultured human melanocytes. Pigment cell research. 2003;16(1):81-4.

186. Singh SK, Sarkar C, Mallick S, Saha B, Bera R, Bhadra R. Human placental lipid induces melanogenesis through p38 MAPK in B16F10 mouse melanoma. Pigment cell research. 2005;18(2):113-21.

187. Li L, Hu D-N, Zhao H, McCormick SA, Nordlund JJ, Boissy RE. Uveal melanocytes do not respond to or express receptors for α-melanocyte-stimulating hormone. Investigative ophthalmology & visual science. 2006;47(10):4507-12.

188. Hu D-N, McCormick SA, Seedor JA, Ritterband DC, Shah MK. Isolation, purification and cultivation of conjunctival melanocytes. Experimental eye research. 2007;84(4):655-62.

189. Zhou X, Fu X, Qu J, Lu F, Hu D. Study on Melanogenesis of Mongolian Uveal Melanocytes in Vitro. Investigative Ophthalmology & Visual Science. 2004;45(13):1216-.

190. Hu D-n, Stjernschantz J, McCORMICK SA. Effect of Prostaglandins A2, E1, F2 α and Latanoprost on Cultured Human Iridal Melanocytes. Experimental eye research. 2000;70(1):113-20.

191. HU DN. Regulation of growth and melanogenesis of uveal melanocytes. Pigment Cell Research. 2000;13:81-6.

192. Hu D-N, Ritch R, McCormick S, Pelton-Henrion K. Isolation and cultivation of human iris pigment epithelium. Investigative ophthalmology & visual science. 1992;33(8):2443-53.

193. McGuinness R. Impedance-based cellular assay technologies: recent advances, future promise. Current opinion in pharmacology. 2007;7(5):535-40.

194. Gu W, Zhao Y. Cellular electrical impedance spectroscopy: an emerging technology of microscale biosensors. Expert review of medical devices. 2010;7(6):767-79.

195. Torrents J, Juan-Garcia P, Aguado A. Electrical impedance spectroscopy as a technique for the surveillance of civil engineering structures: considerations on the galvanic insulation of samples. Measurement Science and Technology. 2007;18(7):1958.

196. Wu J, Ben Y, Chang H-C. Particle detection by electrical impedance spectroscopy with asymmetric-polarization AC electroosmotic trapping. Microfluidics and Nanofluidics. 2005;1(2):161-7.

197. Casas O, Bragos R, Riu P, Rosell J, Tresanchez M, Warren M, et al. In Vivo and In Situ Ischemic Tissue Characterization Using Electrical Impedance Spectroscopy a. Annals of the New York Academy of Sciences. 1999;873(1):51-8.

198. Da Silva JE, De Sá JM, Jossinet J. Classification of breast tissue by electrical impedance spectroscopy. Medical and Biological Engineering and Computing. 2000;38(1):26-30.

199. Giaever I, Keese CR. Electric cell-substrate impedance sensing concept to commercialization. Electric cell-substrate impedance sensing and cancer metastasis: Springer; 2012. p. 1-19.

200. Xu Y, Xie X, Duan Y, Wang L, Cheng Z, Cheng J. A review of impedance measurements of whole cells. Biosensors and Bioelectronics. 2016;77:824-36.

201. Gawad S, Cheung K, Seger U, Bertsch A, Renaud P. Dielectric spectroscopy in a micromachined flow cytometer: theoretical and practical considerations. Lab on a Chip. 2004;4(3):241-51.

202. Morgan H, Sun T, Holmes D, Gawad S, Green NG. Single cell dielectric spectroscopy. Journal of Physics D: Applied Physics. 2006;40(1):61.

203. Sun T, Green NG, Morgan H. Analytical and numerical modeling methods for impedance analysis of single cells on-chip. Nano. 2008;3(01):55-63.

204. Yang L, Ruan C, Li Y. Detection of viable Salmonella typhimurium by impedance measurement of electrode capacitance and medium resistance. Biosensors and Bioelectronics. 2003;19(5):495-502.

205. Asami K. Characterization of biological cells by dielectric spectroscopy. Journal of Non-Crystalline Solids. 2002;305(1-3):268-77.

206. Schwan HP, Kay CF. Specific resistance of body tissues. Circulation Research. 1956;4(6):664-70.

207. Hasted JB. Aqueous dielectrics: Chapman and Hall; 1973.

208. Giaever I, Keese CR. Micromotion of mammalian cells measured electrically. Proceedings of the National Academy of Sciences. 1991;88(17):7896-900.

209. Krinke D, Jahnke H-G, Pänke O, Robitzki AA. A microelectrode-based sensor for label-free in vitro detection of ischemic effects on cardiomyocytes. Biosensors and Bioelectronics. 2009;24(9):2798-803.

210. Arndt S, Seebach J, Psathaki K, Galla H-J, Wegener J. Bioelectrical impedance assay to monitor changes in cell shape during apoptosis. Biosensors and Bioelectronics. 2004;19(6):583-94.

211. Wang L, Yin H, Xing W, Yu Z, Guo M, Cheng J. Real-time, label-free monitoring of the cell cycle with a cellular impedance sensing chip. Biosensors and Bioelectronics. 2010;25(5):990-5.

212. K'Owino IO, Sadik OA. Impedance spectroscopy: a powerful tool for rapid biomolecular screening and cell culture monitoring. Electroanalysis: An International Journal Devoted to Fundamental and Practical Aspects of Electroanalysis. 2005;17(23):2101-13.

213. Yarlagadda RR. Analog and digital signals and systems: Springer; 2010.

214. Gawad S, Schild L, Renaud P. Micromachined impedance spectroscopy flow cytometer for cell analysis and particle sizing. Lab on a Chip. 2001;1(1):76-82.

215. Wang J, Wu C, Hu N, Zhou J, Du L, Wang P. Microfabricated electrochemical cell-based biosensors for analysis of living cells in vitro. Biosensors. 2012;2(2):127-70.

216. Narayanan S, Nikkhah M, Strobl JS, Agah M. Analysis of the passivation layer by testing and modeling a cell impedance micro-sensor. Sensors and Actuators A: Physical. 2010;159(2):241-7.

217. Schäfer S, Eick S, Hofmann B, Dufaux T, Stockmann R, Wrobel G, et al. Time-dependent observation of individual cellular binding events to field-effect transistors. Biosensors and bioelectronics. 2009;24(5):1201-8.

218. Susloparova A, Koppenhöfer D, Vu X, Weil M, Ingebrandt S. Impedance spectroscopy with field-effect transistor arrays for the analysis of anti-cancer drug action on individual cells. Biosensors and Bioelectronics. 2013;40(1):50-6.

219. Chen N-C, Chen C-H, Chen M-K, Jang L-S, Wang M-H. Single-cell trapping and impedance measurement utilizing dielectrophoresis in a parallel-plate microfluidic device. Sensors and Actuators B: Chemical. 2014;190:570-7.

220. Jiang X, Spencer MG. Electrochemical impedance biosensor with electrode pixels for precise counting of CD4+ cells: A microchip for quantitative diagnosis of HIV infection status of AIDS patients. Biosensors and Bioelectronics. 2010;25(7):1622-8.

221. Chun H, Chung TD, Kim HC. Cytometry and velocimetry on a microfluidic chip using polyelectrolytic salt bridges. Analytical chemistry. 2005;77(8):2490-5.

222. Cheung K, Gawad S, Renaud P. Impedance spectroscopy flow cytometry: On-chip label-free cell differentiation. Cytometry Part A. 2005;65(2):124-32.

223. Pänke O, Weigel W, Schmidt S, Steude A, Robitzki AA. A cell-based impedance assay for monitoring transient receptor potential (TRP) ion channel activity. Biosensors and Bioelectronics. 2011;26(5):2376-82.

224. Abdolahad M, Janmaleki M, Taghinejad M, Taghnejad H, Salehi F, Mohajerzadeh S. Single-cell resolution diagnosis of cancer cells by carbon nanotube electrical spectroscopy. Nanoscale. 2013;5(8):3421-7.

225. Thomas Jr C, Springer P, Loeb G, Berwald-Netter Y, Okun L. A miniature microelectrode array to monitor the bioelectric activity of cultured cells. Experimental cell research. 1972;74(1):61-6.

226. Zudaire E, Cuesta N, Murty V, Woodson K, Adams L, Gonzalez N, et al. The aryl hydrocarbon receptor repressor is a putative tumor suppressor gene in multiple human cancers. The Journal of clinical investigation. 2008;118(2):640-50.

227. Charrier L, Yan Y, Nguyen HTT, Dalmasso G, Laboisse CL, Gewirtz AT, et al. ADAM-15/metargidin mediates homotypic aggregation of human T lymphocytes and heterotypic interactions of T lymphocytes with intestinal epithelial cells. Journal of Biological Chemistry. 2007;282(23):16948-58.

228. Saxena NK, Sharma D, Ding X, Lin S, Marra F, Merlin D, et al. Concomitant activation of the JAK/STAT, PI3K/AKT, and ERK signaling is involved in leptin-mediated promotion of invasion and migration of hepatocellular carcinoma cells. Cancer research. 2007;67(6):2497-507.

229. Radke SM, Alocilja EC. Design and fabrication of a microimpedance biosensor for bacterial detection. IEEE sensors journal. 2004;4(4):434-40.

230. Varshney M, Li Y. Interdigitated array microelectrodes based impedance biosensors for detection of bacterial cells. Biosensors and bioelectronics. 2009;24(10):2951-60.

231. Wang L, Wang H, Mitchelson K, Yu Z, Cheng J. Analysis of the sensitivity and frequency characteristics of coplanar electrical cell–substrate impedance sensors. Biosensors and Bioelectronics. 2008;24(1):14-21.

232. Brischwein M, Herrmann S, Vonau W, Berthold F, Grothe H, Motrescu ER, et al. Electric cell-substrate impedance sensing with screen printed electrode structures. Lab on a Chip. 2006;6(6):819-22.

233. Methods for Measuring Cell Proliferation: Cell Biolabs, INC. Available from: https://www.cellbiolabs.com/news/methods-measuring-cell-proliferation [Accessed 13 May 2020].

234. Cell proliferation: Applied BioPhysics. Available from: https://www.biophysics.com/cellProliferation.php [Accessed 13 May 2020].

235. Xiao C, Luong JH. On-line monitoring of cell growth and cytotoxicity using electric cell-substrate impedance sensing (ECIS). Biotechnology progress. 2003;19(3):1000-5.

236. Yun Y, Dong Z, Tan Z, Schulz MJ. Development of an electrode cell impedance method to measure osteoblast cell activity in magnesium-conditioned media. Analytical and bioanalytical chemistry. 2010;396(8):3009-15.

237. Xu Y, Lv Y, Wang L, Xing W, Cheng J. A microfluidic device with passive air-bubble valves for real-time measurement of dose-dependent drug cytotoxicity through impedance sensing. Biosensors and Bioelectronics. 2012;32(1):300-4.

238. Campbell CE, Laane MM, Haugarvoll E, Giaever I. Monitoring viral-induced cell death using electric cell–substrate impedance sensing. Biosensors and Bioelectronics. 2007;23(4):536-42.

239. Müller J, Thirion C, Pfaffl MW. Electric cell-substrate impedance sensing (ECIS) based real-time measurement of titer dependent cytotoxicity induced by adenoviral vectors in an IPI-2I cell culture model. Biosensors and Bioelectronics. 2011;26(5):2000-5.

240. ECIS Wound Healing/Cell-Migration Assay: Applied Biophysiscs. Available from: https://www.biophysics.com/cellMigration.php [Accessed 13 May 2020].

241. Cai H. Monitoring the Barrier Function of Cell Monolayers using ECIS®: AppliedBiophysiscs

Available from: https://www.biophysics.com/teerBarrierFunction.php [Accessed 13 May 2020].

242. Silverio V, de Freitas SC. Microfabrication techniques for microfluidic devices. Complex Fluid-Flows in Microfluidics: Springer; 2018. p. 25-51.

243. Rai-Choudhury P. Handbook of microlithography, micromachining, and microfabrication: microlithography: Iet; 1997.

244. Merriam-Webster. Etching: Merriam-Webster. Available from: https://www.merriam-webster.com/dictionary/etching [Accessed 13 May 2020].

245. Liu K, Fan ZH. Thermoplastic microfluidic devices and their applications in protein and DNA analysis. Analyst. 2011;136(7):1288-97.

246. Hamilton N. Quantification and its applications in fluorescent microscopy imaging. Traffic. 2009;10(8):951-61.

247. Ayala I, Baldassarre M, Caldieri G, Buccione R. Invadopodia: a guided tour. European journal of cell biology. 2006;85(3-4):159-64.

248. Yamamoto E, Kohama GI, Sunakawa H, Iwai M, Hiratsuka H. Mode of invasion, bleomycin sensitivity, and clinical course in squamous cell carcinoma of the oral cavity. Cancer. 1983;51(12):2175-80.

249. Fusenig NE, Breitkreutz D, Dzarlieva RT, Boukamp P, Bohnert A, Tilgen W. Growth and differentiation characteristics of transformed keratinocytes from mouse and human skin in vitro and in vivo. Journal of Investigative Dermatology. 1983;81(1):S168-S75.

250. Timpson P, Mcghee EJ, Erami Z, Nobis M, Quinn JA, Edward M, et al. Organotypic collagen I assay: a malleable platform to assess cell behaviour in a 3-dimensional context. JoVE (Journal of Visualized Experiments). 2011(56):e3089.

251. Nyström M, Thomas G, Stone M, Mackenzie I, Hart I, Marshall J. Development of a quantitative method to analyse tumour cell invasion in organotypic culture. The Journal of Pathology: A Journal of the Pathological Society of Great Britain and Ireland. 2005;205(4):468-75.

252. Sutherland RM, McCredie JA, Inch WR. Growth of multicell spheroids in tissue culture as a model of nodular carcinomas. Journal of the National Cancer Institute. 1971;46(1):113-20.

253. Hattermann K, Held-Feindt J, Mentlein R. Spheroid confrontation assay: a simple method to monitor the three-dimensional migration of different cell types in vitro. Annals of Anatomy-Anatomischer Anzeiger. 2011;193(3):181-4.

254. Li C, Wei Y, Zhang S, Tan W. Advanced methods to analyze steroid estrogens in environmental samples. Environmental Chemistry Letters. 2020:1-17.

255. Walker CW, Watson JE. Adsorption of estrogens on laboratory materials and filters during sample preparation. Journal of environmental quality. 2010;39(2):744-8.

256. Drzymala SS, Weiz S, Heinze J, Marten S, Prinz C, Zimathies A, et al. Automated solid-phase extraction coupled online with HPLC-FLD for the quantification of zearalenone in edible oil. Analytical and bioanalytical chemistry. 2015;407(12):3489-97.

257. Botelho JC, Ribera A, Cooper HC, Vesper HW. Evaluation of an isotope dilution HPLC tandem mass spectrometry candidate reference measurement procedure for total 17-β estradiol in human serum. Analytical chemistry. 2016;88(22):11123-9.

258. On J, Pyo H, Myung S-W. Effective and sensitive determination of eleven disinfection byproducts in drinking water by DLLME and GC–MS. Science of The Total Environment. 2018;639:208-16.

259. Martins AF, dos Santos JB, Todeschini BH, Saldanha LF, da Silva DS, Reichert JF, et al. Occurrence of cocaine and metabolites in hospital effluent-A risk evaluation and development of a HPLC method using DLLME. Chemosphere. 2017;170:176-82.

260. Pacáková V, Loukotková L, Bosáková Z, Štulík K. Analysis for estrogens as environmental pollutants–A review. Journal of separation science. 2009;32(5-6):867-82.

261. Li W, Hong B, Li Z, Li Q, Bi K. GC–MS method for determination and pharmacokinetic study of seven volatile constituents in rat plasma after oral administration of the essential oil of Rhizoma Curcumae. Journal of pharmaceutical and biomedical analysis. 2018;149:577-85.

262. Tsikas D, Zoerner AA. Analysis of eicosanoids by LC-MS/MS and GC-MS/MS: a historical retrospect and a discussion. Journal of Chromatography B. 2014;964:79-88.

263. Moraes FC, Rossi B, Donatoni MC, de Oliveira KT, Pereira EC. Sensitive determination of 17β-estradiol in river water using a graphene based electrochemical sensor. Analytica chimica acta. 2015;881:37-43.

264. Li J, Song J, Bi S, Zhou S, Cui J, Liu J, et al. Electrochemical estrogen screen method based on the electrochemical behavior of MCF-7 cells. Journal of hazardous materials. 2016;313:238-43.

265. Barton H, Berbel-Filho WM, Consuegra S, Francis L, Tizaoui C, Conlan RS, et al. Ultrasensitive environmental assessment of xeno-estrogens in water samples using label-free graphene immunosensors. Analytical biochemistry. 2018;548:102-8.

266. Liu M, Ke H, Sun C, Wang G, Wang Y, Zhao G. A simple and highly selective electrochemical label-free aptasensor of 17β-estradiol based on signal amplification of bi-functional graphene. Talanta. 2019;194:266-72.

267. Grange R, Thompson J, Lambert D. Radioimmunoassay, enzyme and non-enzyme-based immunoassays. British journal of anaesthesia. 2014;112(2):213-6.

268. Uraipong C, Allan RD, Li C, Kennedy IR, Wong V, Lee NA. A survey of 17α-ethinylestradiol and mestranol residues in Hawkesbury River, Australia, using a highly specific enzyme-linked immunosorbent assay (ELISA) demonstrates the levels of potential biological significance. Ecotoxicology and environmental safety. 2017;144:585-92.

269. Heppell SA, Denslow ND, Folmar LC, Sullivan CV. Universal assay of vitellogenin as a biomarker for environmental estrogens. Environmental Health Perspectives. 1995;103(suppl 7):9-15.

270. Ni X, Xia B, Wang L, Ye J, Du G, Feng H, et al. Fluorescent aptasensor for 17β-estradiol determination based on gold nanoparticles quenching the fluorescence of Rhodamine B. Analytical biochemistry. 2017;523:17-23.

271. Matthews J, Zacharewski T. Differential binding affinities of PCBs, HO-PCBs, and aroclors with recombinant human, rainbow trout (Onchorhynkiss mykiss), and green anole (Anolis carolinensis) estrogen receptors, using a semi-high throughput competitive binding assay. Toxicological Sciences. 2000;53(2):326-39.

272. Leusch FD, De Jager C, Levi Y, Lim R, Puijker L, Sacher F, et al. Comparison of five in vitro bioassays to measure estrogenic activity in environmental waters. Environmental science & technology. 2010;44(10):3853-60.

273. Gier K, Preininger C, Sauer U. A chip for estrogen receptor action: detection of biomarkers released by MCF-7 cells through Estrogenic and anti-estrogenic effects. Sensors. 2017;17(8):1760.

274. Scrimshaw MD, Lester JN. In-vitro assays for determination of oestrogenic activity. Analytical and bioanalytical chemistry. 2004;378(3):576-81.

275. Shabana Islam PF. Assay Methods Protocol: Cell Invasion Assay. In: Corning Incorporated LST, MA USA, editor.: Corning Incorporated, Life Sciences Tewksbury, MA USA; 2012-2018.

276. Chatatikun M, Yamauchi T, Yamasaki K, Aiba S, Chiabchalard A. Anti melanogenic effect of Croton roxburghii and Croton sublyratus leaves in **α**-MSH stimulated B16F10 cells. Journal of traditional and complementary medicine. 2019;9(1):66-72.

277. Solly K, Wang X, Xu X, Strulovici B, Zheng W. Application of real-time cell electronic sensing (RT-CES) technology to cell-based assays. Assay and drug development technologies. 2004;2(4):363-72.

278. Vichai V, Kirtikara K. Sulforhodamine B colorimetric assay for cytotoxicity screening. Nature protocols. 2006;1(3):1112.

279. Körner W, Hanf V, Schuller W, Kempter C, Metzger J, Hagenmaier H. Development of a sensitive E-screen assay for quantitative analysis of estrogenic activity in municipal sewage plant effluents. Science of the Total Environment. 1999;225(1-2):33-48.

280. Pupinyo N, Heiskanen A, Chailapakul O, Gorton L, Emnéus J, Laiwattanapaisal W. Impedimetric melanoma invasion assay device using a simple paper membrane and stencil-printed electrode on PMMA substrate. Sensing and Bio-Sensing Research. 2020 May 21:100354.

281. Justus CR, Leffler N, Ruiz-Echevarria M, Yang LV. In vitro cell migration and invasion assays. JoVE (Journal of Visualized Experiments). 2014(88):e51046.

282. Ng K, Gao B, Yong KW, Li Y, Shi M, Zhao X, et al. Paper-based cell culture platform and its emerging biomedical applications. Materials Today. 2017;20(1):32-44.

283. Frequently Asked Questions of Matrigel: Corning. Available from: http://www.corning.com [Accessed 20 November 2019].

284. Calcein, AM, cell-permeant dye: Thermofisher. Available from: http://www.thermofisher.com [Accessed 13 May 2020].

285. eBioscience Propidium Iodide Staining Solution: Thermofisher. Available from: http://www.thermofisher.com [Accessed 13 May 2020].

286. Ito S. A chemist's view of melanogenesis. Pigment cell research. 2003;16(3):230-6.

287. Price ER, Horstmann MA, Wells AG, Weilbaecher KN, Takemoto CM, Landis MW, et al. **α**-Melanocyte-stimulating hormone signaling regulates expression of microphthalmia, a gene deficient in Waardenburg syndrome. Journal of Biological Chemistry. 1998;273(49):33042-7.

288. Yamaguchi Y, Brenner M, Hearing VJ. The regulation of skin pigmentation. Journal of Biological Chemistry. 2007;282(38):27557-61.

289. Pampaloni F, Reynaud EG, Stelzer EH. The third dimension bridges the gap between cell culture and live tissue. Nature reviews Molecular cell biology. 2007;8(10):839.

290. Kapuscinski J. DAPI: a DNA-specific fluorescent probe. Biotechnic & Histochemistry. 1995;70(5):220-33.

291. Gonçalez M, Correa MA, Chorilli M. Skin delivery of kojic acid-loaded nanotechnology-based drug delivery systems for the treatment of skin aging. BioMed research international. 2013;2013.

292. Ki D-H, Jung H-C, Noh Y-W, Thanigaimalai P, Kim B-H, Shin S-C, et al. Preformulation and formulation of newly synthesized QNT3-18 for development of a skin whitening agent. Drug development and industrial pharmacy. 2013;39(4):526-33.

293. Kumar KS, Vani MG, Wang SY, Liao JW, Hsu LS, Yang HL, et al. In vitro and in vivo studies disclosed the depigmenting effects of gallic acid: A novel skin lightening agent for hyperpigmentary skin diseases. Biofactors. 2013;39(3):259-70.

294. Gamal W, Wu H, Underwood I, Jia J, Smith S, Bagnaninchi P. Impedance-based cellular assays for regenerative medicine. Philosophical Transactions of the Royal Society B: Biological Sciences. 2018;373(1750):20170226.

295. Anh-Nguyen T, Tiberius B, Pliquett U, Urban GA. An impedance biosensor for monitoring cancer cell attachment, spreading and drug-induced apoptosis. Sensors and Actuators A: Physical. 2016;241:231-7.

296. Choosing The Proper ECIS® Array [Technical note]. Applied Biophysiscs. Available from: https://www.biophysics.com/public/pdf/TN01ArrayChoices.pdf [Accessed 25 March 2020].

297. Prins GS, Patisaul HB, Belcher SM, Vandenberg LN. CLARITY-BPA academic laboratory studies identify consistent low-dose Bisphenol A effects on multiple organ systems. Basic & clinical pharmacology & toxicology. 2019;125:14-31.

298. Pellitero MA, Kitsara M, Eibensteiner F, del Campo FJ. Rapid prototyping of electrochemical lateral flow devices: stencilled electrodes. Analyst. 2016;141(8):2515-22.

299. Morrin A, Killard AJ, Smyth MR. Electrochemical characterization of commercial and home-made screen-printed carbon electrodes. Analytical letters. 2003;36(9):2021-39.

300. Fanjul-Bolado P, Hernández-Santos D, Lamas-Ardisana PJ, Martín-Pernía A, Costa-García A. Electrochemical characterization of screen-printed and conventional carbon paste electrodes. Electrochimica Acta. 2008;53(10):3635-42.

301. Mei B-A, Munteshari O, Lau J, Dunn B, Pilon L. Physical interpretations of Nyquist plots for EDLC electrodes and devices. J Phys Chem C. 2017;122(1):194-206.

302. Shaw LM. Tumor cell invasion assays. Cell Migration: Springer; 2005. p. 97-105.

303. Caviglia C, Zor K, Montini L, Tilli V, Canepa S, Melander F, et al. Impedimetric toxicity assay in microfluidics using free and liposome-encapsulated anticancer drugs. Analytical chemistry. 2015;87(4):2204-12.

304. Tomita Y, Montague PM, Hearing VJ. Anti-T4-tyrosinase monoclonal antibodies—specific markers for pigmented melanocytes. Journal of investigative dermatology. 1985;85(5):426-30.

305. Palumbo A. Melanogenesis in the Ink Gland of Sepia officinalis. Pigment Cell Research. 2003;16(5):517-22.

306. Haining RL, Achat-Mendes C. Neuromelanin, one of the most overlooked molecules in modern medicine, is not a spectator. Neural regeneration research. 2017;12(3):372.

VITA

NAME   Naricha Pupinyo

DATE OF BIRTH   12 November 1992

PLACE OF BIRTH   Bangkok, Thailand

INSTITUTIONS ATTENDED   Faculty of Allied Health Sciences, Chulalongkorn
                        University

HOME ADDRESS   21/32 Nannalin Park Home, Nongchok, Bangkok, 10530,
                        Thailand

PUBLICATION   1. Julaluk Noiphung, Kwanrutai Talalak, Irin Hongwarittorrn,
                        Naricha Pupinyo, Pannawich Thirabowonkitphithan,
                        Wanida Laiwattanapaisal, A novel paper-based assay for
                        the simultaneous determination of Rh typing and forward
                        and reverse ABO blood groups, Biosensors and
                        Bioelectronics, Volume 67, 15 May 2015, Pages 485-489,
                        ISSN 0956-5663
                        2. Pupinyo N, Chatatikun M, Chiabchalard A,
                        Laiwattanapaisal W. In situ paper-based 3D cell culture for
                        rapid screening of the anti-melanogenic activity. Analyst.
                        2019;144(1):290-8.
                        3. Pupinyo N, Heiskanen A, Chailapakul O, Gorton L,
                        Emnéus J, Laiwattanapaisal W. Impedimetric melanoma
                        invasion assay device using a simple paper membrane and
                        stencil-printed electrode on PMMA substrate. Sensing and
                        Bio-Sensing Research. 2020 May 21:100354.

AWARD RECEIVED   Popular Vote Poster Award in the 9th CU-TU Medical
                        Technology Student's Research Conference 2014
                        Runner-Up award of Falling Walls Lab Thailand 2019